Discretization and approximation of the shape operator, the Laplace–Beltrami operator, and the Willmore energy of surfaces

Klaus Hildebrandt

A dissertation submitted
to the Fachbereich Mathematik und Informatik, Freie Universität Berlin
in partial fulfillment of the requirements for the degree of
doctor rerum naturalium

Defended December 7, 2012

Referees:
Prof. Dr. Konrad Polthier, Freie Universität Berlin
Prof. Dr. Max Wardetzky, Georg–August–Universität Göttingen

Contents

Introduction

Discrete differential geometry is an active mathematical field that concerns the construction and understanding of discrete counterparts to notions and concepts of classical and modern differential geometry of smooth manifolds. It is a theory in its own right that explores structures of discrete manifolds. Nevertheless, the relation between the continuous and the discrete theories is of central interest. Two basic aspects of a discretization are its consistency and convergence. The discrete objects and solutions of discrete problems or equations should approximate their continuous counterparts. In addition, an explicit goal of discrete differential geometry is to transfer the structure of the continuous theory to the discrete setting. We want to construct discrete objects that share fundamental properties and characteristics, *e.g.*, invariance under a transformation group, of their continuous counterparts. The development in this field has been precipitated by its applicability in areas like computer graphics, computational geometry, computational physics, and architectural geometry.

This thesis deals with discrete differential geometric properties of polyhedral surfaces in $\mathbb{R}^3$. We develop a description of the curvatures of polyhedral surfaces based on a generalization of the shape operator, and we construct discretizations of the (strong form of the) Laplace–Beltrami operator and of the Willmore energy. The focus of our analysis is on approximation properties of the introduced discretizations. In particular, we show that the generalized shape operators can be used to approximate the classical shape operator of a smooth surface, and we prove the consistency of the discrete Laplace–Beltrami operators and the discrete Willmore energies. In addition, we consider a prob-

lem in geometry processing: the fairing of polyhedral surfaces. We develop a scheme for fairing under spatial constraints.

Metric structure of polyhedral surfaces

This thesis is divided into four chapters. The first chapter concerns the approximation of metric properties of a smooth surface from corresponding properties of a nearby polyhedral surface and the construction of Lebesgue and Sobolev function spaces on polyhedral surfaces. The results presented in this chapter provide the basis for the subsequent chapters. Many of them are taken from [64, 106].

We begin the chapter by reviewing basic structures of a polyhedral surface M_h in $\mathbb{R}^3$. In particular, we equip M_h with a differentiable structure and a metric tensor field. The problem is that M_h is a topological, but (in general) not a differentiable submanifold of $\mathbb{R}^3$. However, as a consequence of Munkres' work [82, 83] on differentiable structures on topological manifolds, there is a unique differentiable structure on M_h that is compatible with the topology on M_h induced by $\mathbb{R}^3$. In Section 1.2, we explicitly construct charts that form an atlas of this differentiable structure on M_h. Then we can define tensor fields on M_h. The metric tensor field induced by $\mathbb{R}^3$ is flat in the interior of the triangles and edges and has cone singularities at the vertices. Hence it is a *cone metric*.

The approximation of metric properties of a smooth surface M by a nearby polyhedral surface M_h is treated in Sections 1.5 and 1.6. To quantitatively compare objects, like the normal vector fields, the metric tensor fields, and the area forms of the surfaces, we use the orthogonal projection π_M onto M to construct a map between the surfaces. Then we pullback the objects from M_h to M and use appropriate norms on M (L^∞-norms in our case) to measure the distance between corresponding objects. Using the orthogonal projection onto M for this purpose is common practice [44, 64, 80, 66]. In [64], it was shown that if a sequence of polyhedral surfaces converges to M in the Hausdorff distance, then the following are equivalent: the convergence of the normal vectors, the convergence of the area forms, and the convergences of the metric tensors. In Section 1.6, we slightly extend this convergence result by deriving explicit upper bounds on the distances of the metric tensors and the area forms. The estimates are linear in the Hausdorff distance and quadratic in the distance of the normal vector fields. Asymptotically, these bounds agree with estimates for the approximation of the surface area derived by Morvan and Thibert [81].

In Section 1.3, we review basics of the theory of the Sobolev spaces $W^{1,p}$ on polyhedral surfaces that was developed in [106]. This theory forms the ana-

lytic foundation for the generalization of the shape operator and the Laplace–Beltrami operator in the following chapters. An important property is that the pullback of functions via the orthogonal projection establishes an isomorphism of the Sobolev spaces $W^{1,p}$ on M_h and M. In addition to functions on a smooth or polyhedral surface $\mathcal{M}$, we consider vector fields in $T^{\mathcal{M}}\mathbb{R}^3$, the restriction to $\mathcal{M}$ of the tangent bundle of $\mathbb{R}^3$. Since this is a trivial bundle, the definitions of the Lebesgue and Sobolev function spaces on $\mathcal{M}$ directly generalize to corresponding spaces $\mathcal{X}_{L^p}(\mathcal{M})$ and $\mathcal{X}_{W^{1,p}}(\mathcal{M})$ of vector fields in this bundle. In Section 1.3.1, we introduce these spaces and define the *divergence* and *curl* of vector fields in $\mathcal{X}_{W^{1,p}}(\mathcal{M})$.

Generalized shape operators

Curvature is a central concept in the study of geometric properties of surfaces in $\mathbb{R}^3$ and appears in many interesting geometric and physical problems. Examples are the study and construction of surface with constant mean curvature and the analysis and integration of curvature flows. The estimation of curvatures of a smooth surface from an approximating discrete surface is important for the numerical treatment of such problems and for various applications in engineering and computer graphics.

In classical differential geometry, the curvatures of a smooth surface M in $\mathbb{R}^3$ are represented by the shape operator S, a tensor field on the tangent bundle of M. Since the definition of S involves second derivatives of the embedding of the surface, it does not apply to polyhedral surfaces. Consequently, there are different approaches for describing the curvatures of polyhedral surfaces. An overview will be given later in this introduction. Here, we follow a functional analytic approach. We introduce two generalized shape operators that are functionals on an appropriate Sobolev space of weakly differentiable vector fields and can be defined rigorously on polyhedral surfaces.

To motivate the construction, let us consider the two tensor fields

$$\bar{S} : X \mapsto S(X^\top) - HN\,\langle X, N\rangle \quad \text{and} \quad \hat{S} : X \mapsto S(N \times X),$$

on the bundle $T^{\mathcal{M}}\mathbb{R}^3$, where H and N denote the mean curvature and surface normal field of M and X is a vector field in $T^M\mathbb{R}^3$ with tangential part $X^\top$. What makes the two tensor fields interesting for us is that they satisfy the (vector-valued) integral equations

$$\int_M \bar{S}\,X \,\mathrm{d}vol = \int_M N \operatorname{div} X \,\mathrm{d}vol \quad \text{and} \quad \int_M \hat{S}\,X \,\mathrm{d}vol = -\int_M N \operatorname{curl} X \,\mathrm{d}vol,$$

and that the right-hand sides of both equations can be evaluated on polyhedral surfaces. We define the generalized shape operators on a smooth or polyhedral

surface $\mathcal{M}$ as the vector-valued continuous functionals

$$\bar{\Sigma} : X \mapsto \int_{\mathcal{M}} N \operatorname{div} X \, \mathrm{d}vol \quad \text{and} \quad \hat{\Sigma} : X \mapsto -\int_{\mathcal{M}} N \operatorname{curl} X \, \mathrm{d}vol$$

on $\mathcal{X}_{W^{1,1}}(\mathcal{M})$. In contrast to the classical shape operator, the generalized operators describe the curvatures in the sense of distributions and, therefore, cannot be evaluated at a single point of the surface. Nevertheless, Lemma 2.3 shows that on a smooth surface, the tensor fields $\bar{S}$ and $\hat{S}$ are the only continuous tensor fields that satisfy

$$\bar{\Sigma}(X) = \int_M \bar{S}\, X \, \mathrm{d}vol \quad \text{and} \quad \hat{\Sigma}(X) = \int_M \hat{S}\, X \, \mathrm{d}vol$$

for all $X \in \mathcal{X}_{W^{1,p}}(M)$.

Approximation results

In Sections 2.2-2.5, we establish two types of approximation results: the approximation of the generalized shape operators in the operator norm and pointwise approximation of the classical shape operator of a smooth surface.

The approximation in the operator norm guarantees that the generalized shape operators of a smooth surface can be approximated by their counterparts on a nearby polyhedral surface. It could be called approximation of the curvatures in an integrated sense, since it implies that integrals of $\bar{S}$ or $\hat{S}$ over a smooth surface can be approximated. To compare the generalized shape operators of a smooth surface M and a nearby polyhedral surface M_h, we pullback the operator of M_h to M via the orthogonal projection. The isomorphy of the spaces $\mathcal{X}_{W^{1,p}}$ guarantees that the pullback is a continuous functional. Hence, the distance of the generalized shape operators can be measured in the corresponding operator norm. We show that it is bounded by a constant times the sum of the Hausdorff distance and the distance of the normal vector fields.

Our approach for constructing pointwise approximations of the shape operator is to test the generalized shape operators with certain vector fields whose support is localized around a point. For this, we introduce the concept of *r-local functions*. If, for a $r \in \mathbb{R}^+$, a function ψ is r-local at a point y, then its support is contained in the geodesic ball of radius r around y. In addition, ψ is positive, has unit L^1-norm, and its $W^{1,1}$-norm satisfies a certain bound that depends on r. For the first step of our construction, we employ such a function to build the tensor $\bar{S}^\psi$, which is the $(1,1)$-tensor on $\mathbb{R}^3$ that, with respect to the standard basis $\{e_1, e_2, e_3\}$ of $\mathbb{R}^3$, has the components

$$(\bar{S}^\psi)_{ij} = \left\langle e_i, \bar{\Sigma}(\psi\, e_j) \right\rangle_{\mathbb{R}^3}.$$

If M_h is near M and ψ is r-local at $y \in M_h$, then $\bar{S}^\psi$ approximates the tensor $\bar{S}(x)$, where $x = \pi_M(y) \in M$. For the second step, we use $\bar{S}^\psi$ and the

surface normals of M_h to construct a tensor S^ψ, which approximates the shape operator $S(x)$ of M at x. We prove the bound

$$\left\| S(x) - S^\psi \right\| \leq C\,(r + \frac{\delta}{r}),$$

where δ denotes the sum of the Hausdorff distance of the surfaces and the distance of the surface normal fields and C is a constant. The estimate assumes no correlation between r and δ. To get convergence, r has to be asymptotically larger than δ. The optimal choice is $r = \sqrt{\delta}$, which results in an approximation order of $\sqrt{\delta}$. For a certain type of r-local functions, the bound improves to $C\,(r^2 + \frac{\delta}{r})$. Then $r = \delta^{\frac{1}{3}}$ yields an approximation order of $\delta^{\frac{2}{3}}$. In the last two sections of the chapter, we discuss the construction of r-local functions, and we present numerical experiments that confirm our approximation estimates.

Discrete Laplace–Beltrami operators

The Laplace–Beltrami operator of a Riemannian manifold is the counterpart on a curved manifold to the Laplace operator of a flat Euclidean space. According to Berger [15], the study of this operator and the associated heat and wave equations on a general Riemannian manifold has started rather recently in late 1940s. Evaluating the operator of a smooth function at a point of the manifold involves derivatives of the metric. Therefore, the classical definition (of the strong form) of the operator does not extend to polyhedral surfaces in $\mathbb{R}^3$. However, to formulate second-order equations, like Poisson's equation, only the weak form of the Laplace–Beltrami operator is needed. In contrast to the strong form, the weak form does not require derivatives of the metric and can be defined on polyhedral surfaces. In [64], it was shown that for a sequence of polyhedral surfaces that converge to a smooth surface in Hausdorff distance, the convergence of the weak Laplace–Beltrami operators in the operator norm is equivalent to the convergence of the surface normals.

A natural finite element space on a polyhedral surface is the space S_h of continuous functions that are linear in each triangle. In Section 3.3, we review a discretization of the weak Laplace–Beltrami operator with these elements. As shown in [91], the resulting discrete operator can be described using the cotangents of the inner angles of the triangles of the polyhedral surface. Therefore, it is often referred to as the *cotan Laplacian*. The weak Laplace–Beltrami operator can be used to discretize second-order boundary value problems on polyhedral surfaces. Convergence of solutions of the discrete Dirichlet problem of Poisson's equation was shown by Dziuk [44].

This raises the question of whether one can construct a consistent discretization of the strong Laplace–Beltrami operator, *i.e.*, a discretization that converges pointwise. Based on the cotan weights, various constructions of discrete

Laplacians have been proposed, see [107, 74, 97, 26] and references therein. However, pointwise convergence results for these operators could only be established for special types of meshes [110] (*e.g.*, meshes with certain valences) and counter-examples to consistency have been reported [110, 64].

Consistent discrete Laplace–Beltrami operators

In Section 3.5, we present a principle for constructing consistent discretizations of the strong Laplace–Beltrami operator. The construction involves r-local functions as it did for the pointwise approximation of curvature in Chapter 2.

The basis of the construction is a pointwise approximation estimate, which we derive in Section 3.4. We consider a smooth function u on a smooth surface M, a polyhedral surface M_h that is inscribed to M, and a piecewise linear function u_h on M_h that interpolates u at the vertices of M_h. Then we derive the bound

$$\left| \Delta u(x) - \int_{M_h} \left\langle \operatorname{grad}_{M_h} u_h, \operatorname{grad}_{M_h} \psi \right\rangle_{\mathbb{R}^3} \mathrm{d}vol_{M_h} \right| \leq C\,(r + \frac{h}{r}),$$

where ψ is a r-local function at $y \in M_h$, $x = \pi_M(y) \in M$, and h is the mesh size of M_h. The integral above equals the weak Laplace–Beltrami operator of u_h applied to ψ. This means that we can approximate $\Delta u(x)$ by testing the weak Laplace–Beltrami operator of u_h with r-local functions. As for the approximation of the shape operator, the bound improves to $C\,(r^2 + \frac{h}{r})$ for certain r-local functions. The optimal choice of r yields approximation orders of $h^{\frac{1}{2}}$ and $h^{\frac{2}{3}}$, respectively.

The discrete operators Δ_h, we want to build, are an endomorphism of S_h. For the construction, we need a r-local function at every vertex of M_h. Then we specify the value $\Delta_h u_h$ takes at a vertex v by testing the weak Laplace–Beltrami operator of u_h with the function that is r-local at v. From the pointwise approximation estimates, we deduce approximation estimates for the discrete Laplace–Beltrami operators in the L^∞-norm.

Like the cotan Laplacian, the constructed discrete operators can be expressed in terms of the cotan weights. We show that they can be represented by a matrix that is the product of the cotan matrix and a matrix that evaluates the r-local functions at the vertices of M_h. This representation simplifies the implementation of the proposed operators, especially when the cotan matrix is already implemented. Section 3.7 shows numerical experiments that confirm the established bounds.

Discrete Willmore energies for polyhedral surfaces

The Willmore energy of a smooth surface M in $\mathbb{R}^3$ is the nonlinear geometric functional

$$W(M) = \int_M H^2 \mathrm{d}vol.$$

$W(M)$ agrees, modulo multiples of the total Gauß curvature $\int_M K \,\mathrm{d}vol$, with the functionals

$$\int_M (\kappa_1^2 + \kappa_2^2)\mathrm{d}vol \quad \text{and} \quad \int_M (\kappa_1 - \kappa_2)^2 \mathrm{d}vol. \tag{1}$$

The Gauß–Bonnet theorem implies that the total Gauß curvature is constant under variations of a surface that keep the boundary and tangent planes at the boundary fixed. Hence, under such boundary constraints a minimizer of the Willmore energy is also a minimizer of the other two functionals. This means it has the least curvature (as a minimizer of the first functional in (1)) and the least difference in the principal curvatures (second functional). In addition, the second functional in (1) has the remarkable property that it is invariant under Möbius transformations of $\mathbb{R}^3$, see [17].

In Section 3.6, we introduce a construction of discrete Willmore energies on polyhedral surfaces, and, for inscribed polyhedral surfaces, we establish an upper bound on the difference of the continuous and discrete Willmore energies. The construction is based on the discrete strong Laplace–Beltrami operators. On smooth surfaces, the Willmore energy is linked to the Laplace–Beltrami operator through the mean curvature vector field $\mathbf{H}$, which is the product of the mean curvature H and the surface normal field. The mean curvature vector field equals the Laplace–Beltrami operator of the embedding of the surface, thus the Willmore energy equals the squared L^2-norm of the mean curvature vector. Since the embedding of a polyhedral surface is continuous and piecewise linear (hence in the domain of the discrete Laplace–Beltrami operators), the construction of the discrete Laplace–Beltrami operators extends to a construction of discrete mean curvature vectors and discrete Willmore energies. As a direct consequence of the consistency of the discrete Laplace–Beltrami operators, we obtain estimates for the pointwise approximation of the mean curvature vector field of a surface. Then we use these facts to prove consistency of the corresponding discrete Willmore energies. The consistency order agrees with that of the discrete Laplace–Beltrami operators.

Constraint-based fairing

The fourth chapter is concerned with fairing (or smoothing) of polyhedral surfaces. We introduce a fairing method that allows us to prescribe a bound

on the maximum deviation of every vertex of a polyhedral surface from its initial position. The scheme is modeled as a constrained non-linear optimization problem, where a discrete fairness energy (*e.g.*, a discrete Willmore energy) is minimized while inequality constraints ensure that the maximum deviation of the vertices is bounded.

An important application of surface smoothing is the removal of noise from 3D laser scan data. Though a laser scanner can capture the geometry of an object with high precision [73], the resulting data still contains noise. Surface smoothing methods are applied, in a post process, after a surface has been created from a number of range images. A benefit of our scheme over alternative approaches is that it can preserve the measuring accuracy of the data while smoothing out the noise. A second application of our scheme is the removal of aliasing and terracing artifacts from isosurfaces, which appear when a surface is extracted from volumetric data. Our scheme assures that the surface remains within the domain consisting of the voxels that contain the initial surface and their 1-neighbors. In addition, our scheme was recently applied by Váša and Rus [104] for removing artifacts induced by quantization of the vertex positions, which is used for mesh compression. The fairing method offers the benefit that the vertices are kept within the cubical cells specified by the quantization.

The choice of a numerical solver focuses on two goals: the method should be able to handle larger data sets and the running time should be comparable to that of alternative schemes, like those that integrate Willmore flow. We solve the problem with an active set Newton method with gradient projection.

Related work

The reader may believe that giving a complete overview of the literature on discrete differential geometry of polyhedral surfaces is hopeless. Instead, we focus on those developments that have had the most influence on this work.

Curvatures of polyhedral surfaces

Since the classical definition of curvatures does not apply to polyhedral surfaces, different concepts for describing their curvature have been introduced. We distinguish three classes: discrete curvatures, curvature measures, and polynomial surface approximation.

Discrete curvatures. Polyhedral minimal surfaces can be defined as stationary points of the area functional with respect to variation of the vertices and suitable boundary conditions. This definition led to the construction of interesting polyhedral minimal surfaces [91, 71, 93, 92]. In the continuous case, the

first variation of the area functional satisfies

$$\delta_V \text{area}(M) = \int_M \langle \mathbf{H}, V \rangle_{\mathbb{R}^3} \, \mathrm{d}vol.$$

Discretizing this equation by considering variations of the vertices of a polyhedral surface yields a discrete mean curvature vector field. Analogous to the continuous case, the discrete mean curvature vector field agrees with the image of the embedding of M_h under the cotan Laplacian.

Another prominent example of a discrete curvature is the discrete Gauß curvature that is defined at any vertex v of a polyhedral surface as the angle defect, *i.e.* 2π minus the sum of the angles at v of the triangles that contain v. There are different ways to motivate this definition, see [7, 8]. One of these uses the fact that on a smooth surface the integral of the Gauß curvature over a small enough region equals the signed area of the Gauß image of the region in the two-sphere $\mathbb{S}^2$. For polyhedral surfaces, the latter is a polygon in $\mathbb{S}^2$ whose area equals the angle defect at the vertex. Another motivation is that a discrete Gauß–Bonnet theorem can be derived based on the discrete Gauß curvature. Local versions of the discrete Gauß–Bonnet theorem can be formulated using an appropriate definition of geodesic curvature of polygons on a polyhedral surface, see [96].

Recently, Bobenko, Pottmann, and Wallner [18] introduced a curvature theory for discrete surfaces based on a notion of mesh parallelity. The discrete curvatures are defined for pairs of a discrete surface and an edgewise parallel Gauß image. The discrete Gauß and mean curvature are localized at the faces and defined using the surface area, the area of the Gauß image, and the mixed area. This curvature theory generalizes and unifies different previously defined classes of special surfaces including discrete isothermic surfaces of constant mean curvature [21], discrete minimal surfaces constructed from orthogonal circle patterns [20], and discrete Delaunay surfaces derived from elliptic billiards [65].

Curvature measures. Federer [47] introduced the first curvature measures, which generalize the k^{th}-mean curvatures (*i.e.* the symmetric polynomials of degree k in the principal curvatures) of a hypersurface of $\mathbb{R}^n$. They are defined for subsets of $\mathbb{R}^n$ with positive reach, a class that contains smooth submanifolds and arbitrary convex subsets. The connection of the k^{th}-mean curvature measures to corresponding classical curvatures can be illustrated by looking at the curvature measure of a smooth hypersurface M. Then for $k \in \{0, 1, ..., n-1\}$, the k^{th}-curvature measure of a Borel set $B \subset \mathbb{R}^n$ is proportional to the integral of the k^{th}-mean curvature over $M \cap B$. The theory of *normal cycles*, see [109, 114, 51, 80], was used to extend the class of sets for which the curvature measures can be defined. The normal cycle is a generalization of the

normal bundle of a hypersurface and can be defined for a broad class of subsets of $\mathbb{R}^n$ that is called *geometric sets* and includes sets of positive reach and arbitrary polyhedra. Based on the theory of normal cycles, Cohen–Steiner and Morvan [32, 33] introduced a new tensor-valued curvature measure, the *second fundamental measure*. A benefit of this measure is that it generalizes the whole second fundamental form (or shape operator) and not only the scalar-valued k^{th}-mean curvatures. Moreover, in [33], upper bounds on the difference (in the sense of measures) of the second fundamental measures of a smooth hypersurface and a nearby geometric set are derived. The case of a polyhedral surface that approximates a smooth surface was already treated earlier in [32]. The approximation of curvatures in the sense of measures is similar in spirit to our approximation of the generalized shape operators in the operator norm. It is an interesting problem to examine the relationship between the two concepts.

A discrete net of curvature lines in a smooth surface is a decomposition of the surface into cells, such that every edge of the decomposition is a segment of a curvature line of the smooth surface. Bauer et al. [10] defined discrete curvatures of such a net using a local polyhedral approximation, which constructs a 1-ring of planar triangles around any vertex of the net. They prove pointwise convergence of discrete curvatures on a net of curvature lines, based on either the convergence in measure of the curvature measures or the weak convergence of the discrete mean curvature vector.

Polynomial surface approximation. Given a sampling of a smooth surface, bivariate polynomial interpolation can be used to estimate the curvatures at a sample point x. First, a plane P in $\mathbb{R}^3$ that contains x and is not parallel to the surface normal at x (usually an estimation of the tangent plane at x) is constructed. Locally around x, the smooth surface can be represented as a graph over P. Then a selection of the sample points is projected onto P and serves as nodes for a bivariate polynomial interpolation, see [77, 53, 29]. The curvature at x of the resulting graph is used to approximate the curvature of the smooth surface at x. Since the sampling is irregular, a problem of this approach is that the interpolation problem may be ill-conditioned or even may not have a unique solution, see [111] for an example.

Heine [58] uses isoparametric finite elements (with polynomials of order two or higher) to obtain pointwise approximations of the curvatures of a smooth surface. The isoparametric elements are constructed over a polyhedral surface that approximates the smooth surface. In contrast to the discretizations considered in this thesis, the isoparametric element scheme requires additional information about the smooth surface. For example, to construct quadratic elements, the points of the smooth surface corresponding to the midpoints of the edges of the polyhedral surface are used. The weak formulation of the shape

operator used in this construction is related to one of our generalized shape operators.

Discrete Laplace–Beltrami operators

Discrete Laplace–Beltrami operators are basic objects in discrete differential geometry [23], discrete complex analysis [43, 78], and numerics of geometric partial differential equations [44]. In addition, different applications in fields like computer graphics [37, 74], geometry and image processing [97, 26], computational biology [25], and neuroscience [11, 99] use discretizations of the Laplace–Beltrami operator.

Among the different discretizations of the Laplace–Beltrami operator on polyhedral surfaces, the cotan Laplacian, is probably the most prominent. Several modifications of this discrete operator have been proposed. Based on an intrinsic Delaunay triangulation of a polyhedral surface, Bobenko and Springborn [24] propose a modified cotan Laplacian that has non-negative weights. This implies that the discrete operator satisfies a maximum principle, which, in general, is not satisfied by the cotan Laplacian. For an example of a cotan-discrete minimal surface that does not satisfy the maximum principle, we refer to [95]. Wardetzky et al. [108] analyze structural properties of discrete Laplace–Beltrami operators. Building on the continuous setting, they propose a set of desirable properties for discrete Laplace–Beltrami operators and prove a theoretical limitation: discrete Laplacians cannot satisfy all the properties. For example, the cotan Laplacian satisfies all but one of the properties, namely the maximum principle. In addition to the analysis, they introduce a construction of discrete Laplace–Beltrami operators that uses the outer differential of discrete 1-forms. A discrete Laplace–Beltrami operator is obtained by specifying an L^2-product on the space of discrete 1-forms. An extension of this idea is used by Alexa and Wardetzky [3] to define discrete Laplacians on surfaces with arbitrary polygonal faces, which may even be non-planar and non-convex. For extensions of the discrete Laplace–Beltrami operators to discrete Laplace–de Rham operators that act on discrete k-forms, we refer to [94, 38, 106, 5, 66] and references therein. Discrete anisotropic Laplace–Beltrami operators were introduced in [31, 59] in the context of feature preserving surface fairing. Demlow [36] constructs discrete Laplace–Beltrami operators using higher-order finite elements and proves consistency and convergence of the discrete operators. Similar to the method of Heine for curvature approximation, a piecewise polynomial approximation of a smooth surface is used, where the polynomials are defined over a polyhedral surface.

To our knowledge, only one other consistent discretization of the strong Laplace–Beltrami operator on polyhedral surfaces has been proposed besides our approach. It is called the *mesh Laplacian* and was introduced by Belkin

et al. [13]. The construction is based on a discretization of the heat kernel and is related to graph Laplacians used in data analysis and machine learning [57, 12]. Similar to our approach, the value of Δu at a point of a smooth surface is approximated by an integral over a region on a polyhedral surface. The diameter of the region depends on the size of the heat kernel that is used. To get convergence, the size of the heat kernel must be asymptotically larger than the mesh size. The consistency results for the mesh Laplacian have been generalized by Belkin et al. [14] to point clouds in $\mathbb{R}^d$ and by Dey et al. [40] to convergence of the spectrum of the Laplace–Beltrami operator. In Section 3.5.2, we discuss this construction and show that the consistency order we obtain improves the rates established for the mesh Laplacian.

Willmore energy

Boundary value problems for the Willmore energy are of fourth order, which makes discretizing the Willmore energy and the associated flow on polyhedral surfaces a difficult task. Based on a discretization of the mean curvature vector, Hsu, Kusner, and Sullivan [67] introduced a discrete Willmore energy for polyhedral surfaces and used Brakke's Surface Evolver [27] to compute minimizers with different genus. Bobenko [19] proposed a discrete Willmore energy for polyhedral surfaces that preserves the Möbius symmetry of the continuous energy. In [22] the flow of this discrete energy is studied. The question of whether these discrete energies approximate their smooth counterparts is still open. Dziuk [45] introduced a consistent discretization of the Willmore energy for polyhedral surfaces that are inscribed to a smooth surface. However, this discretization differs from the discrete energies considered in this work. Evaluating the energy requires derivatives of the embedding of the smooth surfaces, so it cannot be evaluated if only the polyhedral surface is known.

Clarenz et al. [30] use a weak form of the Willmore flow equation for a finite element discretization. To discretize the fourth-order equation with piecewise linear elements over a polyhedral surface, they use a mixed finite element method with position and mean curvature vector as variables. For alternative finite element discretizations of the Willmore flow with piecewise linear elements, we refer to Dziuk [45], Barrett et al. [9], and Olischläger and Rumpf [88]. A discretization of the Willmore flow with higher-order finite elements was introduced by Hari et al. [56] and a level set method was used by Droske and Rumpf [41]. Convergence results for the discretization of the Willmore flow have been established by Deckelnick and Dziuk [34] for the special case of surfaces that are graphs over a domain in the plane. For the general case of parametrized surfaces, such results are still missing.

Surface fairing

Many methods for surface fairing are based on a parabolic differential equation that is integrated over a time interval. The length of the integration interval is a parameter that controls the strength of the fairing effect. Different kinds of equations have been used, ranging from the linear diffusion of the embedding of a surface [101] to geometric flows, like the second-order mean curvature flow [39] and the fourth-order Willmore flow [113, 30, 22, 107]. Anisotropic geometric diffusion schemes [31, 100, 6, 59, 68] preserve or even enhance features, like sharp corners or edges, by locally suppressing or intensifying the diffusion depending on the principal curvatures and directions. Anisotropic geometric diffusion derives from the Perona–Malik filter [90] in image processing. A related technique, the bilateral filter [102], has been transferred to surface smoothing by Fleishman et al. [49] and Jones et al. [69]. Several extension and adjustments of the basic bilateral filtering of surfaces have been proposed, see [112, 16] and references therein. Comparable results can be achieved by methods based on Wiener filtering [89, 55, 2].

In contrast to schemes that integrate a parabolic equation, constraint-based fairing methods solve an optimization problem. Weak constraints are used for the least-square meshes [98, 84] that minimize a weighted sum of two quadratic energies: the biharmonic energy and a weighted sum of the squared distances of each vertex to its initial position. Extending this approach, Volodine et al. [105] present a scheme to compute minimizers of the biharmonic energy under the constraint that the sum of the squared distances is less than a prescribed value. Hard constraints have been considered for reducing aliasing effects in isosurfaces extracted from binary volume data [52, 86]. Similar to our method, these schemes minimize a fairness energy subject to hard constraints. However, there are differences. They focus on isosurfaces extracted from a regular grid. For example, the formulation of the constraints involves the volume grid. Furthermore, they use simpler fairness energies. In [52], a spring energy with zero rest length is used. As a result, the minimizers are of low regularity, *e.g.*, sharp bendings appear where the surface touches the constraints. Additionally, the solvers they apply seem to be less efficient than the solver we propose to use.

Summary of the main achievements

- Since a polyhedral surface has planar triangles, its *curvatures* are concentrated at the edges and vertices. Hence, roughly speaking, they cannot be described by functions but by distributions. In Chapter 2, we implement this idea by introducing generalized shape operators that can be defined rigorously for smooth and polyhedral surfaces.

- The definition of the generalized shape operators as elements of normed spaces is chosen such that the distance between the operators of a smooth and nearby polyhedral surface can be measured. We prove estimates for the approximation in the operator norm and for the pointwise approximation of the classical shape operator. To our knowledge, these are the first pointwise approximation results for the shape operator of a smooth surface from a nearby polyhedral surface in this generality.
- A construction of consistent discrete strong Laplace–Beltrami operators on polyhedral surfaces based on the weak Laplace–Beltrami operator is introduced. Our consistency order largely improves the order that was established for an alternative approach, the mesh Laplacian.
- Based on the discrete Laplacians, we define a discrete Willmore energy for polyhedral surfaces and prove its consistency. To our knowledge, this is the first consistency result for a discrete Willmore energy on polyhedral surfaces in this generality.
- Our fairing method provides control over the maximum deviation of the resulting smoothed surface from the input surface. It allows us to remove noise from measured surface data while preserving the measuring accuracy of the data.

Publications

The results presented in this thesis are published in the refereed articles [60], [61], and [62]. The latter received the *Best Paper Award* (1^{st} prize) at the *ACM Siggraph/Eurographics Symposium on Geometry Processing 2011*. Moreover, results of Chapters 2 and 3 were presented at the Oberwolfach workshop *Discrete Differential Geometry* in July 2012 and are summarized in the Oberwolfach report [63].

Open problems

Before closing the introduction, we want to mention some open questions and problems related to this thesis.

- The pointwise approximation results in Chapter 2 and 3 hold for any choice of a r-local function. We show that the approximation order improves (from $h^{\frac{1}{2}}$ to $h^{\frac{2}{3}}$) if a certain class of r-local functions (those that have the r^2-property) is used. Furthermore, the constant in our estimates depends on the $W^{1,1}$-norm of the r-local function. However, it is unclear what particular choice of a r-local function yields the best approximation.

- Are the bounds for the pointwise approximation of the shape operator and the Laplace–Beltrami operator sharp? In particular, for r-local functions that have the r^2-property, our experiments indicate that it may be possible to prove an approximation order of h.
- We introduce a consistent discretization of the Willmore energy. This motivates the question of whether convergence of solutions to boundary value problems for the discrete Willmore energy can be established. Moreover, it would interesting to use the discrete strong Laplace–Beltrami operators to discretize other fourth-order problems.
- Another interesting question is whether our construction of discrete Willmore energies could be transferred to a Möbius invariant setting.
- Concerning the fairing of surfaces, an interesting problem is to develop a strategy for estimating the accuracy of scan data. Combining this with our fairing method could help to automate the smoothing process.

Acknowledgements

It is my pleasure to thank all those who encouraged and supported me during the writing of this thesis. I would like to thank my advisor Konrad Polthier for introducing me to the field of discrete differential geometry and for his continuous support. I am grateful to Max Wardetzky for inspiring discussions, constructive and critical remarks, and for being my second referee. I wish to thank Carsten Lange, Ulrich Reitebuch, and Ulrich Bauer for stimulating discussions and Mimi Tsuruga for proof-reading a manuscript of this thesis.

Finally, this thesis would not have been possible without my family and friends who accompanied me during the last few years. I am deeply indebted to my wife Miriam for her love and endless support.

1
Polyhedral surfaces in $\mathbb{R}^3$

1.1 Topological and simplicial structures

The discrete manifolds we consider are polyhedral surfaces in $\mathbb{R}^3$. They carry a topological and a simplicial structure. The building blocks of a polyhedral surface are simplices.

Definition 1.1 (simplex) *A* k-dimensional simplex (*or* k-simplex) σ *in* $\mathbb{R}^n$ *is the convex hull of a set* P *of* $k+1$ *affinely independent points in* $\mathbb{R}^n$*. Any simplex spanned by a subset of* P *is called a* face *of* σ*.*

There are special names for low-dimensional simplices: we call a 2-simplex a *triangle*, a 1-simplex an *edge*, and a 0-simplex a *vertex*. By gluing together simplices, we can construct a *simplicial complex*. We restrict our attention to finite simplicial complexes.

Definition 1.2 (simplicial complex) *A* simplicial complex K *in* $\mathbb{R}^n$ *is a finite collection of simplices in* $\mathbb{R}^n$ *satisfying the following conditions:*

1. If a simplex is in K, then all its faces are in K.
2. If $\sigma, \tau \in K$ are simplices, then $\sigma \cap \tau$ is a face of σ and of τ.

The *dimension* of a simplicial complex is the maximum dimension of its simplices. The (closed) *star* of a simplex σ in a simplicial complex K is defined as

$$star(\sigma, K) = \{\tau \in K \mid \exists v \in K \text{ that has } \sigma \text{ and } \tau \text{ as a face}\}.$$

The *underlying space* U of a simplicial complex K is the set formed by the union of all simplices of K equipped with the subspace topology induced from $\mathbb{R}^n$. A *simplicial decomposition* of a subspace U of $\mathbb{R}^n$ is a simplicial complex K in $\mathbb{R}^n$ such that U is the underlying space of K.

Definition 1.3 (polyhedral surface) *A* polyhedral surface *in* $\mathbb{R}^n$ *is a topological 2-submanifold of* $\mathbb{R}^n$ *furnished with a simplicial decomposition.*

Notation 1.4 *Throughout the text, M will denote a smooth and M_h a polyhedral surface in $\mathbb{R}^3$. Both surfaces are assumed to be compact, connected, oriented, and without boundary. For statements that refer to both types of surfaces we use the calligraphic letter $\mathcal{M}$ to denote the surface.*

1.2 Metric and smooth structures

By definition, polyhedral surfaces in $\mathbb{R}^3$ are topological submanifolds; but, in general, they are not smooth submanifolds. Therefore, results of classical differential geometry are not directly applicable to them. However, polyhedral surfaces exhibit interesting geometric structures and possess counterparts to many differential geometric properties of smooth surfaces.

The goal of this section is to equip a polyhedral surface with two differential geometric structures, namely a smooth structure and a metric tensor field. Let us begin with a notion of distance between points on the surface. Let $\mathcal{M}$ be a smooth or polyhedral surface in $\mathbb{R}^3$. A curve in $\mathcal{M}$ is a continuous map γ from an interval to $\mathcal{M}$; we say that γ is *admissible* if it is rectifiable as a curve in $\mathbb{R}^3$.

Definition 1.5 (intrinsic distance) *The* intrinsic distance *between two points x and y in $\mathcal{M}$ is*

$$d_{\mathcal{M}}(x, y) = \inf_{\gamma} \textit{length}(\gamma), \tag{1.1}$$

where the infimum is taken over all admissible curves in $\mathcal{M}$ that connect x and y.

The pair $(\mathcal{M}, d_{\mathcal{M}})$ is a metric space, a so-called *length space* [54]. The intrinsic distance of a length space takes the role of the Riemannian distance of a Riemannian manifold. If $\mathcal{M}$ is a smooth submanifold, the intrinsic distance and the Riemannian distance coincide. Local isometries of Riemannian manifolds are usually characterized as diffeomorphisms that preserve the Riemannian metric. The following lemma shows that they can alternatively be described as maps that preserve the Riemannian distance function. For a proof we refer to [28].

Lemma 1.6 (isometries) *A map between two open subsets of Riemannian manifolds is a diffeomorphism and preserves the Riemannian metric if and only if it preserves the Riemannian distance.*

A *minimizing geodesic* in $\mathcal{M}$ is an admissible curve $\gamma : I \mapsto \mathcal{M}$ that satisfies

$$d_{\mathcal{M}}(\gamma(s), \gamma(t)) = \text{length}(\gamma_{|[s,t]})$$

for all $s, t \in I$, where I is an interval in $\mathbb{R}$. The following lemma is a direct consequence of the Hopf–Rinow theorem for locally-compact length spaces, which can be found in the book of Gromov [54], and our assumption that $\mathcal{M}$ is compact and connected.

Lemma 1.7 (minimizing geodesics) *Any pair of points in $\mathcal{M}$ can be joined by a minimizing geodesic.*

Now, we show how to construct an atlas of a smooth (even complex) structure for a polyhedral surface M_h. The construction follows Troyanov [103]. The standard cone with angle θ is the set

$$C_\theta = \{(r, \phi) \,|\, r \geq 0, \phi \in \mathbb{R}/\theta\mathbb{Z}\}/_{(0,\phi)\sim(0,\widetilde{\phi})}$$

equipped with the cone metric $\mathrm{d}s^2 = \mathrm{d}r^2 + r^2\mathrm{d}\phi^2$. The metric is flat if θ equals 2π and otherwise has a singularity at the center. The cone C_θ is isometric to $\mathbb{C}$ with the metric $\mathrm{d}s^2 = |z|^{2\beta}\,|\mathrm{d}z|^2$, where $\beta = \frac{\theta}{2\pi} - 1$. Explicitly, the isometry is given by

$$\begin{aligned} F : C_\theta &\mapsto \mathbb{C} \\ (r, \phi) &\mapsto \left(\frac{\theta}{2\pi} r\, e^{i\phi}\right)^{\frac{2\pi}{\theta}} . \end{aligned}$$

Every point of M_h has a neighborhood that is isometric to a neighborhood of the center of a cone C_θ with a certain angle θ. For every vertex v of M_h, the angle θ of the cone equals the sum of the angles at v of the triangles incident to v; for all other points, the angle θ of the cone equals 2π. For any point $x \in M_h$, the concatenation of the local isometry and the map F establishes a chart for a local neighborhood around x. The transition functions between the charts around two distinct points are holomorphic maps since they are compositions of holomorphic functions of the form $z \mapsto a\,z + b$ and $z \mapsto z^\gamma$, where the domains of functions of the second type do not include the origin. Hence, we can use these charts to construct an atlas of a smooth (even complex) structure on M_h. This smooth structure is compatible with the topology on M_h induced by $\mathbb{R}^3$. In fact it is the only smooth structure with this property. This follows from the work of Munkres [82, 83], who showed that smooth surfaces that are homeomorphic are also diffeomorphic.

By construction, each of the charts of the atlas is an isometry with respect to the metric tensor $\mathrm{d}s^2 = |z|^{2\beta}\,|\mathrm{d}z|^2$ on $\mathbb{C}$. Therefore, the transition functions between any pair of charts are isometries (where the values of β and hence the metrics $\mathrm{d}s^2$ on $\mathbb{C}$ may be different for the two charts). For any chart, we can pullback the metric tensor field from the image to the domain, which provides us with a metric tensor field in local neighborhoods on the polyhedral surface. Since the transition functions between the charts are isometries, the locally defined tensor fields consistently describe a metric tensor field g_h on M_h. This metric is flat in the interior of all triangles and edges and has conical singularities at the vertices. Therefore, we call g_h the cone metric. The distance function on M_h derived from this metric tensor agrees with the intrinsic distance on M_h. Furthermore, for every point in the interior of a triangle, this tensor agrees with the restriction to the plane of the triangle of the standard scalar product of $\mathbb{R}^3$.

1.3 Lebesgue and Sobolev spaces

The operators that we consider in the following chapters act on Sobolev spaces of once weakly differentiable functions or vector fields. To be able to define these operators on a polyhedral surface, we need a theory of Sobolev spaces $W^{1,p}$ on polyhedral surfaces. Such a theory was developed by Wardetzky in his dissertation [106]. In this section, we define the Lebesgue space L^p and Sobolev spaces $W^{1,p}$ on polyhedral surfaces, and then extend the construction to spaces of vector fields.

The area form $\mathrm{d}vol_{M_h}$, induced by the cone metric g_{M_h}, is a Borel regular measure on M_h. Thus, we can define the function space of Lebesgue-integrable functions on polyhedral surfaces in the same way as on smooth surfaces. Let $\mathcal{M}$ denote a smooth or polyhedral surface. For any positive integer $p < \infty$, we define $L^p(\mathcal{M})$ as the space of measurable functions on $\mathcal{M}$ whose p^{th} power is Lebesgue-integrable, where, as usual, we identify two functions in L^p if they are equal almost everywhere (*a.e.*) on $\mathcal{M}$. Equipped with the L^p-norm

$$\|u\|_{L^p} = \left(\int_{\mathcal{M}} |u|^p \,\mathrm{d}vol_{\mathcal{M}}\right)^{\frac{1}{p}} \tag{1.2}$$

$L^p(\mathcal{M})$ is a Banach space. When $p = 2$, the space $L^2(\mathcal{M})$ is a Hilbert space, and the scalar product is

$$\langle u, v\rangle_{L^2} = \int_{\mathcal{M}} u\, v \,\mathrm{d}vol_{\mathcal{M}}.$$

A measurable function u is *essentially bounded* on $\mathcal{M}$ if there exists a constant c for which $|u| < c$ holds *a.e.* on $\mathcal{M}$. The greatest lower bound of such a

constant c is called the *essential supremum* of u, which we abbreviate by ess $\sup_{x\in M_h} |u(x)|$. The space $L^\infty(\mathcal{M})$ consists of classes of essentially bounded functions, where again functions are identified if they agree *a.e.* on $\mathcal{M}$. The functional

$$\|u\|_{L^\infty} = \operatorname*{ess\,sup}_{x\in\mathcal{M}} |u(x)| \tag{1.3}$$

defines a norm on $L^\infty(\mathcal{M})$ and makes it a Banach space.

The smooth structure, derived in the last section, equips M_h with a tangent bundle TM_h and a notion of smooth tangential vector fields on M_h (the singularities are only visible in the metric, not in the differentiable structure). We denote by $\mathfrak{X}_{L^p}(\mathcal{M})$ the space of integrable tangential vector fields X on $\mathcal{M}$ whose pointwise norm $\sqrt{g_{\mathcal{M}}(X,X)}$ is in $L^p(\mathcal{M})$, and we define the norm

$$\|X\|_{L^p} = \left\| \sqrt{g_{\mathcal{M}}(X,X)} \right\|_{L^p}$$

on $\mathfrak{X}_{L^p}(\mathcal{M})$. Now, we define a space of test vector fields $\mathfrak{X}(\mathcal{M})$. For this, we distinguish between the case when $\mathcal{M}$ is smooth and the case when $\mathcal{M}$ is polyhedral. On a smooth surface M, let $\mathfrak{X}(M)$ be the space of smooth tangential vector fields. Following [106], we impose additional assumptions on the test vector fields on M_h, which are needed to control the influence of the cone singularities. We define $\mathfrak{X}(M_h)$ to be the space of continuous vector fields on M_h that are smooth outside the cone singularities and whose pointwise norm and divergence (both classically defined almost everywhere on M_h) is in $L^\infty(M_h)$.

Definition 1.8 (Sobolev spaces) *For any positive integer $p < \infty$, let $W^{1,p}(\mathcal{M})$ be the space of all functions $u \in L^p(\mathcal{M})$ for which there exists a vector field $\operatorname{grad} u \in \mathfrak{X}_{L^p}(\mathcal{M})$, called the* weak gradient *of u, that satisfies*

$$\int_{\mathcal{M}} g_{\mathcal{M}}(\operatorname{grad} u, X)\, dvol_{\mathcal{M}} = \int_{\mathcal{M}} u\, \operatorname{div} X\, dvol_{\mathcal{M}}$$

for all $X \in \mathfrak{X}(\mathcal{M})$. If $p = 2$, we write $H^1(\mathcal{M}) = W^{1,2}(\mathcal{M})$.

The norms and semi-norms on the spaces $W^{1,p}(\mathcal{M})$ are

$$|u|_{W^{1,p}} = \|\operatorname{grad} u\|_{L^p}$$

and

$$\|u\|_{W^{1,p}} = \left(\|u\|_{L^p}^p + |u|_{W^{1,p}}^p\right)^{\frac{1}{p}}.$$

For properties of the weak gradient and the Sobolev space on polyhedral surfaces (including the uniqueness of the weak derivative, Rellich's compactness lemma, and Poincaré's inequality) we refer to [106].

On a smooth surface M, we additionally consider the spaces $C^k(M)$ of k-times continuously differentiable functions. On $C^1(M)$ and $C^2(M)$ we define the semi-norms

$$|u|_{C^1} = \|\operatorname{grad} u\|_{L^\infty} \qquad \text{and} \qquad |u|_{C^2} = \|\operatorname{hess} u\|_\infty ,$$

where $\operatorname{hess} u$ denotes the Hessian of u and

$$\|\operatorname{hess} u\|_\infty = \operatorname*{ess\,sup}_{x\in M} \max_{\substack{v,w\in T_xM \\ \|v\|_g=\|w\|_g=1}} |\operatorname{hess} u(v,w)| .$$

Furthermore, on $C^0(M)$, $C^1(M)$, and $C^2(M)$ we consider the norms

$$\begin{aligned} \|u\|_{C^0} &= \|u\|_{L^\infty} , \\ \|u\|_{C^1} &= \|u\|_{C^0} + |u|_{C^1} , \quad \text{and} \\ \|u\|_{C^2} &= \|u\|_{C^1} + |u|_{C^2} . \end{aligned}$$

Then the pairs $\{C^0(M), \| \ \|_{C^0}\}$, $\{C^1(M), \| \ \|_{C^1}\}$, and $\{C^2(M), \| \ \|_{C^2}\}$ are Banach spaces.

1.3.1 Vector fields

In addition to vector fields in the tangent bundle $T\mathcal{M}$, we consider vector fields in $T^{\mathcal{M}}\mathbb{R}^3$, the restriction to $\mathcal{M}$ of the tangent bundle of ambient $\mathbb{R}^3$. This bundle is trivial and we identify it with $\mathcal{M} \times \mathbb{R}^3$. Then a vector field in this bundle is a map $\mathcal{M} \mapsto \mathcal{M} \times \mathbb{R}^3$ that is the identity in the first component. To simplify notation, we omit this first component, thus we identify vector fields in $T^{\mathcal{M}}\mathbb{R}^3$ with maps from $\mathcal{M}$ to $\mathbb{R}^3$. For any such vector field X, we denote by $X_i = \langle X, e_i\rangle_{\mathbb{R}^3}$ its components with respect to the standard basis $\{e_1, e_2, e_3\}$ of $\mathbb{R}^3$. We define $\mathcal{X}_{L^p}(\mathcal{M})$ and $\mathcal{X}_{W^{1,p}}(\mathcal{M})$ to be the spaces of vector fields in $T^{\mathcal{M}}\mathbb{R}^3$ with all three component functions in $L^p(\mathcal{M})$ and $W^{1,p}(\mathcal{M})$, respectively. An example of a vector field in $T^{\mathcal{M}}\mathbb{R}^3$ is the surface normal field $N : \mathcal{M} \mapsto \mathbb{R}^3$. On a smooth surface M, the components of N are smooth; on a polyhedral surface M_h, the components of N are constant over every triangle and discontinuous at the edges and vertices. For any $X \in \mathcal{X}_{L^p}(\mathcal{M})$, we denote by $X^\perp = \langle X, N\rangle_{\mathbb{R}^3} N$ the normal component and by $X^\top = X - X^\perp$ the tangential component of X. Both components, $X^\perp$ and $X^\top$, are vector fields in $\mathcal{X}_{L^p}(\mathcal{M})$. We denote the subspaces of $\mathcal{X}_{L^p}(\mathcal{M})$ consisting of vector fields with vanishing normal or tangential component by $\mathcal{X}^\top_{L^p}(\mathcal{M})$ and $\mathcal{X}^\perp_{L^p}(\mathcal{M})$, respectively.

Let $I : \mathcal{M} \mapsto \mathbb{R}^3$ be the embedding of $\mathcal{M}$ in $\mathbb{R}^3$. Then $\mathrm{d}I$ maps vector fields in $T\mathcal{M}$ onto tangential vector fields in $T^{\mathcal{M}}\mathbb{R}^3$. On a smooth surface M, $\mathrm{d}I$ maps smooth vector fields in TM to smooth vector fields in $T^M\mathbb{R}^3$. Since the embedding of a polyhedral surface is only Lipschitz continuous, this is not the

case for polyhedral surfaces. For example, the image $\mathrm{d}I(X)$ of a continuous vector field X in TM_h is, in general, not continuous in $T^{M_h}\mathbb{R}^3$. However, for polyhedral and for smooth surfaces, $\mathrm{d}I$ is an isometry of the spaces $\mathfrak{X}_{L^p}(\mathcal{M})$ and $\mathcal{X}^\top_{L^p}(\mathcal{M})$. This implies that the image $\mathrm{d}I(\operatorname{grad} u)$ of the weak gradient of a function $u \in W^{1,p}(\mathcal{M})$ is in $\mathcal{X}^\top_{L^p}(\mathcal{M})$. For simplicity, we will identify the spaces $\mathfrak{X}_{L^p}(\mathcal{M})$ and $\mathcal{X}^\top_{L^p}(\mathcal{M})$; in particular, we will treat the weak gradient of a function as an element of $\mathcal{X}^\top_{L^p}(\mathcal{M})$. Furthermore, for any point $x \in \mathcal{M}$ at which the normal vector is defined, we will identify the tangent space $T_x\mathcal{M}$ with its image $\mathrm{d}I(T_x\mathcal{M})$, which is the subspace of $\mathbb{R}^3$ that is orthogonal to $N(x)$. We call the orthogonal complement of $T_x\mathcal{M}$ in $\mathbb{R}^3$ the *normal space* $T_x^\perp\mathcal{M}$.

Next, we define the divergence and curl of vector fields in $\mathcal{X}_{W^{1,p}}(\mathcal{M})$.

Definition 1.9 (divergence and curl) *The* divergence *and the* curl *are the linear operators*

$$\mathit{div}, \mathit{curl} : \mathcal{X}_{W^{1,p}}(\mathcal{M}) \mapsto L^p(\mathcal{M})$$

given almost everywhere on $\mathcal{M}$ by

$$\mathit{div}\, X = \sum_{i=1}^{3} \langle \mathit{grad}\, X_i, e_i \rangle_{\mathbb{R}^3} \tag{1.4}$$

and

$$\mathit{curl}\, X = \sum_{i=1}^{3} \langle \mathit{grad}\, X_i \times e_i, N \rangle_{\mathbb{R}^3}\,, \tag{1.5}$$

where $\times$ is the cross product of $\mathbb{R}^3$ and $p < \infty$ is a positive integer.

On a polyhedral surface M_h, eqs. (1.4) and (1.5) are defined only in the interior of the triangles. However, this suffices to get well-defined operators div and curl on $\mathcal{X}_{W^{1,p}}(M_h)$.

Lemma 1.10 *The operators div and curl are continuous with operator norm less or equal to one.*

Proof. For any $X \in \mathcal{X}_{W^{1,p}}(\mathcal{M})$,

$$\|\operatorname{div} X\|_{L^p} = \left\| \sum_{i=1}^{3} \langle \operatorname{grad} X_i, e_i \rangle_{\mathbb{R}^3} \right\|_{L^p} \leq \sum_{i=1}^{3} \|\operatorname{grad} X_i\|_{L^p} \leq \|X\|_{W^{1,p}}$$

and

$$\|\operatorname{curl} X\|_{L^p} = \left\| \sum_{i=1}^{3} \langle \operatorname{grad} X_i \times e_i, N \rangle_{\mathbb{R}^3} \right\|_{L^p} \leq \sum_{i=1}^{3} \|\operatorname{grad} X_i\|_{L^p} \leq \|X\|_{W^{1,p}}\,.$$

This proves the lemma. □

To motivate the definition, let us consider a smooth surface M and a smooth vector field $X \in T^M\mathbb{R}^3$. Using the orthogonal projection π_M onto M (see Section 1.5), this field can be extended to a smooth vector field $\tilde{X}$ on a (small enough) open neighborhood of M in $\mathbb{R}^3$ by setting

$$\tilde{X}(x) = X(\pi_M(x)).$$

Then the classical divergence and curl of $\tilde{X}$ in $\mathbb{R}^3$ agree with the divergence and curl of X for all points of M:

$$\operatorname{div} X = \sum_{i=1}^{3} \langle \operatorname{grad} X_i, e_i \rangle_{\mathbb{R}^3} = \sum_{i=1}^{3} \left\langle \operatorname{grad}_{\mathbb{R}^3} \tilde{X}_i, e_i \right\rangle_{\mathbb{R}^3} = \operatorname{div}_{\mathbb{R}^3} \tilde{X}$$

and

$$\begin{aligned} \operatorname{curl} X &= \sum_{i=1}^{3} \langle \operatorname{grad} X_i \times e_i, N \rangle_{\mathbb{R}^3} = \sum_{i=1}^{3} \left\langle \operatorname{grad}_{\mathbb{R}^3} \tilde{X}_i \times e_i, N \right\rangle_{\mathbb{R}^3} \\ &= \left\langle \operatorname{curl}_{\mathbb{R}^3} \tilde{X}, N \right\rangle_{\mathbb{R}^3}. \end{aligned}$$

Here we use the property that $\tilde{X}$ is constant along any straight line that meets M normally. Hence, $\operatorname{grad} X_i = \operatorname{grad}_{\mathbb{R}^3} \tilde{X}_i$. The extrinsic definitions of divergence and curl of vector fields in $T^M\mathbb{R}^3$ are consistent with the intrinsic definitions of divergence of vector fields in TM in the sense that for any $Y \in TM$, the divergence and curl of Y agree with the divergence and curl of the corresponding field $\mathrm{d}I(Y)$. Since we identify Y and $\mathrm{d}I(Y)$, we also use the same notation for the intrinsically defined and the extrinsically defined divergence. We want to remark that the extrinsic definition of a divergence of vector fields in $T^M\mathbb{R}^3$ is also known as the tangential divergence, see [46].

The contribution of the normal component of a vector field X to the divergence has a simple geometric interpretation

$$\operatorname{div} X^\perp = \langle \operatorname{grad} \langle X, N \rangle_{\mathbb{R}^3}, N \rangle_{\mathbb{R}^3} + \langle X, N \rangle_{\mathbb{R}^3} \operatorname{div} N = -H \langle X, N \rangle_{\mathbb{R}^3}, \tag{1.6}$$

where H is the mean curvature of M (see Section 1.4). Furthermore, on smooth surfaces the divergence and the curl of X are related by

$$\operatorname{curl} X = \operatorname{div}(X \times N). \tag{1.7}$$

This implies that the curl of a normal vector field vanishes,

$$\operatorname{curl} X = \operatorname{curl} X^\top. \tag{1.8}$$

In Lemma 2.5, we establish error estimates for the approximation of divergence and curl of a smooth surface by the divergence and curl of polyhedral surfaces.

1.4 Shape operator of smooth surfaces in $\mathbb{R}^3$

Let D denote the flat connection of $\mathbb{R}^3$. Since the surface normal field N of a smooth surface M has constant length and points in the normal direction, for every tangential vector field $X \in \mathcal{X}^\top(M)$, the derivative $\mathrm{D}_X N$ is again a tangential vector field. The *shape operator* (or *Weingarten map*) S is the tensor field

$$\begin{aligned} S : \mathcal{X}^\top(M) &\mapsto \mathcal{X}^\top(M) \\ X &\mapsto -\mathrm{D}_X N. \end{aligned} \tag{1.9}$$

A basic property of the shape operator is that for every $x \in M$, $S(x)$ is self-adjoint with respect to the scalar product on $T_x M$ inherited from $\mathbb{R}^3$. The eigenvalues and eigendirections of $S(x)$ are the principal curvatures $\kappa_i(x)$ and the principal curvature directions of M at x, and we call $\kappa_{\max}(x) = \max\{|\kappa_1(x)|, |\kappa_2(x)|\}$ the maximum curvature at x. Furthermore, the trace and the determinant of $S(x)$ are called the mean curvature and the Gauß curvature of M at x and are denoted by $H(x)$ and $K(x)$.

In the following chapter, we will consider vector fields that are not necessarily tangential. Then it is convenient to consider an extended shape operator that is defined on $\mathcal{X}(M)$. For simplicity of presentation, we denote both operators by S and rely on the context to make the distinction. The extended shape operator is defined by

$$\begin{aligned} S : \mathcal{X}(M) &\mapsto \mathcal{X}(M) \\ X &\mapsto -\mathrm{D}_{X^\top} N. \end{aligned}$$

The extended operator agrees with the classical operator for tangential vector fields, and normal vector fields are in its kernel.

1.5 Polyhedral surfaces near smooth surfaces

In the previous sections, we constructed a metric tensor and function spaces on polyhedral surfaces. In this section, we consider a polyhedral surface that approximates a smooth surface and analyze relations between corresponding metric properties and function spaces. First, we use the orthogonal projection onto the smooth surface to obtain a bi-Lipschitz mapping between the surfaces. Considering this map for comparing two surfaces, where one of them is smooth, is common practice, see [44, 64, 80, 66]. Using this map, we pullback the metric tensor g_{M_h} of the polyhedral surface to the smooth surface. The difference between the two metric tensors on M can be described by a symmetric tensor field, the *metric distortion tensor*. In Section 1.5.5, we follow [64] and derive a

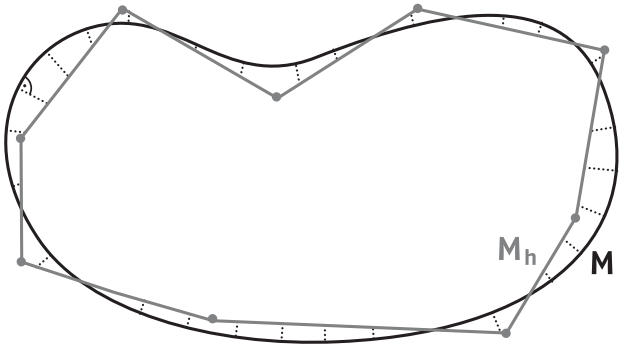

FIGURE 1.1. An illustration of the correspondence between the smooth and the polyhedral surface is shown. The correspondence is obtained by restricting the orthogonal projection onto M to the surface M_h.

closed form representation of the this tensor in terms of the Hausdorff distance, the normal distance, and the curvature of M. Again following [64], we show in Section 1.5.6 that the pullback of functions via the orthogonal projection induces an isomorphism of corresponding function spaces L^p and $W^{1,p}$ on the two surfaces.

1.5.1 Orthogonal projection onto M

Let M be a compact smooth surface in $\mathbb{R}^3$. The distance function $\delta_M : \mathbb{R}^3 \mapsto \mathbb{R}_0^+$ is defined as

$$\delta_M(y) = \inf_{x \in M} \|x - y\|_{\mathbb{R}^3} . \tag{1.10}$$

Since M is compact, for every $y \in \mathbb{R}^3$ there is at least one point $x \in M$ that attains the minimum distance to y. Then the straight line passing through x and y meets M orthogonally; therefore, x is called an *orthogonal projection* of y onto M. In general, x is not unique with this property; however, there exists an open neighborhood U_M of M in $\mathbb{R}^3$, such that every point of U_M has a unique orthogonal projection onto M. The induced *projection map* $\pi_M : U_M \mapsto M$ is smooth, a proof of this is contained in a note by Foote [50].

1.5.2 Reach of a surface

The *reach* of M is the supremum of all positive numbers r such that the orthogonal projection onto M is unique in the open r-tube around M, where an open r-tube around M is the set of all points y in $\mathbb{R}^3$ that fulfill $\delta_M(y) < r$. Locally around a point $x \in M$, the reach equals the reciprocal of $\kappa_{\max}(x)$. As a consequence, the reach of M is bounded above by

$$\operatorname{reach}(M) \leq \inf_{x \in M} \frac{1}{\kappa_{\max}(x)}. \tag{1.11}$$

The inequality is strict, *e.g.* equality holds if M is a sphere in $\mathbb{R}^3$, but in general the reach additionally depends on global properties of the surface. Still, every embedded compact smooth surface has positive reach. For a general treatment of sets with positive reach we refer to the book of Federer [48].

1.5.3 Differential of the projection map

Let y be a point in the open reach(M)-tube around M and let $x = \pi_M(y)$ be the projection of y onto M. The signed distance of y to M is

$$\sigma_M(y) = \langle y - \pi_M(y), N(x) \rangle_{\mathbb{R}^3} . \tag{1.12}$$

Differentiating this equation at y into a direction $v \in \mathbb{R}^3$ yields

$$\mathrm{d}_y \sigma_M(v) = \langle N(\pi_M(y)), v \rangle_{\mathbb{R}^3} , \tag{1.13}$$

where we apply the fact that the images of $\mathrm{D}N$ and $\mathrm{d}\pi_M$ are orthogonal to N and $y - \pi_M(y)$ is parallel to N. Using the signed distance function, we can represent the projection π_M as

$$\pi_M(y) = y - \sigma_M(y)\ N(\pi_M(y)). \tag{1.14}$$

Differentiation of this equation yields

$$\mathrm{d}_y \pi_M(v) = v - \mathrm{d}_y \sigma_M(v)\, N(x) - \sigma_M(y)\, \mathrm{D}_{\mathrm{d}_y \pi_M(v)} N.$$

Using the definition of the shape operator (1.9) and equation (1.13), we get

$$(Id - \sigma_M(y)\, S(x)) \mathrm{d}_y \pi_M = Id - \langle N(x), \cdot \rangle_{\mathbb{R}^3}\, N(x). \tag{1.15}$$

The right-hand side of this equation describes the orthogonal projection in $\mathbb{R}^3$ onto the tangent plane $T_x M$.

1.5.4 Normal graphs

Let us consider a polyhedral surface M_h that approximates a smooth surface M and use the orthogonal projection onto M to construct a map between the surfaces.

Definition 1.11 (normal graphs) *A polyhedral surface M_h is a* normal graph *over a smooth surface M if M_h is a subset of the open reach(M)-tube around M and the restriction of the projection map π_M to M_h is a bijection. We denote the restricted projection map by Ψ. Furthermore, we denote by Φ the inverse map of Ψ, which parametrizes M_h over M.*

The parametrization Φ of any normal graph M_h over M can be written as

$$\Phi(x) = I(x) + \phi(x)N(x),$$

where I is the embedding of M and

$$\phi(x) = \sigma_M(\Phi(x)).$$

We will use the map Φ to pullback functions, vector fields, and tensors from M_h to M. We will add the subindex "M_h" to objects defined on M_h and the subindex "h" to the pullback to M of such an object. For example, we denote the surface normal of M by N, the surface normal of M_h by N_{M_h}, and the pullback to M of N_{M_h} by $N_h = N_{M_h} \circ \Phi$.

Let $x \in M$ be a point such that $\Phi(x)$ is in the interior of a triangle of M_h. Then $N_h(x)$ is well-defined, and T_xM and $T_{\Phi(x)}M_h$ are the subspaces of $\mathbb{R}^3$ orthogonal to $N(x)$ and $N_h(x)$, respectively. As a tool in the proofs in this chapter, we will use the following projections

$$\begin{aligned} P_{N_h(x)} &: T_xM \mapsto T_{\Phi(x)}M_h \\ P_{N_h(x)}(v) &= v - \langle v, N_h(x)\rangle_{\mathbb{R}^3} N_h(x) \end{aligned} \tag{1.16}$$

and

$$\begin{aligned} P_{N(x)} &: T_{\Phi(x)}M_h \mapsto T_xM \\ P_{N(x)}(w) &= w - \langle w, N(x)\rangle_{\mathbb{R}^3} N(x). \end{aligned} \tag{1.17}$$

By the definition of normal graphs, $N(x)$ and $N_h(x)$ are never orthogonal. Thus, both maps have full rank and the inverse maps

$$\begin{aligned} P^{-1}_{N_h(x)} &: T_{\Phi(x)}M_h \mapsto T_xM \\ P^{-1}_{N_h(x)}(w) &= w - \frac{\langle w, N(x)\rangle_{\mathbb{R}^3}}{\langle N, N_h(x)\rangle_{\mathbb{R}^3}} N_h(x) \end{aligned} \tag{1.18}$$

and

$$\begin{aligned} P^{-1}_{N(x)} &: T_xM \mapsto T_{\Phi(x)}M_h \\ P^{-1}_{N(x)}(v) &= v - \frac{\langle v, N_h(x)\rangle_{\mathbb{R}^3}}{\langle N, N_h(x)\rangle_{\mathbb{R}^3}} N(x) \end{aligned} \tag{1.19}$$

exist.

Lemma 1.12 *The map Ψ is a homeomorphism of M_h and M, and for every triangle $T \in M_h$ the restriction of Ψ to the interior of T is a diffeomorphism onto its image.*

Proof. We first show that Ψ is a homeomorphism. Ψ is continuous, because it is the restriction to M_h of the smooth map π_M, and Ψ is bijective by assumption. Now we only need to show that Ψ is a closed map. Since M_h is compact, a closed subset A of M_h is compact; and since Ψ is continuous, $\Psi(A)$ is compact in M and hence $\Psi(A)$ is closed.

To prove the second part of the lemma, consider a point y in the interior of a triangle T of M_h with corresponding point $x = \Psi(y)$. The differential of Ψ at y equals the restriction of $\mathrm{d}_y\pi_M$ to T_yM_h. From equation (1.15) we get

$$\mathrm{d}_y\Psi(v) = (Id - \phi(x)\ S(x))^{-1} P_{N(x)}(v), \tag{1.20}$$

for any $v \in T_yM_h$. As stated above, $P_{N(x)}$ has full rank and $Id - \sigma_M S$ has full rank by equation (1.11). This means that $\mathrm{d}_y\Psi$ has full rank, and consequently, the restriction of Ψ to the interior of T is a diffeomorphism onto its image. □

1.5.5 Metric distortion

Let us consider a polyhedral surface M_h that is a normal graph over a smooth surface M. Using the bijection Φ, we can compare the metrics g of M and g_{M_h} of M_h. For this, we pullback the metric g_{M_h} to M, *i.e.*, we consider the metric

$$g_h(X,Y) = g_{M_h}(\mathrm{d}\Phi\, X, \mathrm{d}\Phi\, Y) = \langle \mathrm{d}\Phi\, X, \mathrm{d}\Phi\, Y\rangle_{\mathbb{R}^3}\,, \tag{1.21}$$

which is defined almost everywhere on M. Then there exists a uniquely defined (almost everywhere on M) g-symmetric tensor field A, that satisfies

$$g_h(X,Y) = g\,(A\,X, Y) = \langle A\,X, Y\rangle_{\mathbb{R}^3} \qquad a.e. \tag{1.22}$$

for all tangential vector fields X, Y on M. We call this tensor field the *metric distortion tensor* A. The following theorem describes a representation of the tensor in terms of the pointwise distance of the surfaces, the shape operator of M, and the projections P_N and P_{N_h}. This representation will be a basic ingredient for the proofs of bounds on the approximation of metric properties of a smooth surface by those of a polyhedral normal graph.

Theorem 1.13 (distortion tensor) *Consider a polyhedral surface M_h that is a normal graph over a smooth surface M. Then the metric distortion tensor satisfies*

$$A = (Id - \phi S)(P_N \circ P_{N_h})^{-1}(Id - \phi S) \tag{1.23}$$

almost everywhere on M, and there are (possibly different) orthonormal frames in which $Id - \phi S$ and $P_N \circ P_{N_h}$ are represented by the matrices

$$\begin{pmatrix} 1-\phi\kappa_1 & 0 \\ 0 & 1-\phi\kappa_2 \end{pmatrix} \quad \textit{and} \quad \begin{pmatrix} \langle N, N_h\rangle^2_{\mathbb{R}^3} & 0 \\ 0 & 1 \end{pmatrix}, \tag{1.24}$$

respectively.

Proof. Equation (1.20) implies

$$\mathrm{d}\Phi = P_N^{-1}(Id - \phi S) \qquad a.e.,$$

where P_N^{-1} is defined in (1.19). From the explicit representations of the inverse of $P_{N_h}^{-1}$ and P_N^{-1}, see (1.18) and (1.19), we get

$$\begin{aligned}
\left\langle P_N^{-1}X, P_N^{-1}Y\right\rangle_{\mathbb{R}^3} &= \left\langle P_N^{-1}X, Y - \frac{\langle Y, N_h\rangle_{\mathbb{R}^3}}{\langle N, N_h\rangle_{\mathbb{R}^3}} N \right\rangle_{\mathbb{R}^3} \\
&= \left\langle P_N^{-1}X, Y\right\rangle_{\mathbb{R}^3} - \frac{\langle Y, N_h\rangle_{\mathbb{R}^3}}{\langle N, N_h\rangle_{\mathbb{R}^3}} \left\langle P_N^{-1}X, N\right\rangle_{\mathbb{R}^3} \\
&= \left\langle P_N^{-1}X - \frac{\left\langle P_N^{-1}X, N\right\rangle_{\mathbb{R}^3}}{\langle N, N_h\rangle_{\mathbb{R}^3}} N_h, Y \right\rangle_{\mathbb{R}^3} \\
&= \left\langle P_{N_h}^{-1}\left(P_N^{-1}X\right), Y\right\rangle_{\mathbb{R}^3}. \\
&= \left\langle (P_N \circ P_{N_h})^{-1}X, Y\right\rangle_{\mathbb{R}^3}.
\end{aligned}$$

Using the fact that Id and S are self-adjoint yields

$$\begin{aligned}
\langle \mathrm{d}\Phi\, X, \mathrm{d}\Phi\, Y\rangle_{\mathbb{R}^3} &= \left\langle P_N^{-1}(Id - \phi S)\, X, P_N^{-1}(Id - \phi S)\, Y\right\rangle_{\mathbb{R}^3} \\
&= \left\langle (P_N \circ P_{N_h})^{-1}(Id - \phi S)\, X, (Id - \phi S)\, Y\right\rangle_{\mathbb{R}^3} \\
&= \left\langle (Id - \phi S)(P_N \circ P_{N_h})^{-1}(Id - \phi S)\, X, Y\right\rangle_{\mathbb{R}^3} \\
&= \langle A\, X, Y\rangle_{\mathbb{R}^3}.
\end{aligned}$$

The matrix representation of $Id - \phi S$ follows directly from the definition of the principal curvatures. The length of $P_N N_h$ satisfies

$$\begin{aligned}
\|P_N N_h\|_{\mathbb{R}^3}^2 &= \langle N_h - \langle N_h, N\rangle_{\mathbb{R}^3} N, N_h - \langle N_h, N\rangle_{\mathbb{R}^3} N\rangle_{\mathbb{R}^3} \\
&= 1 - \langle N, N_h\rangle_{\mathbb{R}^3}^2.
\end{aligned}$$

Then

$$\begin{aligned}
P_N \circ P_{N_h}(X) &= P_N\left(X - \langle X, N_h\rangle_{\mathbb{R}^3} N_h\right) \\
&= X - \langle X, N_h\rangle_{\mathbb{R}^3} N_h - \langle X - \langle X, N_h\rangle_{\mathbb{R}^3} N_h, N\rangle_{\mathbb{R}^3} N \\
&= X - \langle X, N_h\rangle_{\mathbb{R}^3} N_h - \langle X, N\rangle_{\mathbb{R}^3} N + \langle X, N_h\rangle_{\mathbb{R}^3} \langle N_h, N\rangle_{\mathbb{R}^3} N \\
&= X - \langle X, N_h\rangle_{\mathbb{R}^3} (N_h - \langle N_h, N\rangle_{\mathbb{R}^3} N) \\
&= X - \langle X, N_h - \langle N_h, N\rangle_{\mathbb{R}^3} N\rangle_{\mathbb{R}^3} (N_h - \langle N_h, N\rangle_{\mathbb{R}^3} N) \\
&= X - \langle X, P_N N_h\rangle_{\mathbb{R}^3} P_N N_h \\
&= X - (1 - \langle N, N_h\rangle_{\mathbb{R}^3}^2) \left\langle X, \frac{P_N N_h}{\|P_N N_h\|_{\mathbb{R}^3}} \right\rangle_{\mathbb{R}^3} \frac{P_N N_h}{\|P_N N_h\|_{\mathbb{R}^3}}.
\end{aligned}$$

Hence, the matrix representation of $P_N \circ P_{N_h}$ in the frame $\{\frac{P_N N_h}{\|P_N N_h\|_{\mathbb{R}^3}}, N \times \frac{P_N N_h}{\|P_N N_h\|_{\mathbb{R}^3}}\}$ has the above-stated form. □

The area distortion is measured by a function α that is given almost everywhere on M by

$$\mathrm{d}vol_h = \alpha \, \mathrm{d}vol. \tag{1.25}$$

Corollary 1.14 (area distortion) *The area distortion α satisfies*

$$\alpha = \frac{1 - \phi H + \phi^2 K}{\langle N, N_h \rangle_{\mathbb{R}^3}} \tag{1.26}$$

almost everywhere on M.

Proof. The area distortion equals the determinate of the metric distortion,

$$\alpha = \sqrt{\det A}.$$

Thus, (1.26) follows from

$$\det A = \frac{\det(Id - \phi S)^2}{\det(P_N \circ P_{N_h})},$$

where we use the representation of A derived in Theorem 1.13. □

1.5.6 Isomorphy of function spaces

The pullback of functions (via orthogonal projection onto M) allows us to pullback functions on M_h to M. In this section, we show that this map establishes an isomorphism between the function spaces L^p and $W^{1,p}$ on M and M_h. Let us start with a definition.

Definition 1.15 (isomorpic spaces) *A continuous linear operator $L : V \mapsto W$ between to Banach spaces is an* isomorphism *if it is bijective and the inverse is continuous. If there exits an isomorphism between two Banach spaces, then they are called* isomorphic*.*

Lemma 1.16 (isomorphy of Lebegues spaces) *Let M_h be a normal graph over M, and let Ψ be the restriction to M_h of the orthogonal projection onto M. Then the pullback of functions, $u \mapsto u \circ \Psi$, is an isomorphism of $L^p(M)$ and $L^p(M_h)$ for $1 \leq p < \infty$.*

Proof. Let u be in $L^p(M)$. Since Ψ is continuous, $u \circ \Psi$ is measurable. The L^p-norm of $u \circ \Psi$ can be expressed using the metric distortion tensor

$$\|u \circ \Psi\|_{L^p(M_h)} = \left(\int_M |u|^p \, \alpha \, \mathrm{d}vol \right)^{\frac{1}{p}}. \tag{1.27}$$

Then, using equation (1.27) and Hölder's inequality, we get

$$\begin{aligned}\|u\circ\Psi\|^p_{L^p(M_h)} &= \int_M |u|^p\ \alpha\,\mathrm{d}vol\\ &\le \|\alpha\|_{L^\infty}\int_M |u|^p\ \mathrm{d}vol\\ &= \|\alpha\|_{L^\infty}\,\|u\|^p_{L^p(M)}\,.\end{aligned}$$

Thus the pullback is a well-defined and continuous operator from $L^p(M)$ to $L^p(M_h)$. The inverse of the pullback is the operator that maps v to $v\circ\Phi$. Since Φ is continuous, $v\circ\Phi$ is measurable for any $v\in L^p(M_h)$. Furthermore,

$$\begin{aligned}\|u\circ\Psi\|^p_{L^p(M_h)} &= \int_M |u|^p\ \alpha\,\mathrm{d}vol\\ &\ge \frac{1}{\|\alpha^{-1}\|_{L^\infty}}\int_M |u|^p\ \mathrm{d}vol\\ &= \left\|\alpha^{-1}\right\|^{-1}_{L^\infty}\,\|u\|^p_{L^p(M)}\,.\end{aligned}$$

Thus, the inverse operator is well-defined and continuous. □

We omit a proof of the next lemma and refer to [106] instead.

Lemma 1.17 (isomorphy of Sobolev spaces) *Let M_h be a normal graph over M, and let Ψ be the restriction to M_h of the orthogonal projection onto M. Then the pullback of functions, $u\mapsto u\circ\Psi$, is an isomorphism of $W^{1,p}(M)$ and $W^{1,p}(M_h)$ for $1\le p<\infty$.*

The gradients of a function $u\in W^{1,p}(M)$ with respect to the metrics g and g_h are related by

$$\operatorname{grad}_h u = A^{-1}\operatorname{grad} u.$$

Furthermore, for any point $x\in M$ such that $\Phi(x)$ is in the interior of a triangle of M_h, $\operatorname{grad} u$ at x and $\operatorname{grad}_{M_h}(u\circ\Psi)$ at $\Phi(x)$ satisfy

$$\begin{aligned}\operatorname{grad}_{M_h}(u\circ\Psi)(\Phi(x)) &= \mathrm{d}_x\Phi\operatorname{grad}_h u(x)\\ &= \mathrm{d}_x\Phi A^{-1}\operatorname{grad} u(x)\\ &= P_{N_h(x)}(Id-\phi(x)S(x))^{-1}\operatorname{grad} u(x).\end{aligned}\tag{1.28}$$

Then for any function $u\in W^{1,p}(M)$, the $W^{1,p}$-norm of $u\circ\Psi$ is given by

$$\begin{aligned}\|u\circ\Psi\|^p_{W^{1,p}(M_h)} &= \|u\circ\Psi\|^p_{L^p(M_h)} + \left\|\operatorname{grad}_{M_h}(u\circ\Psi)\right\|^p_{L^p(M_h)}\\ &= \int_M |u|^p\ \alpha\,\mathrm{d}vol + \int_M \left\|P_{N_h}(Id-\phi S)^{-1}\operatorname{grad} u\right\|^p_{\mathbb{R}^3}\ \alpha\,\mathrm{d}vol\\ &= \int_M |u|^p\ \alpha\,\mathrm{d}vol + \int_M \left\langle A^{-1}\operatorname{grad} u,\operatorname{grad} u\right\rangle^{\frac{p}{2}}_{\mathbb{R}^3}\ \alpha\,\mathrm{d}vol.\end{aligned}$$

Lemma 1.18 (equivalence of Sobolev semi-norms) *Let $1 \leq p < \infty$ and $u \in W^{1,p}(M)$. Then*

$$c_W \, |u|^p_{W^{1,p}} \leq |u \circ \Psi|^p_{W^{1,p}(M_h)} \leq C_W \, |u|^p_{W^{1,p}} \,, \tag{1.29}$$

where $c_W = \left\|\alpha^{-1}\right\|^{-1}_{L^\infty} \| A\|^{-\frac{p}{2}}_\infty$ and $C_W = \|\alpha\|_{L^\infty} \left\|A^{-1}\right\|^{\frac{p}{2}}_\infty$.

Proof. The semi-norm of $u \circ \Psi$ is

$$|u \circ \Psi|^p_{W^{1,p}(M_h)} = \left\|\operatorname{grad}_{M_h}(u \circ \Psi)\right\|^p_{L^p(M_h)} . \tag{1.30}$$

Using Hölder's inequality, we get

$$\begin{aligned}
\left\|\operatorname{grad}_{M_h}(u \circ \Psi)\right\|^p_{L^p(M_h)} &= \int_M \left\langle A^{-1} \operatorname{grad} u, \operatorname{grad} u \right\rangle^{\frac{p}{2}}_{\mathbb{R}^3} \, \alpha \, \mathrm{d}vol \\
&\leq \|\alpha\|_{L^\infty} \left\|A^{-1}\right\|^{\frac{p}{2}}_\infty \int_M \langle \operatorname{grad} u, \operatorname{grad} u \rangle^{\frac{p}{2}}_{\mathbb{R}^3} \, dvol \\
&= \|\alpha\|_{L^\infty} \left\|A^{-1}\right\|^{\frac{p}{2}}_\infty \|\operatorname{grad} u\|^p_{L^p}
\end{aligned}$$

and

$$\begin{aligned}
\left\|\operatorname{grad}_{M_h}(u \circ \Psi)\right\|^p_{L^p(M_h)} &= \int_M \left\langle A^{-1} \operatorname{grad} u, \operatorname{grad} u \right\rangle^{\frac{p}{2}}_{\mathbb{R}^3} \, \alpha \, \mathrm{d}vol \\
&\geq \left\|\alpha^{-1}\right\|^{-1}_{L^\infty} \| A\|^{-\frac{p}{2}}_\infty \int_M \langle \operatorname{grad} u, \operatorname{grad} u \rangle^{\frac{p}{2}}_{\mathbb{R}^3} \, \mathrm{d}vol \\
&= \left\|\alpha^{-1}\right\|^{-1}_{L^\infty} \| A\|^{-\frac{p}{2}}_\infty \|\operatorname{grad} u\|^p_{L^p} \,.
\end{aligned}$$

□

Remark 1.19 *Isomorphy of the spaces $\mathcal{X}_{L^p}(M)$ and $\mathcal{X}_{W^{1,p}}(M)$ and their respective counterparts $\mathcal{X}_{L^p}(M_h)$ and $\mathcal{X}_{W^{1,p}}(M_h)$ directly follows from isomorphy of the functions spaces.*

1.6 Approximation of the metric tensor

After having introduced the metric distortion tensor in the last section, we now define quantitative measures for the metric distortion, the area distortion, the distance of the surfaces and their normal vector fields. Then in Section 1.6.3, we derive explicit upper bounds on the metric distortion, the area distortion, and a third term (which, as we will see in Chapter 3, is the norm of the difference of weak Laplace–Beltrami operators of M and M_h). The estimates are a quantitative version of convergence results derived in [64].

1.6.1 Spatial distance of M and M_h

Since M_h is a normal graph over M, the *height* of M_h over M, given by $\sup_{x\in M_h} \delta_M(x)$, is a canonical measure for the spatial distance of M and M_h. This is confirmed by the following lemma, which states that the height agrees with the Hausdorff distance and the Fréchet distance of M and M_h.

Lemma 1.20 (equivalence of distances) *Let M_h be a normal graph over a smooth surface M and let $\delta_H(M, M_h)$ and $\delta_F(M, M_h)$ denote the Hausdorff distance and the Fréchet distance of M and M_h. Then we have*

$$\delta_H(M, M_h) = \delta_F(M, M_h) = \sup_{x\in M_h} \delta_M(x).$$

Proof. Since Ψ is a homeomorphism of M_h and M, we have

$$\delta_F(M, M_h) \leq \sup_{x\in M_h} \delta_M(x).$$

By definition, the Hausdorff distance of M and M_h is the maximum of

$$\sup_{x\in M_h} \delta_M(x) \qquad \text{and} \qquad \sup_{x\in M} \inf_{y\in M_h} \|x - y\|_{\mathbb{R}^3}.$$

Hence, we have

$$\sup_{x\in M_h} \delta_M(x) \leq \delta_H(M, M_h).$$

Furthermore, the Hausdorff distance of two surfaces is smaller than their Fréchet distance,

$$\delta_H(M, M_h) \leq \delta_F(M, M_h).$$

The combination of the three inequalities proves the lemma. □

For our purposes, we prefer to use, instead of the height, the *relative height* of M_h over M

$$\delta(M, M_h) = \sup_{x\in M_h} \left(\delta_M(x)\, \kappa_{\max}(\Psi(x))\right), \tag{1.31}$$

which measures the height relative to the curvature of M. The resulting statements do not lose generality, since for any smooth surface M, the relative height of every normal graph M_h over M is bounded by a constant times its height,

$$\delta(M, M_h) \leq \|\kappa_{\max}\|_{L^\infty} \sup_{x\in M_h} \delta_M(x), \tag{1.32}$$

where $\|\kappa_{\max}\|_{L^\infty} < \infty$ since M is compact. The converse inequality does not hold in general, *e.g.*, the relative height of two parallel planes vanishes whereas the height can be arbitrarily large. The relative height has some more properties: since M_h is in the open reach(M)-tube around M, we have $\delta_M(x) < (\kappa_{\max}(\Psi(x)))^{-1}$ for all $x \in M_h$, which implies $\delta(M, M_h) \in [0, 1)$. Furthermore, $\delta(M, M_h)$ is invariant under scaling of M and M_h.

1.6.2 Distances of vectors and tensors on M

To compare objects on M and M_h, like vector fields or tensor fields, we pullback the object from M_h to M. Our convention is to denote the pullback of the object with a subscript "h" (see Section 1.5.4). Then the distance between the objects can be measured with an appropriate norm on M. We call the distance

$$\|N - N_h\|_{L^\infty}$$

the *normal distance* of M and M_h. For any (sufficiently regular) $(1,1)$-tensor field T on M, we define

$$\|T\|_\infty = \operatorname*{ess\,sup}_{x\in M} \max_{\substack{v\in T_xM \\ \|v\|_g=1}} \|T\,v\|_g\,.$$

Then the norm of $A - Id$ is a measure for the metric distortion between M and M_h

$$\begin{aligned}
\|A - Id\|_\infty &= \operatorname*{ess\,sup}_{x\in M} \max_{\substack{v\in T_xM \\ \|v\|_g=1}} \|(A - Id)\,v\|_g \\
&= \operatorname*{ess\,sup}_{x\in M} \max_{\substack{v,w\in T_xM \\ \|v\|_g=\|w\|_g=1}} |g((A - Id)\,v, w)| \\
&= \operatorname*{ess\,sup}_{x\in M} \max_{\substack{v,w\in T_xM \\ \|v\|_g=\|w\|_g=1}} |g(Av, w) - g(v, w)| \\
&= \operatorname*{ess\,sup}_{x\in M} \max_{\substack{v,w\in T_xM \\ \|v\|_g=\|w\|_g=1}} |g_h(v, w) - g(v, w)|\,.
\end{aligned}$$

Similarly, $\|\alpha - 1\|_{L^\infty}$ measures the area distortion between M and M_h

$$\|\alpha - 1\|_{L^\infty} = \operatorname*{ess\,sup}_{x\in M} \max_{\substack{v,w\in T_xM \\ \|v\|_g=\|w\|_g=1}} |\mathrm{d}vol(v, w) - \mathrm{d}vol_h(v, w)|\,.$$

1.6.3 Bounds on the metric distortion

Now that we have defined measures for the metric and area distortion the spatial and normal distance on the surfaces, we can formulate bounds on the on the metric and area distortions in terms of the relative height of the surfaces.

Definition 1.21 (ϵ-normal graph) *A polyhedral surface M_h is an* ϵ-normal graph *over a smooth surface M if M_h is a normal graph over M and satisfies $\delta(M, M_h) < \epsilon$ and $\|N - N_h\|_{L^\infty} < \sqrt{2}\epsilon$.*

Theorem 1.22 (approximation of metric tensor) *Let M be a smooth surface in $\mathbb{R}^3$. Then for every $\epsilon \in (0, 1)$ there exists a constant C such that for*

every polyhedral surface M_h that is an ϵ-normal graph over M, the estimates

$$\|A - Id\|_\infty \leq C\,(\delta(M, M_h) + \|N - N_h\|^2_{L^\infty}), \tag{1.33}$$

$$\|\alpha - 1\|_{L^\infty} \leq C\,(\delta(M, M_h) + \|N - N_h\|^2_{L^\infty}), \quad \textit{and} \tag{1.34}$$

$$\left\|\alpha\, A^{-1} - Id\right\|_\infty \leq C\,(\delta(M, M_h) + \|N - N_h\|^2_{L^\infty}) \tag{1.35}$$

hold. The constant C depends only on ϵ.

Proof. From Theorem 1.13, we know that A can be constructed from the tensors $(Id - \phi S)$ and $(P_N \circ P_{N_h})^{-1}$. Let us consider these two tensors first. The estimate

$$\|\phi\, S\|_\infty \leq \delta(M, M_h)$$

follows directly from the definition of $\delta(M, M_h)$. At any point of M where N_h is defined, the eigenvalues of $(P_N \circ P_{N_h})^{-1}$ are 1 and $\langle N_h, N\rangle^{-2}_{\mathbb{R}^3}$. By our assumption that $\|N - N_h\|_{L^\infty} < \sqrt{2}\epsilon$, we have

$$\langle N, N_h\rangle_{\mathbb{R}^3} = \left(1 - \frac{1}{2}\,\|N - N_h\|^2_{\mathbb{R}^3}\right) > \left(1 - \epsilon^2\right).$$

Then

$$\begin{aligned}
&\left\|(P_N \circ P_{N_h})^{-1} - Id\right\|_\infty = \left\|1 - \langle N_h, N\rangle^{-2}_{\mathbb{R}^3}\right\|_{L^\infty} \\
&\leq \left\|\langle N_h, N\rangle^{-2}_{\mathbb{R}^3}\right\|_{L^\infty} \left\|1 - \langle N, N_h\rangle^{2}_{\mathbb{R}^3}\right\|_{L^\infty} \\
&\leq \left(1 - \epsilon^2\right)^{-2} \|(\langle N_h, N\rangle_{\mathbb{R}^3} + 1)(\langle N_h, N\rangle_{\mathbb{R}^3} - 1)\|_{L^\infty} \\
&\leq 2\left(1 - \epsilon^2\right)^{-2} \|\langle N_h, N\rangle_{\mathbb{R}^3} - 1\|_{L^\infty} \\
&\leq \left(1 - \epsilon^2\right)^{-2} \|N - N_h\|^2_{L^\infty},
\end{aligned}$$

where we use

$$\|N - N_h\|^2_{\mathbb{R}^3} = 2(1 - \langle N, N_h\rangle_{\mathbb{R}^3})$$

in the last step. Now, we prove the first estimate

$$\begin{aligned}
&\|A - Id\|_\infty = \left\|(Id - \phi S)(P_N \circ P_{N_h})^{-1}(Id - \phi S) - Id\right\|_\infty \\
&= \left\|(Id - \phi S)((P_N \circ P_{N_h})^{-1} - Id)(Id - \phi S) + (Id - \phi S)^2 - Id\right\|_\infty \\
&\leq \|Id - \phi S\|^2_\infty \left\|(P_N \circ P_{N_h})^{-1} - Id\right\|_\infty + \left\|(Id - \phi S)^2 - Id\right\|_\infty \\
&\leq C\,(\delta(M, M_h) + \|N - N_h\|^2_{L^\infty}),
\end{aligned}$$

where C is a constant that depends only on ϵ.

To verify the second estimate, we use the representation (1.26) of α. Our assumptions directly imply

$$\|\phi\, H\|_{L^\infty} < 2\,\delta(M, M_h), \qquad \left\|\phi^2\, K\right\|_{L^\infty} \leq \delta(M, M_h)^2 < \epsilon\,\delta(M, M_h)$$

and we get

$$\begin{aligned}
\|\alpha - 1\|_{L^\infty} &= \left\| \frac{1 - \phi H + \phi^2 K}{\langle N, N_h \rangle_{\mathbb{R}^3}} - 1 \right\|_{L^\infty} \\
&\leq \left\| \langle N, N_h \rangle_{\mathbb{R}^3}^{-1} \right\|_{L^\infty} \left(\|1 - \langle N, N_h \rangle_{\mathbb{R}^3}\|_{L^\infty} + \left\| \phi H + \phi^2 K \right\|_{L^\infty} \right) \qquad (1.36) \\
&\leq \frac{1}{1 - \epsilon^2} \left(\frac{1}{2} \|N - N_h\|_{L^\infty}^2 + (2 + \epsilon) \delta(M, M_h) \right).
\end{aligned}$$

The inverse of A is defined in the interior of the triangles and is given by

$$A^{-1} = (Id - \phi S)^{-1} P_N \circ P_{N_h} (Id - \phi S)^{-1}.$$

By construction of the projections P_N and P_{N_h}, the map $P_N \circ P_{N_h}$ satisfies

$$\|P_N \circ P_{N_h}\|_\infty \leq 1.$$

At any point of M, the map $(Id - \phi(x) S(x))^{-1}$ has the same eigenvectors as the shape operator $S(x)$, and the corresponding eigenvalues are

$$\lambda_i(x) = \frac{1}{1 - \phi(x)\, \kappa_i(x)}.$$

This implies

$$\left\| (Id - \phi S)^{-1} \right\|_\infty \leq \frac{1}{1 - \epsilon}$$

since, by our assumptions, $|\phi(x)\, \kappa_i(x)| < \epsilon$ for all $x \in M$ and $\epsilon < 1$. Using the representation of A^{-1} and the two estimates, we get

$$\begin{aligned}
\left\| A^{-1} \right\|_\infty &\leq \left\| (Id - \phi S)^{-1} \right\|_\infty^2 \|P_N \circ P_{N_h}\|_\infty \\
&\leq \left\| (Id - \phi S)^{-1} \right\|_\infty^2 \leq \left(\frac{1}{1 - \epsilon} \right)^2.
\end{aligned}$$

Now, we can verify the third estimate

$$\begin{aligned}
&\left\| \alpha\, A^{-1} - Id \right\|_\infty \leq \|\alpha\|_{L^\infty} \left\| A^{-1} - Id \right\|_\infty + \|\alpha - 1\|_{L^\infty} \\
&\leq \|\alpha\|_{L^\infty} \left\| A^{-1} \right\|_\infty \|A - Id\|_\infty + \|\alpha - 1\|_{L^\infty} \\
&\leq C \left(\delta(M, M_h) + \|N - N_h\|_{L^\infty}^2 \right).
\end{aligned}$$

In the last step, we use the estimates established above. This completes the proof. □

1.7 Inscribed polyhedral surfaces

In this section, we specialize the approximation estimates to polyhedral surfaces whose vertices lie on the smooth surface M, the so-called inscribed polyhedral surfaces. The resulting bound depends on the mesh size of M_h instead of the relative height and the normal distance of the surfaces.

Definition 1.23 (inscribed surfaces) *We call a polyhedral surface M_h* inscribed *to a smooth surface M if M_h is a normal graph over M and all vertices of M_h are on the surface M.*

For a triangle T_h of a polyhedral surface M_h, let $r_{circ}(T_h)$ and $r_{in}(T_h)$ denote the circumradius and the inner radius of T_h. We define the *mesh size* h and the *shape regularity* ρ of M_h as

$$h = \max_{T_h \in M_h} r_{circ}(T_h) \qquad \text{and} \qquad \rho = \max_{T_h \in M_h} \frac{r_{circ}(T_h)}{r_{in}(T_h)}.$$

For inscribed polyhedral surfaces, the relative height, $\delta(M, M_h)$, and the approximation of the normals, $\|N - N_h\|_{L^\infty}$, can be bounded above in terms of the mesh size h, the shape regularity ρ, and properties of M, compare [85, 4, 81, 80]. We summarize this in the following lemma.

Lemma 1.24 (approximation of normals) *Let M be a smooth surface in $\mathbb{R}^3$. Then there exists an $h_0 \in \mathbb{R}^+$ such that, for every polyhedral surface M_h that is inscribed to M and satisfies $h < h_0$, the inequalities*

$$\delta(M, M_h) \leq C\, h^2 \tag{1.37}$$

and

$$\|N - N_h\|_{L^\infty} \leq C\, h \tag{1.38}$$

hold, where the constant C depends only on M, h_0, and ρ.

For inscribed polyhedral surfaces, we can formulate the bounds on the metric distortion in terms of the mesh size h instead of $\delta(M, M_h)$ and $\|N - N_h\|_{L^\infty}$.

Lemma 1.25 (approximation of metric tensor) *Let M be a smooth surface in $\mathbb{R}^3$. Then there exists a $h_0 \in \mathbb{R}^+$ such that for every polyhedral surface M_h that is inscribed to M and has mesh size $h < h_0$, the estimates*

$$\|\, A - Id\|_\infty \leq C\, h^2, \tag{1.39}$$

$$\|\alpha - 1\|_{L^\infty} \leq C\, h^2, \quad \textit{and} \tag{1.40}$$

$$\left\|\alpha\, A^{-1} - Id\right\|_\infty \leq C\, h^2 \tag{1.41}$$

hold, where the constant C depends only on M, h_0, and ρ.

The lemma directly follows from combining Theorem 1.22 and Lemma 1.24.

2
Generalized shape operators

2.1 Definition of the generalized shape operators

In classical differential geometry, the curvature of a surface in $\mathbb{R}^3$ is described by the shape operator. While the metric tensor is characterized by first derivatives of the embedding of the surface, the shape operator requires second derivatives. Since polyhedral surfaces in $\mathbb{R}^3$ are only Lipschitz submanifolds, the classical shape operator is not defined for them. In this section, we introduce two generalized shape operators that can be defined on polyhedral surfaces. They describe the curvatures of a surface in the sense of distributions. Hence, we can not evaluate the generalized shape operators at a single point, but we can test them with certain functions. However, as we will see in Section 2.4, the generalized shape operator on a polyhedral surface can be used to approximate the classical shape operator of a nearby smooth surface.

Definition 2.1 (generalized shape operators) *We define the generalized shape operators $\bar{\Sigma}$ and $\hat{\Sigma}$ on a smooth or polyhedral surface $\mathcal{M}$ to be the linear operators*

$$\bar{\Sigma} : \mathcal{X}_{W^{1,1}}(\mathcal{M}) \mapsto \mathbb{R}^3 \qquad X \mapsto \int_{\mathcal{M}} N \, div X \, dvol$$

and

$$\hat{\Sigma} : \mathcal{X}_{W^{1,1}}(\mathcal{M}) \mapsto \mathbb{R}^3 \qquad X \mapsto -\int_{\mathcal{M}} N \, curl X \, dvol.$$

The next lemma shows that $\bar{\Sigma}$ and $\hat{\Sigma}$ are elements of the normed space $L(\mathcal{X}_{W^{1,1}}(\mathcal{M}), \mathbb{R}^3)$ of continuous linear maps from $\mathcal{X}_{W^{1,1}}(\mathcal{M})$ to $\mathbb{R}^3$.

Lemma 2.2 *The operators $\bar{\Sigma}$ and $\hat{\Sigma}$ are continuous.*

Proof. Consider a vector field $X \in \mathcal{X}_{W^{1,1}}$. Using Hölder's inequality we have

$$\left\|\bar{\Sigma}(X)\right\|_{\mathbb{R}^3} = \left\| \int_{\mathcal{M}} N \operatorname{div} X \, \mathrm{d}vol \right\|_{\mathbb{R}^3} \leq \|N\|_{L^\infty} \|\operatorname{div} X\|_{L^1} \leq \|X\|_{W^{1,1}}$$

and

$$\left\|\hat{\Sigma}(X)\right\|_{\mathbb{R}^3} = \left\| \int_{\mathcal{M}} N \operatorname{curl} X \, \mathrm{d}vol \right\|_{\mathbb{R}^3} \leq \|N\|_{L^\infty} \|\operatorname{curl} X\|_{L^1} \leq \|X\|_{W^{1,1}}$$

which proves the lemma. □

To motivate the definition, we consider a smooth surface M and discuss the connection of the generalized shape operators to the classical shape operator. For this we consider the two $(1,1)$-tensor fields $\bar{S}, \hat{S} : \mathcal{X}(M) \mapsto \mathcal{X}(M)$ given by

$$\bar{S} : X \mapsto S(X^\top) - HN \langle X, N \rangle \tag{2.1}$$

and

$$\hat{S} : X \mapsto S(N \times X). \tag{2.2}$$

The tensor $\bar{S}$ agrees with the shape operator S for tangential vector fields, and it multiplies the normal part of a vector field by the negative of the mean curvature. Applying the tensor field $\hat{S}$ to a vector field equals first removing the normal part, then rotating the remaining tangential vectors by $\frac{\pi}{2}$ in the corresponding tangent planes and applying the shape operator S to the result. At a point $x \in M$, let b_1 and b_2 be unit vectors that point into the principal curvature directions in $T_x M$. Then in the basis $\{b_1, b_2, N\}$ of $\mathbb{R}^3$, the matrix representations of $\bar{S}(x)$ and $\hat{S}(x)$ are

$$\begin{pmatrix} \kappa_1(x) & 0 & 0 \\ 0 & \kappa_2(x) & 0 \\ 0 & 0 & -H(x) \end{pmatrix} \quad \text{and} \quad \begin{pmatrix} 0 & -\kappa_2(x) & 0 \\ \kappa_1(x) & 0 & 0 \\ 0 & 0 & 0 \end{pmatrix}.$$

The tensors have the property that if at a point $x \in M$, the surface normal $N(x)$ and either of $\bar{S}(x)$ or $\hat{S}(x)$ is known, one can construct the shape operator $S(x)$ by simple algebraic operations. This property will be important when we discuss the pointwise approximation of the shape operator.

The following lemma reveals a connection of the tensors $\bar{S}, \hat{S}$ and the operators $\bar{\Sigma}, \hat{\Sigma}$.

Lemma 2.3 *The tensor field $\bar{S}$ is the only continuous $(1,1)$-tensor field in $T^M\mathbb{R}^3$ that satisfies*

$$\int_M \bar{S}\, X \, dvol = \bar{\Sigma}(X) \tag{2.3}$$

for all $X \in \mathcal{X}(M)$ and $\hat{S}$ is the only continuous $(1,1)$-tensor field in $T^M\mathbb{R}^3$ that satisfies

$$\int_M \hat{S}\, X \, dvol = \hat{\Sigma}(X) \tag{2.4}$$

for all $X \in \mathcal{X}(M)$.

Proof. To show that the tensor field $\bar{S}$ fulfills equation (2.3), we apply the divergence theorem and use equation (1.6)

$$\begin{aligned}\int_M S\, X^\top \, \mathrm{d}vol &= -\int_M \mathrm{D}_{X^\top} N \, \mathrm{d}vol = \int_M N \operatorname{div} X^\top \, \mathrm{d}vol \\ &= \int_M N \operatorname{div} X \, \mathrm{d}vol + \int_M \langle HN, X\rangle_{\mathbb{R}^3}\, N \, \mathrm{d}vol.\end{aligned}$$

To show that the tensor field $\hat{S}$ fulfills equation (2.4), we apply the divergence theorem and use equation (1.7)

$$\begin{aligned}\int_M \hat{S}\, X \, \mathrm{d}vol &= \int_M S\,(N \times X)\, \mathrm{d}vol = \int_M N \operatorname{div}(N \times X)\, \mathrm{d}vol \\ &= -\int_M N \operatorname{curl} X \, \mathrm{d}vol.\end{aligned}$$

To prove the uniqueness of the solution, let us assume that the tensor fields $\bar{S}$ and T are solutions of (2.3) for all $X \in \mathcal{X}(M)$. It follows that

$$\int_M (\bar{S} - T)\, X \, \mathrm{d}vol = 0$$

holds for all $X \in \mathcal{X}(M)$, which, by the fundamental lemma of calculus of variations, implies that $\bar{S}$ equals T. An analogous argument will show the uniqueness of $\hat{S}$. □

2.2 Approximation of the generalized shape operators

In this section, we derive error estimates for the approximation of the generalized shape operators of a smooth surface M by the generalized shape operators of a polyhedral surface M_h that is a normal graph over M. To compare the generalized shape operators of M_h and M, we pullback the operators $\bar{\Sigma}_{M_h}$ and $\hat{\Sigma}_{M_h}$ from M_h to M. More explicitly, we consider the operators $\bar{\Sigma}_h$ and $\hat{\Sigma}_h$ given by

$$\begin{aligned}\bar{\Sigma}_h &: \mathcal{X}_{W^{1,1}}(M) \mapsto \mathbb{R}^3 \\ \bar{\Sigma}_h(X) &= \bar{\Sigma}_{M_h}(X \circ \Psi)\end{aligned}$$

and

$$\hat{\Sigma}_h : \mathcal{X}_{W^{1,1}}(M) \mapsto \mathbb{R}^3$$
$$\hat{\Sigma}_h(X) = \hat{\Sigma}_{M_h}(X \circ \Psi).$$

Since the pullback of vector fields induces an isomorphism of $\mathcal{X}_{W^{1,1}}(M_h)$ and $\mathcal{X}_{W^{1,1}}(M)$, $\bar{\Sigma}_h$ and $\hat{\Sigma}_h$ are continuous operators and therefore elements of $L(\mathcal{X}_{W^{1,1}}(M), \mathbb{R}^3)$. We use the operator norm $\| \ \|_{Op}$ to measure the distance between corresponding operators.

Theorem 2.4 (approximation of generalized shape operators) *Let M be a smooth surface in $\mathbb{R}^3$. Then for every $\epsilon \in (0,1)$, there exists a constant C such that for every polyhedral surface M_h that is an ϵ-normal graph over M, the estimates*

$$\left\|\bar{\Sigma} - \bar{\Sigma}_h\right\|_{Op} \leq C\left(\delta(M, M_h) + \|N - N_h\|_{L^\infty}\right) \tag{2.5}$$

and

$$\left\|\hat{\Sigma} - \hat{\Sigma}_h\right\|_{Op} \leq C\left(\delta(M, M_h) + \|N - N_h\|_{L^\infty}\right) \tag{2.6}$$

hold. The constant C depends only on ϵ.

Before we prove the theorem, we establish the following estimates for the divergence and curl. The pullbacks of the divergence and curl of M_h to M are the operators

$$\mathrm{div}_h : \mathcal{X}_{W^{1,1}}(M) \mapsto L^1(M) \quad \text{and} \quad \mathrm{curl}_h : \mathcal{X}_{W^{1,1}}(M) \mapsto L^1(M)$$

given by

$$\mathrm{div}_h(X)(x) = \mathrm{div}_{M_h}(X \circ \Psi)(\Phi(x)) \quad \text{and} \quad \mathrm{curl}_h(X)(x) = \mathrm{curl}_{M_h}(X \circ \Psi)(\Phi(x))$$

for almost all $x \in M$.

Lemma 2.5 (approximation of div and curl) *Let M be a smooth surface in $\mathbb{R}^3$ and $\epsilon \in (0,1)$. Then for every polyhedral surface M_h that is an ϵ-normal graph over M, the estimates*

$$\|div - div_h\|_{Op} \leq \left(\|N_h - N\|_{L^\infty} + \frac{1}{1-\epsilon}\,\delta(M, M_h)\right)$$

and

$$\|curl - curl_h\|_{Op} \leq \left(\|N_h - N\|_{L^\infty} + \frac{1}{1-\epsilon}\,\delta(M, M_h)\right)$$

hold. Here $\| \ \|_{Op}$ is the operator norm on $L(\mathcal{X}_{W^{1,1}}(M), L^1(M))$.

Proof. Let $X \in \mathcal{X}_{W^{1,1}}(M)$ be a vector field with $\|X\|_{W^{1,1}} = 1$, and let X_i be the components of X with respect to the standard basis $\{e_1, e_2, e_3\}$ of $\mathbb{R}^3$. From the definition of the divergence, see (1.4), and (1.28) we obtain

$$\operatorname{div}_h X = \sum_{i=1}^{3} \left\langle P_{N_h} (Id - \phi\, S)^{-1} \operatorname{grad} X_i, e_i \right\rangle_{\mathbb{R}^3}.$$

We can represent $(Id - \phi\, S)^{-1}$ as

$$(Id - \phi\, S)^{-1} = Id + R, \tag{2.7}$$

where the map R is given by

$$R = \phi\, S\, (Id - \phi\, S)^{-1}. \tag{2.8}$$

This can be easily verified using the eigenbasis of S. Then

$$\begin{aligned}
\operatorname{div}_h X &= \sum_{i=1}^{3} \langle P_{N_h} (Id + R) \operatorname{grad} X_i, e_i \rangle_{\mathbb{R}^3} \\
&= \operatorname{div} X - \sum_{i=1}^{3} \langle \operatorname{grad} X_i, N_h \rangle_{\mathbb{R}^3} \langle N_h, e_i \rangle_{\mathbb{R}^3} + \sum_{i=1}^{3} \langle P_{N_h} R \operatorname{grad} X_i, e_i \rangle_{\mathbb{R}^3}.
\end{aligned}$$

This yields an upper bound on the L^1-norm of the difference of the divergence operators

$$\begin{aligned}
\|\operatorname{div} X - \operatorname{div}_h X\|_{L^1} &\leq \left\| \sum_{i=1}^{3} \langle \operatorname{grad} X_i, N_h \rangle_{\mathbb{R}^3} \langle N_h, e_i \rangle_{\mathbb{R}^3} \right\|_{L^1} \\
&+ \left\| \sum_{i=1}^{3} \langle P_{N_h} R \operatorname{grad} X_i, e_i \rangle_{\mathbb{R}^3} \right\|_{L^1} \\
&\leq \left\| N_h^{\top} \right\|_{L^\infty} + \|R\|_{\infty} \leq \|N_h - N\|_{L^\infty} + \|R\|_{\infty},
\end{aligned} \tag{2.9}$$

where we use

$$\begin{aligned}
\left\| N_h^{\top} \right\|_{\mathbb{R}^3}^2 &= \|N_h - \langle N_h, N \rangle_{\mathbb{R}^3} N\|_{\mathbb{R}^3}^2 = 1 + \langle N_h, N \rangle_{\mathbb{R}^3}^2 - 2 \langle N_h, N \rangle_{\mathbb{R}^3}^2 \\
&= 1 - \langle N_h, N \rangle_{\mathbb{R}^3}^2 = (1 + \langle N_h, N \rangle_{\mathbb{R}^3}) (1 - \langle N_h, N \rangle_{\mathbb{R}^3}) \\
&\leq 2 (1 - \langle N_h, N \rangle_{\mathbb{R}^3}) = \|N_h - N\|_{\mathbb{R}^3}^2
\end{aligned}$$

Now, let us consider the curl

$$\begin{aligned}
\operatorname{curl}_h X &= \sum_{i=1}^{3} \langle P_{N_h}(Id+R)\operatorname{grad} X_i \times e_i, N_h\rangle_{\mathbb{R}^3} \\
&= \sum_{i=1}^{3} \langle (\operatorname{grad} X_i - \langle \operatorname{grad} X_i, N_h\rangle_{\mathbb{R}^3} N_h + P_{N_h} R \operatorname{grad} X_i) \times e_i, N_h\rangle_{\mathbb{R}^3} \\
&= \operatorname{curl} X + \sum_{i=1}^{3} \langle \operatorname{grad} X_i \times e_i, N_h - N\rangle_{\mathbb{R}^3} + \sum_{i=1}^{3} \langle P_{N_h} R \operatorname{grad} X_i \times e_i, N_h\rangle_{\mathbb{R}^3},
\end{aligned}$$

where we use

$$\langle \langle \operatorname{grad} X_i, N_h\rangle N_h \times e_i, N_h\rangle_{\mathbb{R}^3} = 0$$

in the last step. Then we get the same upper bound on the L^1-norm of the difference of the curl operators as on the L^1-norm of the difference of the divergence operators:

$$\begin{aligned}
&\|\operatorname{curl} X - \operatorname{curl}_h X\|_{L^1} \qquad (2.10)\\
&\leq \left\| \sum_{i=1}^{3} \langle \operatorname{grad} X_i \times e_i, N_h - N\rangle_{\mathbb{R}^3} \right\|_{L^1} + \left\| \sum_{i=1}^{3} \langle P_{N_h} R \operatorname{grad} X_i \times e_i, N_h\rangle_{\mathbb{R}^3} \right\|_{L^1} \\
&\leq \|N_h - N\|_{L^\infty} + \|R\|_\infty .
\end{aligned}$$

It remains to establish a bound on the term $\|R\|_\infty$. At any point $x \in M$, $R(x)$ has the same eigenvectors as the shape operator $S(x)$, and the eigenvalues $\lambda_i(x)$ of $R(x)$ are given by

$$\lambda_i(x) = \frac{\phi(x)\,\kappa_i(x)}{1-\phi(x)\,\kappa_i(x)}. \qquad (2.11)$$

By the definition of $\delta(M, M_h)$

$$\phi(x)\,\kappa_i(x) \leq \delta(M, M_h)$$

for all $x \in M$, and since M_h is an ϵ-normal graph over M,

$$|1-\phi(x)\,\kappa_i(x)| \geq 1-\epsilon$$

for all $x \in M$. This implies

$$\|R\|_\infty \leq \frac{1}{1-\epsilon}\,\delta(M, M_h). \qquad (2.12)$$

Combining this with (2.9) and (2.10) yields

$$\|\operatorname{div} - \operatorname{div}_h\|_{Op} \leq \left(\|N_h - N\|_{L^\infty} + \frac{1}{1-\epsilon}\,\delta(M, M_h) \right)$$

and

$$\|\mathrm{curl} - \mathrm{curl}_h\|_{Op} \leq \left(\|N_h - N\|_{L^\infty} + \frac{1}{1-\epsilon}\, \delta(M, M_h) \right).$$

This concludes the proof of the lemma. □

Now, we prove the theorem.

Proof of Theorem 2.4. Let $X \in \mathcal{X}_{W^{1,1}}$ be a vector field with $\|X\|_{W^{1,1}} = 1$. Using Hölder's inequality, we have

$$\begin{aligned} \left\|\bar{\Sigma}X - \bar{\Sigma}_h X\right\|_{\mathbb{R}^3} &= \left\| \int_M (N \,\mathrm{div}\, X - N_h \,\mathrm{div}_h X\ \alpha) \mathrm{d}vol \right\|_{\mathbb{R}^3} \qquad (2.13) \\ &\leq \|(N\ - \alpha N_h)\mathrm{div}\, X\,\|_{L^1} + \|\alpha N_h(\mathrm{div}\, X - \ \mathrm{div}_h X)\,\|_{L^1} \\ &\leq \|N\ - \alpha N_h\|_{L^\infty}\, \|\mathrm{div}\, X\,\|_{L^1} + \|\alpha\|_{L^\infty}\, \|\mathrm{div} - \ \mathrm{div}_h\|_{Op} \\ &\leq \|1 - \alpha\|_{L^\infty} + \|N\ - N_h\|_{L^\infty} + \|\alpha\|_{L^\infty}\, \|\mathrm{div} - \ \mathrm{div}_h\|_{Op}\,. \end{aligned}$$

Then Theorem 1.22 and Lemma 2.5 imply that there is a constant C, which depends only on ϵ, such that

$$\left\|\bar{\Sigma} - \bar{\Sigma}_h\right\|_{Op} \leq C(\delta(M, M_h) + \|N\ - N_h\|_{L^\infty}).$$

A similar argumentation proves the second estimate. □

2.3 r-local functions

The tool we use to obtain pointwise approximation estimates from the estimates in the operator norm are functions whose support becomes more and more localized while their L^1-norm remains constant and the growth of the $W^{1,1}$-norm is bounded.

Definition 2.6 (r-local functions) *Let $\mathcal{M}$ be a smooth or polyhedral surface in $\mathbb{R}^3$, and let C_D be a positive constant. For any $x \in \mathcal{M}$ and $r \in \mathbb{R}^+$, we call a function $\varphi : \mathcal{M} \mapsto \mathbb{R}$* r-local *at x (with respect to C_D) if the criteria*

- *(D1)* $\varphi \in W^{1,1}(\mathcal{M})$,
- *(D2)* $\varphi(y) \geq 0$ *for all* $y \in \mathcal{M}$,
- *(D3)* $\varphi(y) = 0$ *for all* $y \in \mathcal{M}$ *with* $d_{\mathcal{M}}(x, y) \geq r$,
- *(D4)* $\|\varphi\|_{L^1} = 1$, *and*
- *(D5)* $|\varphi|_{W^{1,1}(\mathcal{M})} \leq \frac{C_D}{r}$

are satisfied.

A function that is r-local at $x \in M$ can be used to approximate the function value at x of a function f through the integral $\int_M f\,\varphi\,\mathrm{d}vol$. This means that r-local functions are approximations of the delta distribution.

Lemma 2.7 *Let $\varphi \in L^1(M)$ satisfy properties (D2), (D3), and (D4) of Definition 2.6 for some $x \in M$ and $r \in \mathbb{R}^+$, and let $f \in C^1(M)$. Then the estimate*

$$\left| f(x) - \int_M f\,\varphi\, dvol \right| \leq \|grad\, f\|_{L^\infty}\; r \tag{2.14}$$

holds.

Proof. Since φ is non-negative and has a unit L^1-norm, we have

$$\begin{aligned} \left| f(x) - \int_M f\,\varphi\, \mathrm{d}vol \right| &= \left| \int_M (f(x) - f)\,\varphi\, \mathrm{d}vol \right| \\ &\leq \sup_{y \in B_r(x)} |f(x) - f(y)|\,. \end{aligned}$$

For any y in the geodesic ball $B_r(x)$ around x, let γ be a (unit-speed parametrized) minimizing geodesic that connects x and y. Then

$$\begin{aligned} |f(x) - f(y)| &= \left| \int_\gamma g(\mathrm{grad}\, f(\gamma(t)), \dot\gamma(t)) \mathrm{d}t \right| \\ &\leq \|\mathrm{grad}\, f\|_{L^\infty}\; \mathrm{length}(\gamma) \leq \|\mathrm{grad}\, f\|_{L^\infty}\; r. \end{aligned}$$

This implies $\sup_{y \in B_r(x)} |f(x) - f(y)| \leq \|\mathrm{grad}\, f\|_{L^\infty}\, r$, which concludes the proof. □

Certain functions φ even exhibit a higher approximation order.

Definition 2.8 (r^2-property) *Let M be a smooth surface, and let C_Q be a positive constant. For any $x \in M$ and $r \in \mathbb{R}^+$, we say that a function φ has the r^2-property at x (with respect to C_Q) if for every $f \in C^2(M)$ the estimate*

$$\left| f(x) - \int_M f\,\varphi\, dvol \right| \leq C_Q\;\; \|f\|_{C^2}\; r^2 \tag{2.15}$$

holds.

We will discuss the construction of r-local functions and functions with the r^2-property in Section 2.6.

2.4 Pointwise approximation of the shape operator

In this section, we derive estimates for the pointwise approximation of the shape operator of a smooth surface M in $\mathbb{R}^3$. They follow from an estimate on the pointwise approximation of the tensor field $\bar{S}$. For brevity, we restrict our considerations to the tensor field $\bar{S}$ and leave the tensor field $\hat{S}$ aside. Still, an analogous statement to Lemma 2.9 holds for the approximation of the tensor field $\hat{S}$ as well.

2.4.1 Pointwise approximation of $\bar{S}$

Let ψ be r-local at the point $y \in M_h$. Then, we define $\bar{S}^{\psi}_{M_h}$ to be the tensor on $\mathbb{R}^3$ that has the components

$$(\bar{S}^{\psi}_{M_h})_{ij} = \left\langle e_i, \bar{\Sigma}_{M_h}(\psi\, e_j)\right\rangle_{\mathbb{R}^3}. \tag{2.16}$$

We will show that $\bar{S}^{\psi}_{M_h}$ approximates $\bar{S}(\Psi(y))$. To measure the distance between $\bar{S}^{\psi}_{M_h}$ and $\bar{S}(\Psi(y))$, we use the operator norm

$$\|T\|_{\max} = \max_{v\in\mathbb{R}^3, \|v\|_{\mathbb{R}^3}=1} \|Tv\|_{\mathbb{R}^3}$$

on the space of linear maps $T : \mathbb{R}^3 \mapsto \mathbb{R}^3$. Here, we use the subscript max instead of *op* to distinguish this norm from the operator norm on the space $L(\mathcal{X}_{W^{1,1}}(M), \mathbb{R}^3)$ used in the previous sections.

Lemma 2.9 (approximation of $\bar{S}$) *Let M be a smooth surface in $\mathbb{R}^3$ and $\epsilon \in (0,1)$. For every pair consisting of a polyhedral surface M_h that is an ϵ-normal graph over M and a function ψ that is r-local at a point $y \in M_h$, the corresponding tensor $\bar{S}^{\psi}_{M_h}$ satisfies the estimate*

$$\left\|\bar{S}(x) - \bar{S}^{\psi}_{M_h}\right\|_{\max} \leq C(r + \frac{\delta(M,M_h) + \|N - N_h\|_{L^\infty}}{r}), \tag{2.17}$$

where $x = \Psi(y)$ is the orthogonal projection of y onto M. If $\psi \circ \Phi$ has the r^2-property, the bound improves to

$$\left\|\bar{S}(x) - \bar{S}^{\psi}_{M_h}\right\|_{\max} \leq C(r^2 + \frac{\delta(M,M_h) + \|N - N_h\|_{L^\infty}}{r}). \tag{2.18}$$

The constants C depend only on M, ϵ, and C_D (see Definition 2.6) and in the second estimate additionally on C_Q (see Definition 2.8).

Proof. Let $\varphi = \psi \circ \Phi$ be the pullback to M of ψ, and let $i, j \in \{1,2,3\}$. Then

$$\left(\bar{S}^{\psi}_{M_h}\right)_{ij} = \left\langle e_i, \bar{\Sigma}_h(\varphi\, e_j)\right\rangle_{\mathbb{R}^3}, \tag{2.19}$$

where $\bar{\Sigma}_h$ is the pullback to M of $\bar{\Sigma}_{M_h}$. Using (2.3) and (2.19), we get

$$\left|(\bar{S}(x) - \bar{S}^{\psi}_{M_h})_{ij}\right| = \left|(\bar{S}(x))_{ij} - \left\langle e_i, \bar{\Sigma}_h(\varphi\, e_j)\right\rangle_{\mathbb{R}^3}\right| \tag{2.20}$$

$$\leq \left|(\bar{S}(x))_{ij} - \int_M \varphi\,(\bar{S})_{ij}\,\mathrm{d}vol\right| + \left|\left\langle e_i, (\bar{\Sigma} - \bar{\Sigma}_h)(\varphi\, e_j)\right\rangle_{\mathbb{R}^3}\right|. \tag{2.21}$$

In the following, we derive bounds for both summands in (2.21). We start with the second. The equivalence of the Sobolev norms implies

$$\|\varphi\|_{W^{1,1}} \leq C\,\|\psi\|_{W^{1,1}(M_h)}.$$

From the explicit representation of C in terms of the metric and area distortion (Lemmas 1.16 and 1.18), it follows that C depends only on ϵ. Using this, we get

$$\begin{aligned}&\left|\left\langle e_i, (\bar{\Sigma} - \bar{\Sigma}_h)(\varphi\, e_j)\right\rangle_{\mathbb{R}^3}\right| \leq \|\varphi\|_{W^{1,1}} \left\|\bar{\Sigma} - \bar{\Sigma}_h\right\|_{Op} \\ &\leq C\, \|\psi\|_{W^{1,1}(M_h)} \left\|\bar{\Sigma} - \bar{\Sigma}_h\right\|_{Op} \leq C\frac{C_D}{r} \left\|\bar{\Sigma} - \bar{\Sigma}_h\right\|_{Op}.\end{aligned}$$

Furthermore, in Theorem 2.4 we established the bound

$$\left\|\bar{\Sigma} - \bar{\Sigma}_h\right\|_{Op} \leq C\,(\delta(M, M_h) + \|N - N_h\|_{L^\infty}).$$

To derive a bound on the first summand in (2.21), we set

$$\bar{\varphi} = \frac{\varphi}{\|\varphi\|_{L^1}}$$

and split the summand in two parts

$$\left|(\bar{S}(x))_{ij} - \int_M \varphi\,(\bar{S})_{ij}\,\mathrm{d}vol\right| \tag{2.22}$$

$$\leq \left|(\bar{S}(x))_{ij} - \int_M \bar{\varphi}\,(\bar{S})_{ij}\,\mathrm{d}vol\right| + \left|\left\langle e_i, \bar{\Sigma}((\bar{\varphi} - \varphi)\ e_j)\right\rangle_{\mathbb{R}^3}\right|. \tag{2.23}$$

We start with the first part. The function $\bar{\varphi}$ clearly satisfies *(D2)* and *(D4)* of Definition 2.6. Since the support of ψ is contained in the geodesic ball $B_r(y)$, the support of $\bar{\varphi}$ is contained in geodesic ball or radius $\|A\|_\infty^{1/2}$, where A denotes the metric distortion tensor. As a consequence of Theorem 1.22, $\|A\|_\infty^{1/2}$ can be bounded by a constant C_A that depends only ϵ. Hence, $\bar{\varphi}$ satisfies property *(D3)* for the point x and the value $C_A r$. Then Lemma 2.7 implies that there is a constant C depending on M and ϵ such that

$$\left|(\bar{S}(x))_{ij} - \int_M \bar{\varphi}\,(\bar{S})_{ij}\,\mathrm{d}vol\right| \leq C\,r.$$

The second part of (2.23) satisfies

$$\left|\left\langle e_i, \bar{\Sigma}((\bar{\varphi} - \varphi)\ e_j)\right\rangle_{\mathbb{R}^3}\right| = \left|\int_M (\bar{\varphi} - \varphi)\,(\bar{S})_{ij}\,\mathrm{d}vol\right| \tag{2.24}$$

$$= \left|(1 - \|\varphi\|_{L^1}) \int_M \bar{\varphi}\,(\bar{S})_{ij}\,\mathrm{d}vol\right| \leq |\|\varphi\|_{L^1} - 1|\, \left\|(\bar{S})_{ij}\right\|_{L^\infty}.$$

Using Theorem 1.22, we see that there is a constant C depending only on ϵ such that

$$\begin{aligned}|\|\varphi\|_{L^1} - 1| = \left|\int_M (1 - \alpha)\,\varphi\,\mathrm{d}vol\right| &\leq \|\alpha - 1\|_{L^\infty} \left\|\alpha^{-1}\right\|_{L^\infty} \\ &\leq C\,(\delta(M, M_h) + \|N - N_h\|_{L^\infty}^2).\end{aligned}$$

If φ satisfies the r^2-property (with respect to C_Q), then the bound on the term (2.22) improves: there is a constant C depending on M and C_Q such that

$$\left|(\bar{S}(x))_{ij} - \int_M \varphi\,(\bar{S})_{ij}\,\mathrm{d}vol\right| \leq C\,r^2.$$

By collecting the bounds derived above, we prove the estimates (2.17) and (2.18). The term $\delta(M, M_h) + \|N - N_h\|^2_{L^\infty}$, which is part of the bound on (2.24), does not appear in estimate (2.17) because

$$\delta(M, M_h) + \|N - N_h\|^2_{L^\infty} < C\left(r + \frac{\delta(M, M_h) + \|N - N_h\|_{L^\infty}}{r}\right).$$

Either, $r > 1$, which implies $\delta(M, M_h) + \|N - N_h\|^2_{L^\infty} < 3\,r$ by our assumptions, or $r \leq 1$ and hence $\delta(M, M_h) + \|N - N_h\|^2_{L^\infty} \leq (\delta(M, M_h) + \sqrt{2}\epsilon\,\|N - N_h\|_{L^\infty})/r$. □

2.4.2 Pointwise approximation of the shape operator

From the tensor $\bar{S}^\psi_{M_h}$, which approximates $\bar{S}(x)$, we can construct an approximation of $S(x)$. The principle of the construction is to remove the normal part of $\bar{S}^\psi_{M_h}$. In the case of a smooth surface, the definition of $\bar{S}(x)$ directly implies

$$S(x) = (Id - N(x)N(x)^T)\bar{S}(x)(Id - N(x)N(x)^T), \tag{2.25}$$

where $N(x)^T$ denotes the transpose of $N(x)$. This motivates the definition of the tensor

$$S^\psi_{M_h} = (Id - N_{M_h}(y)N_{M_h}(y)^T)\bar{S}^\psi_{M_h}(Id - N_{M_h}(y)N_{M_h}(y)^T). \tag{2.26}$$

Since the piecewise constant normal of the polyhedral surface is discontinuous at the edges and vertices, $N_{M_h}(y)$ is not well-defined if y lies on an edge or a vertex of M_h. To get a well-defined tensor $S^\psi_{M_h}$, we specify what $N_{M_h}(y)$ means in this case: we set $N_{M_h}(y)$ to be the normalized sum of the normals of all triangles that are adjacent to the edge or vertex on which y lies. An alternative would be to assign a triangle to each vertex and each edge and to use the normal of that triangle. For our purposes here, all such constructions yield the same asymptotic estimates.

Theorem 2.10 (pointwise approximation of shape operator) *Let M be a smooth surface in $\mathbb{R}^3$ and $\epsilon \in (0, 1)$. For every pair consisting of a polyhedral surface M_h that is an ϵ-normal graph over M and a function ψ that is r-local at a point $y \in M_h$, the tensor $S^\psi_{M_h}$ satisfies the estimate*

$$\left\|S(x) - S^\psi_{M_h}\right\|_{\max} \leq C(r + \frac{\delta(M, M_h) + \|N - N_h\|_{L^\infty}}{r}),$$

where $x = \Psi(y)$. If $\psi \circ \Phi$ has the r^2-property, the bound improves to

$$\left\| S(x) - S^{\psi}_{M_h} \right\|_{\max} \leq C(r^2 + \frac{\delta(M, M_h) + \|N - N_h\|_{L^\infty}}{r}).$$

The constants C depend only on M, ϵ, and C_D (see Definition 2.6) and in the second estimate additionally on C_Q (see Definition 2.8).

Proof. For simplicity of notation, we leave out the point, x, where the tensor and vector fields are evaluated, *i.e.*, we write $S, \bar{S}, N$, and N_h instead of $S(x), \bar{S}(x), N(x)$, and $N_h(x)$. Using equations (2.25) and (2.26), we get

$$\begin{aligned}
&\left\| S(x) - S^{\psi}_{M_h}(y) \right\|_{\max} \\
&= \left\| (Id - NN^T)\bar{S}(Id - NN^T) - (Id - N_h N_h^T)\bar{S}^{\psi}_{M_h}(Id - N_h N_h^T) \right\|_{\max} \\
&= \left\| (N_h N_h^T - NN^T)\bar{S}(Id - NN^T) + (Id - N_h N_h^T)\bar{S}(N_h N_h^T - NN^T) \right. \\
&+ (Id - N_h N_h^T)(\bar{S}^{\psi}_{M_h} - \bar{S})(N_h N_h^T - NN^T) \\
&\left. + (Id - N_h N_h^T)(\bar{S} - \bar{S}^{\psi}_{M_h})(Id - NN^T) \right\|_{\max} \\
&\leq 2 \left\| N_h N_h^T - NN^T \right\|_{\max} \left\| \bar{S} \right\|_{\max} + (1 + \left\| N_h N_h^T - NN^T \right\|_{\max}) \left\| \bar{S} - \bar{S}^{\psi}_{M_h} \right\|_{\max}.
\end{aligned}$$

Combining this with Lemma 2.9 and the estimate

$$\begin{aligned}
\left\| N_h N_h^T - NN^T \right\|_{\max} &\leq \left\| (N_h - N)N^T \right\|_{\max} + \left\| N_h (N_h^T - N^T) \right\|_{\max} \\
&\leq 2 \left\| (N_h - N) \right\|_{L^\infty}
\end{aligned}$$

proves the theorem. □

The estimates in Lemma 2.9 and Theorem 2.10 depend on r and $\delta(M, M_h) + \|N - N_h\|_{L^\infty}$, and both quantities are independent. The following corollary shows how to choose r to get the optimal approximation order in $\delta(M, M_h) + \|N - N_h\|_{L^\infty}$.

Corollary 2.11 *Under the assumptions of Theorem 2.10 and the additional assumption*

$$r = \sqrt{\delta(M, M_h) + \|N - N_h\|_{L^\infty}}, \tag{2.27}$$

we obtain the estimate

$$\left\| S(x) - S^{\psi}_{M_h} \right\|_{\max} \leq C \sqrt{\delta(M, M_h) + \|N - N_h\|_{L^\infty}}.$$

If $\psi \circ \Phi$ has the r^2-property and

$$r = \left(\delta(M, M_h) + \|N - N_h\|_{L^\infty}\right)^{\frac{1}{3}}, \tag{2.28}$$

we get

$$\left\| S(x) - S^{\psi}_{M_h} \right\|_{\max} \leq C \left(\delta(M, M_h) + \|N - N_h\|_{L^\infty}\right)^{\frac{2}{3}}.$$

Proof. The corollary immediately follows from Theorem 2.10 and the assumptions (2.27) and (2.28), respectively. □

2.5 Inscribed polyhedral surfaces

In this section, we specialize the approximation estimates for the shape operator to inscribed polyhedral surfaces. Using Lemma 1.24, we can formulate approximation estimates that depend on h instead of $\delta(M, M_h)$ and $\|N - N_h\|_{L^\infty}$.

Lemma 2.12 (approximation of generalized shape operator) *Let M be a smooth surface in $\mathbb{R}^3$. Then there exists an $h_0 \in \mathbb{R}^+$ such that for every polyhedral surface M_h that is inscribed to M and satisfies $h < h_0$, the inequalities*

$$\left\|\bar{\Sigma} - \bar{\Sigma}_h\right\|_{Op} \leq C\,h \qquad \text{and} \qquad \left\|\hat{\Sigma} - \hat{\Sigma}_h\right\|_{Op} \leq C\,h$$

hold, where C depends only on M, h_0 and the shape regularity of M_h.

Proof. To prove the lemma, we combine the estimates (2.5) and (2.6) of Theorem 2.4 with (1.37) and (1.38) and choose h_0 and C accordingly. □

Furthermore, specializing Theorem 2.10 to inscribed meshes yields estimates on the pointwise approximation that depend on the mesh size h.

Lemma 2.13 (pointwise approximation of shape operator) *Let M be a smooth surface in $\mathbb{R}^3$. Then there exists an $h_0 \in \mathbb{R}^+$ such that for every pair consisting of a polyhedral surface M_h that is inscribed to M and satisfies $h < h_0$ and a function ψ that is r-local at a point $y \in M_h$ with $r = \sqrt{h}$, the corresponding tensor $S^{\psi}_{M_h}$ satisfies the estimate*

$$\left\|S(x) - S^{\psi}_{M_h}\right\|_{\max} \leq C\,\sqrt{h}, \tag{2.29}$$

where $x = \Psi(y)$. If $\psi \circ \Phi$ has the r^2-property and $r = h^{\frac{1}{3}}$, the error bound improves to

$$\left\|S(x) - S^{\psi}_{M_h}\right\|_{\max} \leq C\,h^{\frac{2}{3}}. \tag{2.30}$$

The constants C depend only on M, h_0, ρ, and C_D and in the second estimate additionally on C_Q.

Proof. The lemma immediately follows from combining Theorem 2.10 with Lemma 1.24. □

2.6 Examples of r-local functions

In this section, we discuss the construction of r-local functions and functions with the r^2-property first on smooth and then on polyhedral surfaces. By a family of r-local functions at $x \in M$, we mean a family $(\varphi_r)_{r\in(0,\rho)}$ such that for all $r \in (0, \rho)$, φ_r is r-local at x with respect to a fixed constant C_D. We consider a family of r-local functions on $\mathbb{R}^2$ and use the Riemannian exponential map to construct a family of r-local functions on M. For functions that have a certain symmetry, this construction yield functions that satisfy the r^2-property. As an example, we consider the *geodesic hat* functions and an approximation of them, the *extrinsic hat* functions. Both hat functions can be constructed on polyhedral surfaces, as well.

2.6.1 Construction of r-local functions

Let $\phi \in W^{1,1}(\mathbb{R}^2)$ be a non-negative function that vanishes in the complement of the open unit ball in $\mathbb{R}^2$ and satisfies $\|\phi\|_{L^1(\mathbb{R}^2)} = 1$. Then $(\phi_r)_{r\in\mathbb{R}^+}$ defined by

$$\phi_r(\cdot) = \frac{1}{r^2}\phi(\frac{\cdot}{r})$$

is a family of r-local functions on $\mathbb{R}^2$ at the origin 0, and the constant C_D assumes the value $|\phi|_{W^{1,1}(\mathbb{R}^2)}$.

We denote by $\exp_x$ the Riemannian exponential map at a point $x \in M$ and by $i(M)$ the injectivity radius of M. Since the surface M is compact, the injectivity radius $i(M)$ of M is a strictly positive number. For any $r < i(M)$,

$$\exp_x : B_r(0) \subset T_xM \mapsto M$$

is a diffeomorphism of $B_r(0)$ and $\exp_x(B_r(0)) = B_r(x)$, where $B_r(x)$ and $B_r(0)$ denote the open geodesic balls of radius r around $x \in M$ and $0 \in T_xM$.

Lemma 2.14 (construction of r-local functions) *Consider a point $x \in M$ and a positive $\rho < i(M)$. Then for any family $(\phi_r)_{r\in(0,\rho)}$ of r-local functions on T_xM at 0, the family $(\varphi_r)_{r\in(0,\rho)}$ given by*

$$\varphi_r(y) = \begin{cases} \frac{1}{\|\phi_r \circ \exp_x^{-1}\|_{L^1(M)}} \phi_r \circ \exp_x^{-1}(y) & \text{for } y \in B_{i(M)}(x), \\ 0 & \text{for all other } y, \end{cases} \tag{2.31}$$

is a family of r-local functions at x.

Proof. The properties *(D2)* and *(D4)* of Definition 2.6 are clearly satisfied, and *(D3)* holds since $\exp_x$ is a radial isometry. Since the restriction of $\exp_x$ to $B_{i(M)}(0)$ is a diffeomorphism, *(D1)* follows from properties of Sobolev spaces under smooth coordinate transformations, see [1, Theorem 3.35]. To show that

(D5) holds, we use $\exp_x : B_{i(M)}(0) \mapsto M$ as a parametrization of M around x. Since the support of φ_r is contained in $\exp_x(B_{i(M)}(0))$ for all $r \in (0, \rho)$, we can calculate $\|\varphi_r\|_{W^{1,1}}$ using only the chart $\exp_x$. Analogous to our discussion on the metric distortion introduced by the cone metric of a polyhedral surface (see Section 1.5), we can represent the metric distortion induced by $\exp_x$ through a metric distortion tensor $A_{\exp_x}$ and the distortion of the area form by a function $\alpha_{\exp_x} = \sqrt{\det(A_{\exp_x})}$. On the compact set $\overline{B_\rho(0)}$, $\alpha_{\exp_x}$ and the eigenvalues of $A_{\exp_x}$ are bounded above and below, and since $\exp_x$ is a diffeomorphism, the lower bounds are strictly larger than zero. Then there are constants c and C such that

$$c \|u\|_{L^1(M)} \leq \left\|u \circ \exp_x^{-1}\right\|_{L^1(\mathbb{R}^2)} \leq C \|u\|_{L^1(M)} \tag{2.32}$$

holds for all $u \in L^1(M)$ whose support is contained in $\overline{B_\rho(0)}$, and there are constants $\tilde{c}$ and $\tilde{C}$ such that

$$\tilde{c} \, |u|_{W^{1,1}(M)} \leq \left|u \circ \exp_x^{-1}\right|_{W^{1,1}(\mathbb{R}^2)} \leq \tilde{C} \, |u|_{W^{1,1}(M)} \tag{2.33}$$

holds for all all $u \in W^{1,1}(M)$ whose support is contained in $\overline{B_\rho(x)}$. Because the support of φ_r is contained in the compact set $\overline{B_\rho(x)}$, we have

$$\left|\phi_r \circ \exp_x^{-1}\right|_{W^{1,1}(M)} \leq \tilde{C} \, |\phi_r|_{W^{1,1}(\mathbb{R}^2)} \tag{2.34}$$

and

$$\left\|\phi_r \circ \exp_x^{-1}\right\|_{L^1(M)} \geq c \, \|\phi_r\|_{L^1(\mathbb{R}^2)} = c \tag{2.35}$$

for all $r \in (0, \rho)$. It follows that the estimate

$$|\varphi_r|_{W^{1,1}(M)} \leq \frac{\tilde{C} \, |\phi_r|_{W^{1,1}(\mathbb{R}^2)}}{c \, |\phi_r|_{L^1(\mathbb{R}^2)}} \leq \frac{\tilde{C} \, |\phi|_{W^{1,1}(\mathbb{R}^2)}}{c} \frac{1}{r} \tag{2.36}$$

is satisfied for all $r \in (0, \rho)$. This means *(D5)* holds as well. □

2.6.2 The r^2-property

After having introduced a construction of r-local functions, we will now discuss the construction of functions that have the r^2-property (Definition 2.8). First, we consider the case of functions on domains in $\mathbb{R}^2$.

Lemma 2.15 *For any positive $\rho \in \mathbb{R}^+$, let $B_\rho(0)$ be the open ball of radius ρ around the origin in $\mathbb{R}^2$. Moreover, let ϕ_r be a r-local function at 0 such that $r < \rho$ and*

$$\phi_r(y) = \phi_r(-y) \tag{2.37}$$

for all $y \in \mathbb{R}^2$. Then the estimate

$$\left| f(0) - \int_{B_\rho(0)} f\,\phi_r \, dvol \right| \leq |f|_{C^2}\ r^2 \tag{2.38}$$

holds for all $f \in C^2(\overline{B_\rho(0)})$.

Proof. From Taylor's theorem, we know that

$$f(y) = f(0) + \left\langle \mathrm{grad}_{\mathbb{R}^2} f_{|0}, y \right\rangle_{\mathbb{R}^2} + \mathrm{Rem}(y) \tag{2.39}$$

and that the remainder Rem satisfies

$$|\mathrm{Rem}(y)| \leq |f|_{C^2}\ \|y\|^2_{\mathbb{R}^2} \tag{2.40}$$

for all $y \in B_\rho(0)$. Plugging (2.39) into the left side of (2.38), we get

$$\begin{aligned}
&\left| f(0) - \int_{B_\rho(0)} f\,\phi_r \,\mathrm{d}vol_{\mathbb{R}^2} \right| \\
&= \left| f(0) - \int_{B_\rho(0)} (f(0) + \left\langle \mathrm{grad}_{\mathbb{R}^2} f_{|0}, \cdot \right\rangle_{\mathbb{R}^2} + \mathrm{Rem})\,\phi_r \,\mathrm{d}vol_{\mathbb{R}^2} \right| \\
&= \left| \int_{B_\rho(0)} (\left\langle \mathrm{grad}_{\mathbb{R}^2} f_{|0}, \cdot \right\rangle_{\mathbb{R}^2} + \mathrm{Rem})\,\phi_r \,\mathrm{d}vol_{\mathbb{R}^2} \right| .
\end{aligned}$$

In the last step, we used properties *(D2)* and *(D4)* of ϕ_r.

The property (2.37) of ϕ_r implies that for any linear functional l on $\mathbb{R}^2$,

$$\int_{B_\rho(0)} l\,\phi_r \,\mathrm{d}vol_{\mathbb{R}^2} = 0. \tag{2.41}$$

Since $\left\langle \mathrm{grad}_{\mathbb{R}^2} f_{|0}, \cdot \right\rangle_{\mathbb{R}^2}$ is a linear functional, we get

$$\begin{aligned}
&\left| f(0) - \int_{B_\rho(0)} f\,\phi_r \,\mathrm{d}vol_{\mathbb{R}^2} \right| = \left| \int_{B_\rho(0)} \mathrm{Rem}\,\phi_r \,\mathrm{d}vol_{\mathbb{R}^2} \right| \\
&\leq \sup_{y \in B_r(0)} |\mathrm{Rem}(y)| \leq |f|_{C^2}\ r^2
\end{aligned}$$

Here, we used (2.40) in the last step. □

In Lemma 2.14, we have seen how r-local functions on M can be obtained from r-local functions on $\mathbb{R}^2$. In the following lemma, we combine this construction with the last lemma to get functions with the r^2-property on M.

Lemma 2.16 (r^2-property) *Consider a point $x \in M$ and a positive $\rho < i(M)$. Let $\phi_r : T_xM \mapsto \mathbb{R}$ be a r-local function at 0 that satisfies $r < \rho$ and $\phi_r(y) = \phi_r(-y)$ for all $y \in T_xM$, and let φ_r be constructed from ϕ_r as described in Lemma 2.14. Then there is a constant C depending only on M and ρ such that*

$$\left| f(x) - \int_M f\, \varphi_r \, dvol \right| \leq C \, \|f\|_{C^2} \, r^2$$

for all $f \in C^2(M)$.

Proof. We consider the function $f \circ \exp_x$ that is smooth on $\overline{B_\rho(0)} \subset T_xM$. From Taylor's theorem we know that there is a remainder function Rem such that

$$f \circ \exp_x(y) = f \circ \exp_x(0) + \left\langle \mathrm{grad}_{\mathbb{R}^2}(f \circ \exp_x)_{|0}, y \right\rangle_{\mathbb{R}^2} + \mathrm{Rem}(y) \tag{2.42}$$

for any $y \in B_\rho(0)$. Moreover, there is a constant C, which depends on M and ρ, such that

$$|\mathrm{Rem}(y)| \leq C \, \|f\|_{C^2} \, \|y\|^2_{\mathbb{R}^2} \tag{2.43}$$

for all $y \in B_\rho(0)$. Let $\alpha_{\exp_x}$ denote the area distortion on $\overline{B_\rho(0)}$ induced by the exponential map. Using (2.31) and (2.42), we get

$$\begin{aligned}
&\left| f(x) - \int_M f\, \varphi_r \, \mathrm{d}vol \right| \\
&= \left| f(x) - \frac{1}{\left\| \phi_r \, \alpha_{\exp_x} \right\|_{L^1(B_\rho(0))}} \int_{B_\rho(0)} f \circ \exp_x \, \phi_r \, \alpha_{\exp_x} \mathrm{d}vol \right| \\
&= \left| f(x) - \frac{1}{\left\| \phi_r \, \alpha_{\exp_x} \right\|_{L^1(B_\rho(0))}} \int_{B_\rho(0)} (f \circ \exp_x(0) \right. \\
&\left. + \left\langle \mathrm{grad}_{\mathbb{R}^2}(f \circ \exp_x)_{|0}, \cdot \right\rangle_{\mathbb{R}^2} + \mathrm{Rem}) \, \phi_r \, \alpha_{\exp_x} \mathrm{d}vol \right|
\end{aligned}$$

We derive bounds for all summands of the last expression. Since φ_r is positive and $\|\varphi_r\|_{L^1(M)} = 1$, we get

$$\left| f(x) - \frac{1}{\left\| \phi_r \, \alpha_{\exp_x} \right\|_{L^1(B_\rho(0))}} \int_{B_\rho(0)} f \circ \exp_x(0) \, \phi_r \, \alpha_{\exp_x} \mathrm{d}vol \right| = 0.$$

The area distortion $\alpha_{\exp_x}$ satisfies the bound

$$\left| \alpha_{\exp_x}(y) - 1 \right| < C \, r$$

for all $y \in B_r(0)$. This follows directly from the representation of the metric tensor in geodesic polar coordinates, which can be found in [72, p. 288]. Using

this estimate and (2.41), we have

$$\begin{aligned}
&\left| \frac{1}{\left\|\phi_r\, \alpha_{\exp_x}\right\|_{L^1(B_\rho(0))}} \int_{B_\rho(0)} \left\langle \mathrm{grad}_{\mathbb{R}^2}(f\circ\exp_x)_{|0}, \cdot \right\rangle_{\mathbb{R}^2} \phi_r\, \alpha_{\exp_x} \mathrm{d}vol_{\mathbb{R}^2} \right| \\
&= \left| \frac{1}{\left\|\phi_r\, \alpha_{\exp_x}\right\|_{L^1(B_\rho(0))}} \int_{B_\rho(0)} \left\langle \mathrm{grad}_{\mathbb{R}^2}(f\circ\exp_x)_{|0}, \cdot \right\rangle_{\mathbb{R}^2} \phi_r\, (\alpha_{\exp_x} - 1) \mathrm{d}vol_{\mathbb{R}^2} \right| \\
&\leq \left\| \alpha_{\exp_x}^{-1} \right\|_{L^\infty(B_\rho(0))} \sup_{y\in B_r(0)} \left| \left\langle \mathrm{grad}_{\mathbb{R}^2}(f\circ\exp_x)_{|0}, y \right\rangle_{\mathbb{R}^2} (\alpha_{\exp_x}(y) - 1) \right| \\
&< C\ \|f\|_{C^1}\ r^2.
\end{aligned}$$

To get a bound for the remaining term, we use (2.43)

$$\left| \frac{1}{\left\|\phi_r\, \alpha_{\exp_x}\right\|_{L^1(B_\rho(0))}} \int_{B_\rho(0)} \mathrm{Rem}\, \phi_r\, \alpha_{\exp_x} \mathrm{d}vol \right| \leq \sup_{y\in B_r(0)} |\mathrm{Rem}(y)| < C\ \|f\|_{C^2}\ r^2.$$

Altogether, we established the bound

$$\left| f(x) - \int_M f\, \varphi_r\, \mathrm{d}vol \right| \leq C\ \|f\|_{C^2}\ r^2,$$

which proves the lemma. □

2.6.3 Geodesic and extrinsic hat functions

As an example of the presented construction of r-local functions, let us consider the function $\phi(\cdot) = \frac{3}{\pi} \max\{0, 1 - \|\cdot\|_{\mathbb{R}^2}\}$ on $\mathbb{R}^2$ (resp. on T_xM). We call the corresponding functions φ_r on M *geodesic hat* functions, since they decay linearly with the geodesic distance to x. Explicitly, φ_r is given by

$$\varphi_r = \frac{\tilde{\varphi}_r}{\|\tilde{\varphi}_r\|_{L^1}},\ \text{where } \tilde{\varphi}_r(y) = \max\{0, 1 - \frac{d_M(x,y)}{r}\}. \tag{2.44}$$

Since the function ϕ has the symmetry (2.37), Lemma 2.16 implies that the functions φ_r have the r^2-property.

To keep computations simple, one can employ the extrinsic distance of points in $\mathbb{R}^3$ instead of the geodesic distance. The *extrinsic hat* function ψ_r is defined as

$$\psi_r = \frac{\tilde{\psi}_r}{\left\|\tilde{\psi}_r\right\|_{L^1}},\ \text{where } \tilde{\psi}_r(y) = \max\{0, 1 - \frac{\|x-y\|_{\mathbb{R}^3}}{r}\}. \tag{2.45}$$

As before, we focus on the properties of ψ_r for small values of r. We fix a small ρ and consider only ψ_r with $r \in (0, \rho)$. Then the ψ_rs satisfy the properties of r-local functions, except that we need to modify property *(D3)*: the support of ψ_r

is not contained in $B_r(x)$, but there is a constant C depending only on M and ρ such that $\mathrm{supp}(\psi_r) \subset B_{Cr}(x)$. Our approximation estimates hold for these functions, as well. However, the additional constant appears in all the bounds.

In addition to being r-local, the extrinsic hat functions have the r^2-property. This is shown in the next lemma.

Lemma 2.17 (extrinsic hat functions) *Consider a point $x \in M$ and a positive $\rho < \min\{i(M), reach(M)\}$. For any $r < \rho$, the extrinsic hat function ψ_r at x satisfies*

$$\left| f(x) - \int_M f\, \psi_r \, dvol \right| < C \, \|f\|_{C^2} \, r^2$$

for all $f \in C^2(M)$. The constant C depends only on M and ρ.

Proof. The foundation of the proof is that locally the approximation of the geodesic distance by the extrinsic distance is of third order. Explicitly, in [13, Lemma 3.2] the estimate

$$|d_M(x,y) - \|x-y\|_{\mathbb{R}^3}| \leq \frac{4}{3 \ \mathrm{reach}(M)^2} \ \|x-y\|^3_{\mathbb{R}^3} \, . \tag{2.46}$$

is shown for any pair $x, y \in M$ with $\|x-y\|_{\mathbb{R}^3} <$reach$(M)/2$.

For $x \in M$ and $r < \rho$, let φ_r,$\tilde{\varphi}_r$,ψ_r, and $\tilde{\psi}_r$ be the corresponding functions defined in (2.44) and (2.45). Then, (2.46) implies

$$\left\| \tilde{\varphi}_r - \tilde{\psi}_r \right\|_{L^\infty} \leq \frac{4}{3 \ \mathrm{reach}(M)^2} \, r^2. \tag{2.47}$$

We use this estimate to prove the lemma. For a first step, we have

$$\left| f(x) - \int_M f\, \psi_r \, \mathrm{d}vol \right| \leq \left| f(x) - \int_M f\, \varphi_r \, \mathrm{d}vol \right| + \left| \int_M f\, (\varphi_r - \psi_r) \, \mathrm{d}vol \right| .$$

Lemma 2.16 implies that the first summand on the right hand side is bounded by $C \, \|f\|_{C^2} \, r^2$. To get a bound on the second summand, we use Hölder's in-

equality and the reverse triangle inequality

$$\begin{aligned}
&\left|\int_M f\,(\varphi_r-\psi_r)\,\mathrm{d}vol\right| \le \|f\|_{L^\infty}\,\|\varphi_r-\psi_r\|_{L^1}\\
&\le \|f\|_{L^\infty}\left\|\frac{\tilde\varphi_r}{\|\tilde\varphi_r\|_{L^1}}-\frac{\tilde\psi_r}{\left\|\tilde\psi_r\right\|_{L^1}}\right\|_{L^1}\\
&\le \|f\|_{L^\infty}\left(\left|\frac{\left\|\tilde\psi_r\right\|_{L^1}-\|\tilde\varphi_r\|_{L^1}}{\left\|\tilde\psi_r\right\|_{L^1}}\right|+\frac{\left\|\tilde\varphi_r-\tilde\psi_r\right\|_{L^1}}{\left\|\tilde\psi_r\right\|_{L^1}}\right)\\
&\le 2\,\|f\|_{L^\infty}\,\frac{\left\|\tilde\varphi_r-\tilde\psi_r\right\|_{L^1}}{\left\|\tilde\psi_r\right\|_{L^1}}\\
&\le 2\frac{\mathrm{area}(\mathrm{supp}(\tilde\psi_r))}{\left\|\tilde\psi_r\right\|_{L^1}}\,\|f\|_{L^\infty}\left\|\tilde\varphi_r-\tilde\psi_r\right\|_{L^\infty}\\
&\le C\,\|f\|_{L^\infty}\left\|\tilde\varphi_r-\tilde\psi_r\right\|_{L^\infty}.
\end{aligned}$$

Combining this bound with (2.47) proves the lemma. □

2.6.4 Hat functions on polyhedral surfaces

The constructions of the hat functions, (2.44) and (2.45), can be transferred to polyhedral surfaces, where the geodesic distance on M is replaced by the geodesic distance on M_h. If M_h is a normal graph over M and

$$r=(\delta(M,M_h)+\|N-N_h\|_{L^\infty})^{\frac{1}{3}},$$

which is the optimal choice of r in the second estimate of Corollary 2.11, then the difference between the extrinsic distances on M and M_h is bounded by

$$|\|x-y\|_{\mathbb{R}^3}-\|\Psi(x)-\Psi(y)\|_{\mathbb{R}^3}|\le 2\,\|\kappa_{\max}\|_{L^\infty}\,\delta(M,M_h)\le 2\,\|\kappa_{\max}\|_{L^\infty}\,r^3.$$

This is the same order as the approximation of the geodesic distance on M by the extrinsic distance on M, see (2.46). Based on this property, one can show that for $r=(\delta(M,M_h)+\|N-N_h\|_{L^\infty})^{\frac{1}{3}}$, the pullback $\psi_r\circ\Phi$ to M of the extrinsic distance ψ_r on M_h has the r^2-property. The proof is similar to that of Lemma 2.17. This result is confirmed by our experiments.

For computations, it is convenient to work with continuous and piecewise linear functions on M_h, *e.g.* with the interpolants of a function. The gradient of such a function is constant in each triangle and one can evaluate the generalized shape operators by summing over the triangles in the support of the function. In the experiments, we use a piecewise linear approximation of the extrinsic hat functions.

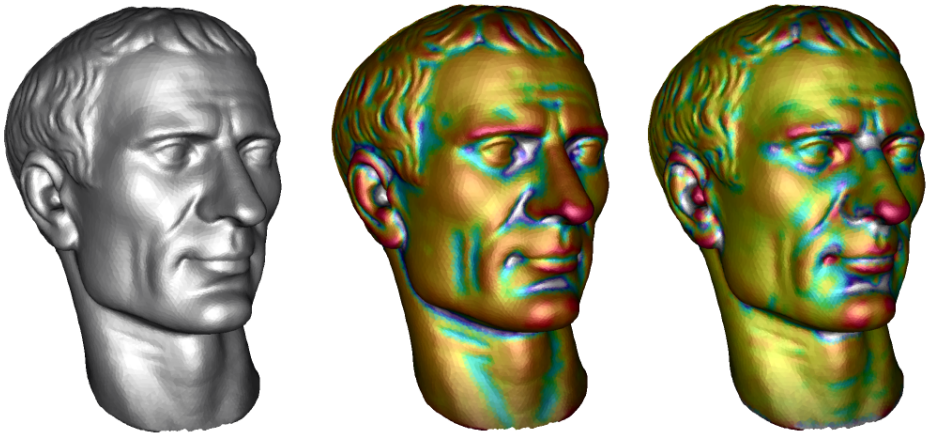

FIGURE 2.1. Mean curvature (middle) and Gaussian curvature (right) computed using the generalized shape operator $\hat{\Sigma}$ and an r-local function on a 3D-scanned model. Color coding from white (negative) to red (positive).

2.7 Experiments

In this Section, we show the results of three experiments concerning the error and the convergence rate of the pointwise approximation of the shape operator. In the first example, we approximate the tensors $\bar{S}(x)$ and $\hat{S}(x)$ at a point x on the unit sphere in $\mathbb{R}^3$ using inscribed polyhedral surfaces with decreasing mesh size h. On each polyhedral surface M_h we consider two functions, ψ and ψ^*. Both functions are continuous and linear on the triangles and hence are determined by their values at the vertices of M_h. The function ψ is an approximation of the extrinsic hat function, see (2.45), and we get ψ^* by disturbing ψ. The disturbance is chosen such that ψ^* is still r-local around x but does not have the r^2-property anymore. At any vertex v of M_h, the functions take the values

$$\psi(v) = \max\{1 - \frac{\|x - v\|_{\mathbb{R}^3}}{\sqrt{h}}, 0\} \tag{2.48}$$

and

$$\psi^*(v) = \max\{1 - \frac{\left\|x + \frac{\sqrt{h}}{20}e - v\right\|_{\mathbb{R}^3}}{\sqrt{h}}, 0\}, \tag{2.49}$$

where h is the mesh size of M_h and e is a fixed unit vector in $\mathbb{R}^3$.

Using ψ and ψ^*, we construct the tensors $\bar{S}^{\psi}_{M_h}$ and $\hat{S}^{\psi}_{M_h}$ with components

$$(\bar{S}^{\psi}_{M_h})_{ij} = \frac{\langle e_i, \bar{\Sigma}_{M_h}(\psi\, e_j)\rangle_{\mathbb{R}^3}}{\|\psi\|_{L^1(M_h)}} \text{ and } (\hat{S}^{\psi}_{M_h})_{ij} = \frac{\left\langle e_i, \hat{\Sigma}_{M_h}(\psi\, e_j)\right\rangle_{\mathbb{R}^3}}{\|\psi\|_{L^1(M_h)}} \tag{2.50}$$

h	$\|\bar{S}(x) - \bar{S}^{\psi}_{M_h}\|$	eoc	$\|\bar{S}(x) - \bar{S}^{\psi^*}_{M_h}\|$	eoc
0.0744108	0.0684689	–	0.0828663	–
0.0304109	0.0275034	1.00	0.0409642	0.79
0.0102627	0.0092561	1.00	0.0197543	0.67
0.0030374	0.0027360	1.00	0.0096611	0.59
0.0008309	0.0007480	1.00	0.0048014	0.54
0.0002176	0.0001959	1.00	0.0023992	0.52
0.0000557	0.0000501	1.00	0.0012003	0.51
0.0000146	0.0000132	1.00	0.0006122	0.50
h	$\|\hat{S}(x) - \hat{S}^{\psi}_{M_h}\|$	eoc	$\|\hat{S}(x) - \hat{S}^{\psi^*}_{M_h}\|$	eoc
0.0744108	0.0114370	–	0.0181622	–
0.0304109	0.0045876	1.00	0.0101977	0.65
0.0102627	0.0015431	1.00	0.0055643	0.56
0.0030374	0.0004560	1.00	0.0029508	0.52
0.0008309	0.0001247	1.00	0.0015321	0.51
0.0002176	0.0000326	1.00	0.0007826	0.50
0.0000557	8.36×10^{-6}	1.00	0.0003958	0.50
0.0000146	2.20×10^{-6}	1.00	0.0002030	0.50

TABLE 2.1. Approximations of the tensors $\bar{S}(x)$ and $\hat{S}(x)$ at a point x on the unit sphere are analyzed. The approximation error and experimental rate of convergence are shown.

and the tensors $\bar{S}^{\psi^*}_{M_h}$ and $\hat{S}^{\psi^*}_{M_h}$ with components

$$(\bar{S}^{\psi^*}_{M_h})_{ij} = \frac{\langle e_i, \bar{\Sigma}_{M_h}(\psi^* e_j)\rangle_{\mathbb{R}^3}}{\|\psi^*\|_{L^1(M_h)}} \text{ and } (\hat{S}^{\psi^*}_{M_h})_{ij} = \frac{\left\langle e_i, \hat{\Sigma}_{M_h}(\psi^* e_j)\right\rangle_{\mathbb{R}^3}}{\|\psi^*\|_{L^1(M_h)}}. \tag{2.51}$$

Table 2.1 lists the approximation errors of the four tensors (measured in the norm $\|\ \|_{\max}$) for inscribed polyhedral surfaces with decreasing mesh size h. In addition, the table shows the experimental order of convergence. Let e_{h_i} and $e_{h_{i+1}}$ be the approximation errors of some quantity for the decreasing mesh sizes h_i and h_{i+1}. Then the *experimental order of convergence (eoc)* of

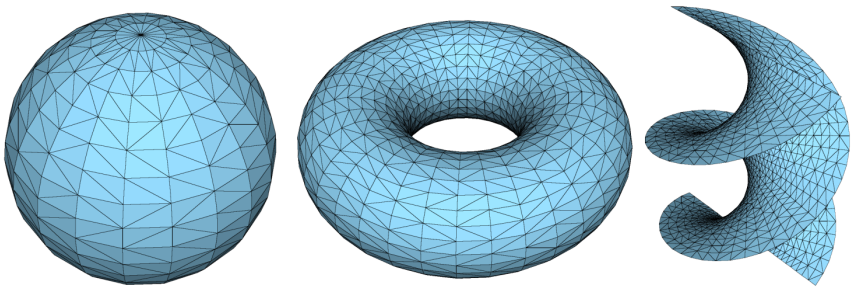

FIGURE 2.2. Some of the surfaces used for the experiments are shown.

h	$\|\bar{S}(x) - \bar{S}^{\psi}_{M_h}\|$	eoc	$\|S(x) - S^{\psi}_{M_h}\|$	eoc
0.0442741	0.0175626	–	0.0155477	–
0.0241741	0.0095546	1.00	0.0084655	1.00
0.0102634	0.0040565	1.00	0.0035977	1.00
0.0035994	0.0014209	1.00	0.0012606	1.00
0.0010920	0.0004308	1.00	0.0003822	1.00
0.0003030	0.0001195	1.00	0.0001060	1.00
0.0000800	0.0000315	1.00	0.0000280	1.00
0.0000206	8.11×10^{-6}	1.00	7.19×10^{-6}	1.00
h	$\|\hat{S}(x) - \hat{S}^{\psi}_{M_h}\|$	eoc	$\|S(x) - \mathcal{S}^{\psi}_{M_h}\|$	eoc
0.0442741	0.0027184	–	0.0036529	–
0.0241741	0.0014769	1.00	0.0020020	0.99
0.0102634	0.0006264	1.00	0.0008539	0.99
0.0035994	0.0002193	1.00	0.0002998	1.00
0.0010920	0.0000665	1.00	0.0000910	1.00
0.0003030	0.0000184	1.00	0.0000252	1.00
0.0000800	4.87×10^{-6}	1.00	6.66×10^{-6}	1.00
0.0000206	1.25×10^{-6}	1.00	1.71×10^{-6}	1.00

TABLE 2.2. The table shows the approximation error and experimental rate of convergence of approximations of the shape operator at a point x on the torus of revolution.

the quantity is defined as

$$\operatorname{eoc}(h_i, h_{i+1}) = \log \frac{e_{h_i}}{e_{h_{i+1}}} \left(\log \frac{h_i}{h_{i+1}} \right)^{-1}. \tag{2.52}$$

All four approximations converge, but the order of convergence differs depending on which function, ψ or ψ^*, we use. The experimental order of convergence of $\bar{S}^{\psi^*}_{M_h}$ and $\hat{S}^{\psi^*}_{M_h}$ is $\frac{1}{2}$. This confirms the sharpness of the estimate (2.29) of Lemma 2.13 (resp. the first estimate in Theorem 2.10). For the second estimate (2.30) of Lemma 2.13, the situation is different. The function ψ leads to an eoc of 1 in our experiments, even if we add normal noise (of order h^2) and even stronger tangential noise to the vertex positions of the polyhedral surfaces. This indicates that it may be possible to improve the bound (2.30). However, when $\sqrt{h}$ is replaced by $h^{\frac{1}{3}}$ in (2.48), we get the expected eoc of $\frac{2}{3}$.

The second example is concerned with the approximation of the classical shape operator of a smooth surface. We consider a point x on a torus of revolution (with radii 1 and 2) and polyhedral surfaces that are inscribed to the torus. On each polyhedral surface we use the function ψ, see (2.48), to compute the tensors $\bar{S}^{\psi}_{M_h}$ and $\hat{S}^{\psi}_{M_h}$, similar to the first example. In this example, we additionally construct approximations of the normal of M at x. For every

h	$\|S(x) - S^{\psi}_{M_h}\|$	eoc	$\|S(x) - S^{\psi}_{M_h,noise}\|$	eoc
0.0385465	0.0009560	–	0.0014489	–
0.0260549	0.0006113	1.10	0.0014966	−0.08
0.0141667	0.0003216	1.10	0.0004560	2.00
0.0060853	0.0001362	1.00	0.0001497	1.30
0.0021316	0.0000476	1.00	0.0000687	0.74
0.0006460	0.0000144	1.00	0.0000194	1.10
0.0001791	3.99×10^{-6}	1.00	5.22×10^{-6}	1.00
h	$\|S(x) - S^{\tilde{\psi}}_{M_h}\|$	eoc	$\|S(x) - S^{\tilde{\psi}}_{M_h,noise}\|$	eoc
0.0385465	0.0002335	–	0.0047959	–
0.0260549	0.0000971	2.20	0.0165850	−3.20
0.0141667	0.0000249	2.20	0.0062470	1.60
0.0060853	4.01×10^{-6}	2.20	0.0213477	−1.50
0.0021316	8.96×10^{-7}	1.40	0.0053238	1.30
0.0006460	7.97×10^{-8}	2.00	0.0132693	−0.76
0.0001791	6.00×10^{-9}	2.00	0.0204679	−0.34

TABLE 2.3. The table shows the error and the experimental rate of convergence for the approximation of the shape operator at a point on the helicoid. The columns on the right show results computed from polyhedral surfaces that are corrupted with noise.

polyhedral surface M_h, we set

$$N^{\tilde{\psi}}_{M_h} = \frac{1}{\left\| \int_{M_h} N_{M_h}\, \tilde{\psi}\, \mathrm{d}vol_h \right\|_{\mathbb{R}^3}} \int_{M_h} N_{M_h}\, \tilde{\psi}\, \mathrm{d}vol_h,$$

where $\tilde{\psi}$ is the continuous and piecewise linear function on M_h that takes the values

$$\tilde{\psi}(v) = \max\{1 - \frac{\|x - v\|_{\mathbb{R}^3}}{2h}, 0\} \tag{2.53}$$

at the vertices v. We use $N^{\tilde{\psi}}_{M_h}$ instead of evaluating $N_{M_h}(\Phi(x))$ to avoid the need to compute the point $\Phi(x)$. Using the estimated normal, we construct the following two approximations of $S(x)$: the first is defined, analogously to (2.26), by

$$S^{\psi}_{M_h} = (Id - N^{\tilde{\psi}}_{M_h} {N^{\tilde{\psi}}_{M_h}}^T) \bar{S}^{\psi}_{M_h} (Id - N^{\tilde{\psi}}_{M_h} {N^{\tilde{\psi}}_{M_h}}^T), \tag{2.54}$$

and the second (denoted by a calligraphic letter) is given by

$$\mathcal{S}^{\psi}_{M_h} = \hat{S}^{\psi}_{M_h}\, C_{N^{\tilde{\psi}}_{M_h}}, \tag{2.55}$$

where

$$C_{N^{\tilde{\psi}}_{M_h}} = \begin{pmatrix} 0 & (N^{\tilde{\psi}}_{M_h})_3 & -(N^{\tilde{\psi}}_{M_h})_2 \\ -(N^{\tilde{\psi}}_{M_h})_3 & 0 & (N^{\tilde{\psi}}_{M_h})_1 \\ (N^{\tilde{\psi}}_{M_h})_2 & -(N^{\tilde{\psi}}_{M_h})_1 & 0 \end{pmatrix}$$

is the matrix representation of the cross product with the vector $-N^{\tilde{\psi}}_{M_h}$. In our experiments, both tensors, $S^{\psi}_{M_h}$ and $\mathcal{S}^{\psi}_{M_h}$, converge to $S(x)$ with the same order as $\bar{S}^{\psi}_{M_h}$ and $\hat{S}^{\psi}_{M_h}$ converge to $\bar{S}(x)$ and $\hat{S}(x)$, see Table 2.2.

The third example is concerned with the approximation of the shape operator from polyhedral surfaces that are corrupted by noise and are no longer inscribed. We consider the shape operator at a point x on the helicoid in $\mathbb{R}^3$ and compute the tensor $S^{\psi}_{M_h}$ (in the same way as in the second example) on inscribed polyhedral surfaces. Then we disturb the polyhedral surfaces by adding random noise of order h^2 to the vertex positions and compute the operator again. We denote the operator computed from the distorted surface by $S^{\psi}_{M_h,noise}$. In our experiments, we found the same order of convergence for both operators, see Table 2.3. In addition, the table lists approximation errors and eoc for the tensors $S^{\tilde{\psi}}_{M_h}$ and $S^{\tilde{\psi}}_{M_h,noise}$ which were computed on the same surfaces but using the function $\tilde{\psi}$, see (2.53), instead of ψ. The main difference between $S^{\psi}_{M_h}$ and $S^{\tilde{\psi}}_{M_h}$ is that the regions on the surfaces that is used to compute $S^{\psi}_{M_h}$ and $S^{\psi}_{M_h,noise}$ is larger than the regions used to estimate $S^{\tilde{\psi}}_{M_h}$ and $S^{\tilde{\psi}}_{M_h,noise}$; the support of ψ is of order $\sqrt{h}$ and the support of $\tilde{\psi}$ is of order h. When computed from the surface without noise, the tensor $S^{\tilde{\psi}}_{M_h}$ converges to $S(x)$ (even with order 2 in our experiments), but when computed from the corrupted surface, the tensor $S^{\tilde{\psi}}_{M_h}$ does no longer converge.

3

Laplace–Beltrami operator and Willmore energy

3.1 Strong and weak form of the Laplace–Beltrami operator

The Laplace–Beltrami operator is a linear second-order differential operator on a Riemannian manifold. We distinguish between two forms of the operator, the strong (or classical) form and the weak form. For simplicity, we denote both, the strong and the weak Laplace–Beltrami operator, by Δ and rely on the context to make the distinction. The strong Laplace–Beltrami operator on a smooth surface M is defined by

$$\begin{aligned} \Delta : C^2(M) &\mapsto C^0(M) \\ u &\mapsto \operatorname{div} \operatorname{grad} u. \end{aligned}$$

Since evaluating Δu at a point of M involves derivatives of the metric, the definition of the strong form of Δ does not hold for polyhedral surfaces. In contrast, the weak form requires less regularity of the surface and can be defined on polyhedral surfaces.

The weak Laplace–Beltrami operator on a smooth or polyhedral surface $\mathcal{M}$ is the continuous linear operator that maps any $u \in H^1(\mathcal{M})$ to the distribution Δu, which lies in $H^1(\mathcal{M})'$, the (topological) dual space of $H^1(\mathcal{M})$, and is given by

$$\langle \Delta u | \varphi \rangle = -\int_{\mathcal{M}} g(\operatorname{grad} u, \operatorname{grad} \varphi) \, \mathrm{d}vol \tag{3.1}$$

for all $\varphi \in H^1(\mathcal{M})$. Here $\langle \cdot | \cdot \rangle$ denotes the pairing of $H^1(\mathcal{M})'$ and $H^1(\mathcal{M})$. The weak form is a generalization of the strong form in the sense that for any

$u \in C^2(M)$, the strong Laplace–Beltrami operator of u is the unique continuous function Δu that satisfies

$$\int_M \Delta u \, \varphi \, dvol = -\int_M g(\operatorname{grad} u, \operatorname{grad} \varphi) \, \mathrm{d}vol$$

for all $\varphi \in H^1(M)$.

3.1.1 A Dirichlet problem

Poisson's equation on a smooth surface M is

$$-\Delta u = f, \tag{3.2}$$

where $u \in C^2(M)$ and $f \in C^0(M)$. The mean value $\bar{u}$ of a function u is

$$\bar{u} = \int_{\mathcal{M}} u \, \mathrm{d}vol. \tag{3.3}$$

Since the mean value of Δu vanishes for all u, a necessary condition on the existence of a solution to (3.2) is that the mean value of f vanishes. The weak form of the Dirichlet problem of Poisson's equation can be formulated for polyhedral surfaces: for any $f \in L^2(\mathcal{M})$ with vanishing mean value, find a $u \in H^1(\mathcal{M})$ such that

$$-\langle \Delta u | \varphi \rangle = \langle f, \varphi \rangle_{L^2} \tag{3.4}$$

holds for all $\varphi \in H^1(\mathcal{M})$. Since the constant functions are in the kernel of Δ, we additionally impose the condition

$$\bar{u} = 0.$$

Then the Dirichlet problem has a unique solution u for any f that satisfies the assumptions mentioned above. For a proof and an analysis of the problem on polyhedral surfaces, including regularity and stability of the solution, we refer to [106].

3.2 Approximation of the weak Laplace–Beltrami operator

In [64], it was shown that if a sequence of polyhedral normal graphs converges to a smooth surface in the Hausdorff distance, then convergence of the normal vectors is equivalent to the convergence of the weak Laplace–Beltrami operators. Based on this result, we derive explicit approximation estimates for the weak Laplace–Beltrami operator in the operator norm.

Let us consider a polyhedral surface M_h that is a normal graph over a smooth surface M. From Section 1.5, we know that the pullback of functions is an

isomorphism of the Sobolev spaces $H^1(M)$ and $H^1(M_h)$. Thus, we can pullback the operator Δ_{M_h} to M by setting

$$\langle \Delta_h u | \varphi \rangle = \langle \Delta_{M_h} u \circ \Psi | \varphi \circ \Psi \rangle$$

for any $\varphi \in H^1(M)$. By means of the metric distortion tensor A and the area distortion α, the operator Δ_h can be represented as

$$\langle \Delta_h u | \varphi \rangle = -\int_M g(A^{-1}\mathrm{grad}\, u, \mathrm{grad}\, \varphi)\alpha \, \mathrm{d}vol. \tag{3.5}$$

This follows from the relation of the weak gradients of M and M_h discussed in Section 1.5. The distance of Δ and Δ_h in the norm of the space of continuous linear operators from $H^1(M)$ to $H^1(M)'$ is

$$\|\Delta - \Delta_h\|_{Op} = \sup_{u,\varphi} |\langle (\Delta - \Delta_h)\, u | \varphi \rangle| \,,$$

where the supremum is taken over all $u, \varphi \in H^1(M)$ with $\|u\|_{H^1} = \|\varphi\|_{H^1} = 1$. Using the representation (3.5) of Δ_h, we get

$$\begin{aligned} \|\Delta - \Delta_h\|_{Op} &= \sup_{u,\varphi} \left| \int_M g((\alpha\, A^{-1} - Id)\mathrm{grad}\, u, \mathrm{grad}\, \varphi)\, \mathrm{d}vol \right| \\ &\leq \left\| \alpha\, A^{-1} - Id \right\|_\infty . \end{aligned}$$

We have already established an upper bound on the last term in Theorem 1.22. Hence, we obtain an approximation estimate for $\|\Delta - \Delta_h\|_{Op}$ that we summarize in the following theorem.

Theorem 3.1 (approximation of weak Laplace–Beltrami operator) *Let M be a smooth surface in $\mathbb{R}^3$. Then for every $\epsilon \in (0,1)$ there exists a constant C, such that for every polyhedral surface M_h that is an ϵ-normal graph over M, the estimate*

$$\|\Delta - \Delta_h\|_{Op} \leq C\, (\delta(M, M_h) + \|N - N_h\|^2_{L^\infty})$$

holds. The constant C depends only on ϵ.

By combining the theorem with Lemma 1.24, we obtain the following corollary for the case of inscribed polyhedral surfaces.

Corollary 3.2 *Let M be a smooth surface in $\mathbb{R}^3$. Then there exists a $h_0 \in \mathbb{R}^+$ such that for every polyhedral surface M_h that is inscribed to M and has mesh size $h < h_0$, the estimates*

$$\|\Delta - \Delta_h\|_{Op} \leq C\, h^2$$

holds, where the constant C depends only on M, h_0, and the shape regularity ρ of M_h.

3.3 Discrete weak Laplace–Beltrami operator

Let S_h denote the finite dimensional subspace of $H^1(M_h)$ consisting of all continuous functions on M_h that are linear over each triangle. Let n be the number of vertices of M_h, and let $\{v_1, v_2, ..., v_n\}$ be the (ordered) set of vertices. For any function $u_h \in S_h(M_h)$, the vector

$$(u_h(v_1), u_h(v_2), ..., u_h(v_n)) \in \mathbb{R}^n$$

is called the *nodal vector*. The mapping between functions in $S_h(M_h)$ and their nodal vectors is a linear isomorphism of S_h and $\mathbb{R}^n$. The Lagrange basis $\{\psi_i\}_{i\in\{1,2,...,n\}}$ of $S_h(M_h)$ consists of the functions whose nodal vectors are the standard basis vectors of $\mathbb{R}^n$.

Now, we construct a discrete weak Laplace–Beltrami operator. The idea behind the construction is to restrict both arguments of $\langle \Delta_{M_h} \cdot | \cdot \rangle$ to functions in S_h. The discrete weak Laplace–Beltrami operator is the linear map

$$\begin{aligned} S_h &\mapsto S_h' \\ u_h &\mapsto \Delta_{M_h} u_{h|S_h}, \end{aligned}$$

where S_h' is the dual space of S_h and $\Delta_{M_h} u_{h|S_h}$ is the restriction of the functional $\Delta_{M_h} u_h \in H^1(\mathcal{M})'$ to S_h. The matrix representation S of the negative of the discrete operator (with respect to the Lagrange basis and the corresponding dual basis of S_h') has the components

$$S_{ij} = \int_{M_h} g_{M_h} \left(\operatorname{grad}_{M_h} \psi_i, \operatorname{grad}_{M_h} \psi_j \right) \mathrm{d}vol_{M_h}.$$

Since the support of any Lagrange basis function ψ_i is the star of the vertex v_i, the component S_{ij} vanishes if $v_j \notin \operatorname{star}(v_i)$. Hence, S is a sparse matrix. Furthermore, the non-vanishing entries S_{ij} depend only on the cotangents of the inner angles of the triangles. For this reason the discrete operator is known as the *cotan Laplacian* and the matrix S as the *cotan matrix*. The cotan weights appear in the work of Pinkall and Polthier [91] on the construction of discrete minimal surfaces and earlier in the work of MacNeal [76] and Duffin [42] on numerical solutions to partial differential equations on planar domains. Explicitly, for two vertices v_i and v_j that share an edge, the entry S_{ij} is given by

$$S_{ij} = -\frac{1}{2}(\cot \alpha_{ij} + \cot \beta_{ij}),$$

where α_{ij} and β_{ij} are the angles opposite to the edge (v_i, v_j) (as illustrated in Figure 3.1). The diagonal entries are

$$S_{ii} = -\sum_{j, j\neq i} S_{ij},$$

where the sum runs over all j such that v_i and v_j share an edge. The last equation implies that for every row of S, the sum of all components vanishes. This is a consequence of the fact that the constant functions are in the kernel of the (weak) Laplace–Beltrami operator.

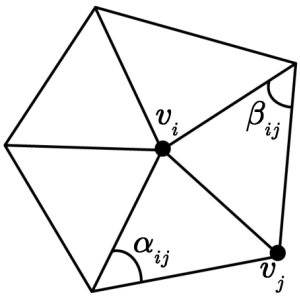

FIGURE 3.1. The definition of the angles α_{ij} and β_{ij} is illustrated.

3.3.1 Discrete Dirichlet problem

The discrete analog of the Dirichlet problem (3.4) is: for any $f \in L^2(M_h)$ with $\bar{f} = 0$, find the function $u_h \in S_h$ that satisfies

$$-\langle \Delta_{M_h} u_h | \varphi_h \rangle = \langle f, \varphi_h \rangle_{L^2} \tag{3.6}$$

for all $\varphi_h \in S_h(M_h)$ and

$$\bar{u}_h = 0. \tag{3.7}$$

The existence and uniqueness of a solution follows from the fact that the kernel of the weak Laplace–Beltrami operator is the one-dimensional space of constant functions. For error estimates on the approximation of the solution of the Dirichlet problem on a smooth surface by a corresponding discrete problem on a polyhedral surface, we refer to [44] and [64].

3.4 Pointwise approximation

In this section, we show how the weak Laplace–Beltrami operator on a polyhedral surface can be used for a pointwise approximation of the strong Laplace–Beltrami operator on a nearby smooth surface. This result is the basis for the construction of the discrete Laplace–Beltrami operators in the next section. Before we state the theorem, we prove an approximation estimate for the gradient of a function by the gradient of an interpolating function.

Let us consider a polyhedral surface M_h that is inscribed to a smooth surface M. As before, we denote by Ψ the restriction to M_h of the orthogonal projection onto M and by Φ its inverse. For brevity, we denote by $\hat{u} = u \circ \Phi$

the pullback to M of a function u on M_h. Let $\hat{S}_h$ be the space that contains any function $\hat{v} \in H^1(M)$ that is a pullback of a function v in S_h. For any continuous function u on M, there are unique functions $u_h \in S_h$ and $\hat{u}_h \in \hat{S}_h$ that interpolate u at the vertices of M_h. The following lemma provides an estimate for the interpolation error, which we will use later in the approximation theorem.

Lemma 3.3 *Let $u \in C^2(M)$ and let $\hat{u}_h \in \hat{S}_h$ be the interpolant of u. Then*

$$\|grad\,(u - \hat{u}_h)\|_{L^\infty} \leq C\,h(|u|_{C^2} + h\;|u|_{C^1}), \tag{3.8}$$

where the constant C depends only on M and the shape regularity of M_h.

Proof. Consider a triangle T_h of M_h and let $T \subset M$ be the projection of T_h onto M. Then $u \circ \Psi\,_{|T_h}$ is in $C^2(T_h)$ and $u_h\,_{|T_h}$ is the linear function that interpolates u at the vertices of T_h. Since T_h is a flat triangle, we can use standard estimates for the approximation error

$$\left\|\mathrm{grad}_{M_h}\,(u \circ \Psi - u_h)\right\|_{L^\infty(T_h)} \leq C\,h\;|u \circ \Psi|_{C^2(T_h)}\,.$$

Furthermore,

$$\begin{aligned}
&\|\mathrm{grad}\,(u - \hat{u}_h)\|_{L^\infty(T)} \\
&\leq \|A\|_\infty^{-\frac{1}{2}} \left\|\sqrt{g(A^{-1}\mathrm{grad}\,(u - \hat{u}_h), \mathrm{grad}\,(u - \hat{u}_h))}\right\|_{L^\infty(T)} \\
&= \|A\|_\infty^{-\frac{1}{2}} \left\|\mathrm{grad}_{M_h}\,(u \circ \Psi - u_h)\right\|_{L^\infty(T_h)}
\end{aligned}$$

and it can be shown, see [44, Lemma 3] and [106, Lemma 3.3.1], that

$$|u \circ \Psi|_{C^2(T_h)} \leq C(|u|_{C^2(T)} + h\;|u|_{C^1(T)}).$$

Since the estimates hold for all triangles of M_h, we have verified (3.8).

□

Our approach to obtain a pointwise approximation is to test the weak Laplace–Beltrami operator with r-local functions, which we introduced in Section 2.3. Slightly different from the last chapter, here we will consider r-local functions that are elements of H^1 (and not only of $W^{1,1}$). This is necessary since we defined the weak Laplacian as an operator on H^1. The construction of r-local functions described in Section 2.6.1 can be used to construct r-local functions that are in H^1, as well. The only change in the construction is that the function ϕ, which is the basis of the construction, has to be in H^1 instead of $W^{1,1}$. The explicit examples of r-local functions derived in Section 2.6.3, the hat functions, are also in H^1.

Theorem 3.4 (pointwise approximation) *Let M be a smooth surface in $\mathbb{R}^3$ and let u be a smooth function on M. Then there exists a $h_0 \in \mathbb{R}^+$ such that for every pair consisting of a polyhedral surface M_h that is inscribed to M and satisfies $h < h_0$ and a function φ that is r-local at a point $y \in M_h$, the estimate*

$$|\Delta u(x) - \langle \Delta_{M_h} u_h | \varphi \rangle| \leq C(r + \frac{h}{r}) \tag{3.9}$$

holds, where $u_h \in S_h(M_h)$ is the interpolant of u and $x = \Psi(y)$. If $\hat{\varphi}$ has the r^2-property (with respect to a constant C_Q), then the bound improves to

$$|\Delta u(x) - \langle \Delta_{M_h} u_h | \varphi \rangle| \leq C(r^2 + \frac{h}{r}). \tag{3.10}$$

The constants C depend only on M, u, h_0, the shape regularity ρ of M_h, and the constants C_D and C_Q of φ.

Proof. The operator Δ_{M_h} and the functions u_h and φ are defined on M_h. First, we pullback Δ_{M_h}, u_h, and φ to M, add some zeros, and use the Cauchy–Schwarz inequality to get

$$\begin{aligned} &|\Delta u(x) - \langle \Delta_{M_h} u_h | \varphi \rangle| = |\Delta u(x) - \langle \Delta_h \hat{u}_h | \hat{\varphi} \rangle| \\ &\leq |\Delta u(x) - \langle \Delta u | \hat{\varphi} \rangle| + |\langle \Delta(u - \hat{u}_h) | \hat{\varphi} \rangle| + |\langle (\Delta - \Delta_h)\hat{u}_h | \hat{\varphi} \rangle| \,. \end{aligned} \tag{3.11}$$

In the following, we derive bounds for each of the three summands of the right-hand side of (3.11). Let us start with the first summand. Since the support of the function φ is contained in the geodesic ball $B_r(y)$, the support of $\hat{\varphi}$ is contained in the $B_{\|A\|_\infty^{1/2} r}(x)$. It follows from Lemma 1.25 that there is a constant C, which depends only on M and h_0, such that $\hat{\varphi}$ satisfies property (D3) for the point x and the radius $C\,r$. Thus, $\hat{\varphi} / \|\hat{\varphi}\|_{L^1}$ satisfies the requirements of Lemma 2.7 and we get

$$\begin{aligned} &|\Delta u(x) - \langle \Delta u | \hat{\varphi} \rangle| \\ &\leq \left| \Delta u(x) - \frac{1}{\|\hat{\varphi}\|_{L^1}} \langle \Delta u | \hat{\varphi} \rangle \right| + \left| (1 - \|\hat{\varphi}\|_{L^1}) \frac{1}{\|\hat{\varphi}\|_{L^1}} \langle \Delta u | \hat{\varphi} \rangle \right| \\ &\leq C(r + h^2). \end{aligned}$$

In the last step, we use the estimate

$$|1 - \|\hat{\varphi}\|_{L^1}| \leq C\,h^2,$$

which follows by combining Lemmas 1.16 and 1.25 and our assumption that $\|\varphi\|_{L^1(M_h)} = 1$.

If $\hat{\varphi}$ satisfies the r^2-property, then using (2.15) instead of Lemma 2.7 yields

$$|\Delta u(x) - \langle \Delta u | \hat{\varphi} \rangle| \leq C(r^2 + h^2).$$

To establish a bound on the second summand, we show that the bound

$$\left\|\operatorname{grad}_{M_h}\varphi\right\|_{L^1(M_h)} \leq C\frac{1}{r}$$

holds for $\|\operatorname{grad}\hat{\varphi}\|_{L^1}$ as well

$$\begin{aligned}
&\|\operatorname{grad}\hat{\varphi}\|_{L^1} = \int_M \|\operatorname{grad}\hat{\varphi}\|_g \,\mathrm{d}vol \\
&\leq \left\|\alpha\, A^{-1}\right\|_\infty^{-\frac{1}{2}} \int_M \sqrt{g(A^{-1}\operatorname{grad}\hat{\varphi}, \operatorname{grad}\hat{\varphi})}\alpha \,\mathrm{d}vol \\
&= \left\|\alpha\, A^{-1}\right\|_\infty^{-\frac{1}{2}} \left\|\operatorname{grad}_{M_h}\varphi\right\|_{L^1(M_h)} \\
&\leq C\frac{1}{r}.
\end{aligned}$$

Then we apply Hölder's inequality and Lemma 3.3 to get

$$\begin{aligned}
&|\langle\Delta(u-\hat{u}_h)|\hat{\varphi}\rangle| = \left|\int_M g(\operatorname{grad}(u-\hat{u}_h), \operatorname{grad}\hat{\varphi})\,\mathrm{d}vol\right| \\
&\leq \|\operatorname{grad}(u-\hat{u}_h)\|_{L^\infty} \|\operatorname{grad}\hat{\varphi}\|_{L^1} \leq C\,\frac{h}{r}.
\end{aligned}$$

A bound on the third summand follows from estimate (1.41) of Lemma 1.25 and Lemma 3.3

$$\begin{aligned}
&\left|\left\langle(\Delta-\hat{\Delta}_h)\hat{u}_h|\hat{\varphi}\right\rangle\right| \\
&= \left|\int_M g((Id-\alpha\ A^{-1})\operatorname{grad}\hat{u}_h, \operatorname{grad}\hat{\varphi})\,\mathrm{d}vol\right| \\
&\leq \left\|Id-\alpha\ A^{-1}\right\|_\infty \|\operatorname{grad}\hat{u}_h\|_{L^\infty} \|\operatorname{grad}\hat{\varphi}\|_{L^1} \\
&\leq C\,\frac{h^2}{r}.
\end{aligned}$$

This bound is quadratic in h and therefore small compared to the bound on the second summand. The combination of the bounds on the three summands completes the proof. □

The theorem is stated in a general setting that assumes no correlation of r and h. The following corollary shows how to choose r to get the optimal approximation order in h.

Corollary 3.5 *Under the assumptions of Theorem 3.4, if* $r = \sqrt{h}$, *then*

$$|\Delta u(x) - \langle\Delta_{M_h} u_h|\varphi\rangle| \leq C\sqrt{h},$$

and if $\hat{\varphi}$ *satisfies (2.15) and* $r = h^{\frac{1}{3}}$, *then*

$$|\Delta u(x) - \langle\Delta_{M_h} u_h|\varphi\rangle| \leq C\,h^{\frac{2}{3}}.$$

3.5 Discrete strong Laplace–Beltrami operators

Based on the approximation results in the last section, we derive a principle for the construction of discrete Laplace–Beltrami operators on polyhedral surfaces that are consistent discretizations of the strong Laplace–Beltrami operator. Then we discuss matrix representations of the operators and compare the consistency rates of our approach and the mesh Laplacian.

In contrast to the discrete weak Laplace–Beltrami operators, which map functions onto functionals, the discrete strong Laplace–Beltrami operators are endomorphisms of S_h. We will describe the discrete strong Laplace–Beltrami operators by their action on the nodal vectors. Let $\{\varphi_i\}_{i\in\{1,2,..n\}}$ be a set of functions such that every φ_i is r-local at the vertex $v_i \in M_h$. Then we define the discrete Laplace–Beltrami operator $\Delta_{M_h}^{\{\varphi_i\}}$ associated to $\{\varphi_i\}$ as

$$\begin{aligned} \Delta_{M_h}^{\{\varphi_i\}} &: S_h \mapsto S_h \\ \begin{pmatrix} u_h(v_1) \\ u_h(v_2) \\ \dots \\ u_h(v_n) \end{pmatrix} &\mapsto \begin{pmatrix} \langle \Delta_{M_h} u_h | \varphi_1 \rangle \\ \langle \Delta_{M_h} u_h | \varphi_2 \rangle \\ \dots \\ \langle \Delta_{M_h} u_h | \varphi_n \rangle \end{pmatrix}. \end{aligned}$$

For each φ_i there is a constant $C_{D,i}$ such that (D5) of Definition 2.6 is satisfied. In the following, we refer to the maximum of the $C_{D,i}$ as the constant C_D of $\{\varphi_i\}$. Similarly, if every $\varphi_i \circ \Phi$ has the r^2-property with respect to a constant $C_{Q,i}$, we denote by C_Q the maximum of the $C_{Q,i}$.

Theorem 3.6 (consistency of discrete operator) *Let M be a smooth surface in $\mathbb{R}^3$, and let u be a smooth function on M. Then there exists a $h_0 \in \mathbb{R}^+$ such that for every pair consisting of a polyhedral surface M_h that is inscribed to M and satisfies $h < h_0$ and a set of functions $\{\varphi_i\}_{i\in\{1,2,..n\}}$ such that every φ_i is r-local at the vertex $v_i \in M_h$ with $r = \sqrt{h}$, the estimate*

$$\sup_{y\in M_h} \left| \Delta u(\Psi(y)) - \Delta_{M_h}^{\{\varphi_i\}} u_h(y) \right| \leq C\sqrt{h} \tag{3.12}$$

holds, where $u_h \in S_h(M_h)$ is the interpolant of u. If every $\hat{\varphi}_i$ has the r^2-property and $r = h^{\frac{1}{3}}$, then we have

$$\sup_{y\in M_h} \left| \Delta u(\Psi(y)) - \Delta_{M_h}^{\{\varphi_i\}} u_h(y) \right| \leq C\, h^{\frac{2}{3}}. \tag{3.13}$$

The constants C depend only on M, u, h_0, the shape regularity ρ of M_h, and the constants C_D and C_Q of $\{\varphi_i\}$.

Proof. Let $v \in S_h$ and $\hat{v} \in \hat{S}_h$ be the interpolants on M_h and M of the function Δu. Then the approximation error satisfies (analogously to Lemma 3.3)

$$\|\Delta u - \hat{v}\|_{L^\infty} \leq C\, h^2 (|\Delta u|_{C^2} + h\ |\Delta u|_{C^1}). \tag{3.14}$$

Theorem 3.4 implies

$$|\Delta u(\Psi(v_i)) - \langle \Delta_{M_h} u_h | \varphi_i \rangle| \leq C\sqrt{h} \tag{3.15}$$

for all i. Since $v(v_i) = \hat{v}(v_i) = \Delta u(\Psi(v_i))$, we have

$$\left\| v - \Delta_{M_h}^{\{\varphi_i\}} u_h \right\|_{L^\infty} \leq C\sqrt{h}. \tag{3.16}$$

Combining (3.14) and (3.16) shows (3.12). A similar argumentation proves the second estimate. □

3.5.1 Matrix representation

We show how the cotan matrix can be used to construct the matrix representation L of $\Delta_{M_h}^{\{\varphi_i\}}$ with respect to the nodal basis. For simplicity, we assume that the φ_i are functions in S_h. Let S denote the cotan matrix and let Φ be the matrix with entries $\Phi_{ij} = \varphi_i(v_j)$. Then L is the sparse matrix given by

$$L = -\Phi\, S. \tag{3.17}$$

The number of entries of L depends on the number of vertices that are in the support of the functions φ_i. When comparing (3.17) to the construction of discrete Laplacians (as described in [107]), we see that Φ takes the role of the inverse mass matrix.

In general, the matrix Φ is not symmetric. But, Φ that are symmetric can be constructed. The matrix can be decomposed into a symmetric and an antisymmetric part

$$\Phi = \Phi^{sym} + \Phi^{asym} = \frac{1}{2}(\Phi + \Phi^T) + \frac{1}{2}(\Phi - \Phi^T),$$

where Φ^T denotes the transpose of Φ. For certain choices of r-local functions $\{\varphi_i\}$, the entries of Φ^{asym} are small compared to the entries of Φ^{sym}. For example, if we use the geodesic or extrinsic hat functions (see Section 2.6) with the same value of r at all vertices. Then it is justified to use

$$L = -\Phi^{sym}\, S,$$

instead of (3.17).

3.5.2 Comparison with the mesh Laplacian

An alternative to our construction of a consistent discrete strong Laplace–Beltrami operator is the *mesh Laplacian* that was proposed by Belkin, Sun, and Wang in [13]. It is based on a discretization of the heat kernel of an embedded

surface. In [14], it is shown that under the assumption that a polyhedral surface is an ϵ-sample of a smooth surface, the consistency error of the mesh Laplacian is bounded by $\mathcal{O}(\frac{\epsilon}{t^2} + t^{\frac{1}{2}})$. Here ϵ denotes the sampling density and t is a parameter that controls the width of the heat kernels. Then the optimal choice $t = \epsilon^{\frac{2}{5}}$ yields a consistency order of $\epsilon^{\frac{1}{5}}$. Under our assumption that the shape regularity of the polyhedral surface is bounded, $\epsilon \sim h$ and the rate can be compared to our results. We want to remark that we are only comparing the bounds that have been proven. As far as we know, it is unclear for both discrete operators, whether the established bounds are optimal.

3.6 Willmore energy

The Willmore energy of a smooth surface M in $\mathbb{R}^3$ is

$$W(M) = \int_M H^2 \mathrm{d}vol, \tag{3.18}$$

where H denotes the mean curvature of M. The mean curvature is connected to the Laplace–Beltrami operator by

$$\mathbf{H} = HN = \Delta I, \tag{3.19}$$

where I is the embedding of M in $\mathbb{R}^3$ and N is the surface normal field. The vector field $H\,N$ is called the mean curvature vector field. Then the Willmore energy of M equals the squared L^2-norm of ΔI. Let $I_{M_h} : M_h \mapsto \mathbb{R}^3$ denote the embedding of the polyhedral surface M_h. Each of the three components of I_{M_h} is a function in S_h. Thus, we can define the discrete mean curvature vector associated to a discrete Laplacian $\Delta_{M_h}^{\{\varphi_i\}}$ analogous to (3.19) by

$$\mathbf{H}_{M_h}^{\{\varphi_i\}} = \Delta_{M_h}^{\{\varphi_i\}} I_{M_h}.$$

If M_h is inscribed to M, Theorem 3.6 implies

$$\sup_{y \in M_h} \|\mathbf{H}(\Psi(y)) - \mathbf{H}_{M_h}^{\{\varphi_i\}}(y)\|_{\mathbb{R}^3} \leq C\sqrt{h} \;\; (\text{resp. } C\,h^{\frac{2}{3}}).$$

We define the discrete Willmore energy of M_h and $\{\varphi_i\}$ analogous to (3.18) as

$$W_{M_h}^{\{\varphi_i\}}(M_h) = \|\mathbf{H}_{M_h}^{\{\varphi_i\}}\|_{L^2(M_h)}^2.$$

The following theorem shows consistency of the discrete Willmore energies.

Theorem 3.7 (consistency of discrete Willmore energies) *Let M be a smooth surface in $\mathbb{R}^3$. Then there exists a $h_0 \in \mathbb{R}^+$ such that for every pair*

consisting of a polyhedral surface M_h that is inscribed to M and satisfies $h < h_0$ and a set of functions $\{\varphi_i\}_{i\in\{1,2,..n\}}$ such that every φ_i is r-local at the vertex $v_i \in M_h$ with $r = \sqrt{h}$, the estimate

$$\left|W(M) - W_{M_h}^{\{\varphi_i\}}(M_h)\right| \leq C\sqrt{h}$$

holds. If every $\hat{\varphi}_i$ has the r^2-property and $r = h^{\frac{1}{3}}$, then we have

$$\left|W(M) - W_{M_h}^{\{\varphi_i\}}(M_h)\right| \leq C\, h^{\frac{2}{3}}.$$

The constants C depend only on M, h_0, the shape regularity ρ of M_h, and the constants C_D and C_Q of $\{\varphi_i\}$.

Proof. To compare $\mathbf{H}$ and $\mathbf{H}_{M_h}^{\{\varphi_i\}}$, we consider the vector field $\mathbf{H}_h^{\{\varphi_i\}} \in \hat{S}_h^3$ given by $\mathbf{H}_h^{\{\varphi_i\}} \circ \Psi = \mathbf{H}_{M_h}^{\{\varphi_i\}}$. We split the approximation error in two terms: the first term measures the difference of $\mathbf{H}$ and $\mathbf{H}_h^{\{\varphi_i\}}$, and the second term measures the difference of the L^2-norms of M and M_h

$$\begin{aligned}
&\left|W(M) - W_{M_h}^{\{\varphi_i\}}(M_h)\right| = \left|\|\mathbf{H}\|_{L^2(M)}^2 - \|\mathbf{H}_{M_h}^{\{\varphi_i\}}\|_{L^2(M_h)}^2\right| \\
&\leq \left|\|\mathbf{H}\|_{L^2(M)}^2 - \|\mathbf{H}_h^{\{\varphi_i\}}\|_{L^2(M)}^2\right| + \|1-\alpha\|_{L^\infty(M)}\, \|\mathbf{H}_h^{\{\varphi_i\}}\|_{L^2(M)}^2 \\
&\leq \|\mathbf{H} - \mathbf{H}_h^{\{\varphi_i\}}\|_{L^\infty(M)} \|\mathbf{H} + \mathbf{H}_h^{\{\varphi_i\}}\|_{L^1(M)} + C\, h^2 \|\mathbf{H}_h^{\{\varphi_i\}}\|_{L^2(M)}^2.
\end{aligned}$$

Here, we use Hölder's inequality and Lemma 1.25 in the last step. By Theorem 3.6, the term

$$\|\mathbf{H} - \mathbf{H}_h^{\{\varphi_i\}}\|_{L^\infty(M)} = \sup_{y\in M_h} \|\Delta I(\Psi(y)) - \Delta_{M_h}^{\{\varphi_i\}} I_{M_h}(y)\|$$

is bounded by $C\sqrt{h}$, resp. $C\, h^{\frac{2}{3}}$. Furthermore, Theorem 3.6 guarantees that there are upper bounds for $\|\mathbf{H} + \mathbf{H}_h^{\{\varphi_i\}}\|_{L^1(M)}$ and $\|\mathbf{H}_h^{\{\varphi_i\}}\|_{L^2(M)}^2$. □

Remark 3.8 *We want to remark that a similar construction of a consistent discrete Willmore energy can be established using the trace of the pointwise approximation of the shape operators, which is discussed in Section 2.4, to approximate the mean curvature.*

3.7 Experiments

In this section, we show results of experiments concerning the consistency error and the consistency order. For a parametrized surface M, we consider inscribed polyhedral surfaces with decreasing mesh size h and approximate the mean

h	$\|\mathbf{H}(x) - \mathbf{H}_h^{\varphi\,\sqrt[3]{h}}\|$	eoc	$\|\mathbf{H}(x) - \mathbf{H}_h^{\varphi\,\sqrt{h}}\|$	eoc
0.9907594	0.1473438	–	0.1655998	–
0.4072441	0.0718663	0.81	0.0816863	0.79
0.1376594	0.0343882	0.68	0.0439559	0.57
0.0407502	0.0151471	0.67	0.0238574	0.50
0.0111478	0.0063759	0.67	0.0126259	0.49
0.0042305	0.0033417	0.67	0.0078440	0.49
0.0015209	0.0016897	0.67	0.0047346	0.49

h	$\|\mathbf{H}(x) - \mathbf{H}_h^{\varphi\,\sqrt[3]{h}}\|$	eoc	$\|\mathbf{H}(x) - \mathbf{H}_h^{\varphi_h}\|$	eoc
0.1819730	0.1159240	–	0.0681956	–
0.0615573	0.0469350	0.83	0.6798970	−2.10
0.0182239	0.0206826	0.67	0.0328904	2.50
0.0049855	0.0087871	0.66	0.5920200	−2.20
0.0018919	0.0045958	0.67	0.1372740	1.50
0.0006802	0.0023197	0.67	0.0918593	0.39
0.0002655	0.0012393	0.67	0.1451020	−0.49

TABLE 3.1. Approximation errors and the experimental orders of convergence for the approximation of the mean curvature vector at a point of a smooth surface are shown.

curvature vector of M at a point $x \in M$ by $\mathbf{H}_{M_h}^{\varphi_r} = \langle \Delta_{M_h} I_{M_h} | \varphi_r \rangle$, where $\varphi_r \in S_h$ is a r-local function on M_h. The tables show the approximation error and the experimental order of convergence, see (2.52). In the first example, we consider a torus of revolution. The upper part of Table 3.1 shows the approximation error $\left\| \mathbf{H}(x) - \mathbf{H}_{M_h}^{\varphi_r} \right\|_{\mathbb{R}^3}$ obtained with two different types of r-local functions and confirms both estimates of Theorem 3.4. The first function is (a piecewise linear approximation of) the extrinsic hat function (see Section 2.6). It is given by

$$\varphi_r = \frac{\tilde{\varphi}_r}{\|\tilde{\varphi}_r\|_{L^1}}, \tag{3.20}$$

h	$W_h^{\{\varphi_i\}}(M_h)$	$\left\|W(M) - W_h^{\{\varphi_i\}}(M_h)\right\|$	eoc
0.6181260	19.8617	2.931210	–
0.3542860	20.9932	1.799680	0.88
0.1909680	21.7347	1.058190	0.86
0.0973871	22.1986	0.594268	0.86
0.0491797	22.4605	0.332392	0.85
0.0247127	22.6066	0.186275	0.84
0.0123872	22.6876	0.105310	0.83
0.0062014	22.7327	0.060178	0.81

TABLE 3.2. Results for the approximation of the Willmore energy of a torus of revolution by a discrete Willmore energy.

where $\tilde{\varphi}_r$ is the function in S_h that at any vertex $v \in M_h$ takes the value

$$\tilde{\varphi}_r(v) = \max\{1 - \frac{\|x - v\|_{\mathbb{R}^3}}{r}, 0\}. \tag{3.21}$$

We set $r = h^{\frac{1}{3}}$ and due to the approximate symmetry of φ_r around x, we obtain an eoc of $h^{\frac{2}{3}}$. The second function sets $r = h^{\frac{1}{2}}$, and we disturb the symmetry around x by translating the center of the extrinsic hat function (away from x) by a random vector of length $\sqrt{h}/20$. The length of the vector is chosen such that the resulting function is still r-local around x but does not have the r^2-property anymore. In the experiments we get the expected eoc of $h^{\frac{1}{2}}$. This is an experimental indication that the bound (3.9) of Theorem 3.4 is sharp. Still, we would like to remark that in this experiment (and in many other similar settings) the eoc is h if we set $r = h^{\frac{1}{2}}$ and do not translate the center of the function. This raises the question of whether it is possible to improve the bound (3.10) of Theorem 3.4) for a special type of functions.

In the second example, we consider polyhedral surfaces that approximate the sphere, but the vertex positions are corrupted with random noise of order h^2. The lower part of Table 3.1 shows that for $r = h^{\frac{1}{3}}$ we still obtain the same eoc, whereas for $r = h$ there is no convergence.

In the third example, we approximate the Willmore energy of a torus of revolution by the discrete Willmore energy that we obtain by using functions of type (3.20) at each vertex of the polyhedral surface. Table 3.2 shows the consistency error and the eoc.

4
Constraint-based fairing

4.1 Fairness energies

Fairness energies are an attempt to establish quantitative measures for the fairness of a shape. Finding a commonly-accepted measure of fairness is a delicate task due to the inherent subjectivity of rating the appearance of a geometry as well as the specific demands of applications. Nevertheless, one can agree on some general criteria: a fairness energy should be independent of the parametrization of the surface, invariant under rigid motions and scaling, and spheres should be among the minimizers of the energy.

Different measures of fairness have been proposed. These can be classified by the order of the highest derivative of the surface needed to evaluate the energy. A first-order quantity that is invariant under reparametrizations and rigid motions is the area of a surface. Since the area is not invariant under scaling, Delingette [35] proposed using the isoperimetric ratio A^3/V^2 as a scale invariant first-order fairness measure for closed surfaces. Here A denotes the area and V is the volume enclosed by the surface. Second-order measures relate to curvature, such as integrals of squares of curvature terms. Prominent examples are the Willmore energy $\int H^2\,dA$, the total curvature $\int(\kappa_1^2+\kappa_2^2)\,dA$, and the energy $\int(\kappa_1-\kappa_2)^2\,dA$ (which many authors also refer to as the Willmore energy). Here κ_1 and κ_2 denote the principal curvatures and $H=\kappa_1+\kappa_2$ the mean curvature. An example of a third-order measure is the curvature variation energy proposed by Moreton and Sequin [79]. The Euler–Lagrange equation of this energy is of sixth order.

For our purposes, we need a fairness energy of at least second order, otherwise we can not expect a continuous minimizer due to the hard constraints. The three examples of second-order energies are closely related to each other. They differ only by a multiple of the integral of the Gauß curvature over the surface. By the Gauß–Bonnet theorem, this integral is constant for compact surfaces without boundary since it depends only on the topology of the surface. For compact surfaces with boundary, the integral of the Gauß curvature is invariant under variations that fix positions and normals at the boundary. Hence in both cases, the three energies have the same minimizers. Either of the three energies is a good candidate for our purposes. An alternative second-order fairness measure would be the integral of the squared Gauß curvature. But by Gauß' Theorema Egregium, this energy only depends on the metric of the surface, which rules out this energy. For example, take a piece of paper and bend it. There is no metric distortion; Gauß curvature does not change.

For our experiments, we use the discrete Willmore energy proposed by Wardetzky et al. [107], which can be derived using non-conforming Crouzeix–Raviart finite elements. The energy is a sum of contributions from hinge stencils

$$E(M) = \sum_{e \in M} \frac{3 \left\| e \right\|^2}{2 \, A_e} cos(\frac{\theta_e}{2})^2, \tag{4.1}$$

where A_e is the combined area of the two triangles adjacent to the edge e, and θ_e is the dihedral angle at e. The non-linear gradient of the energy can be computed efficiently; for an explicit formula see [107]. The reason we do not use the discrete Willmore energies developed in the previous chapter is that the experiments had already been finished before the energies were developed.

4.2 Constrained optimization problem

Our fairing method is modeled as a constrained non-linear optimization problem. The constraints assure that during the smoothing process no point of the surface deviates more than a prescribed distance from its initial position. The definition of the constraints involves a deviation measure that takes into account the maximum deviation. We first define the discrete maximum deviation measure, then describe the optimization problem.

For two polyhedral surfaces M and N that have the same connectivity, we define the discrete *maximum deviation measure* d_∞ as

$$d_\infty(M, N) = max_i \left\| m_i - n_i \right\|_{\mathbb{R}^3}, \tag{4.2}$$

where m_i and n_i are the vertices of M and N, respectively. The measure d_∞ describes a metric on the set of all polyhedral surfaces with fixed connectivity.

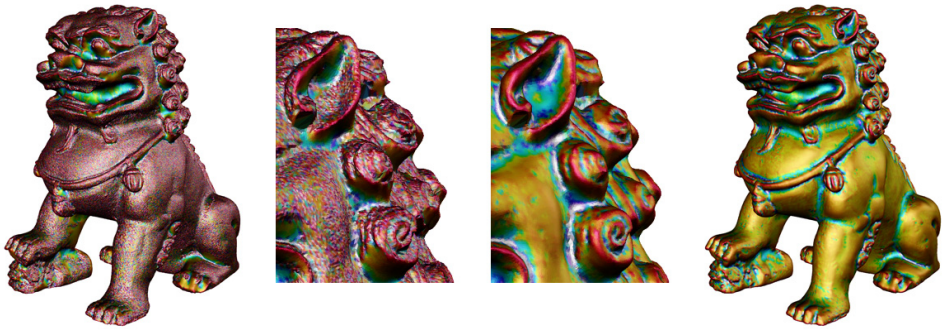

FIGURE 4.1. An original noisy scan of a Chinese lion with 1.3 m triangles and height about 10 cm (left). The smoothed mesh (right) stays within a 0.1 mm distance from the initial mesh. The surfaces are colored by mean curvature with colors ranging from white (negative curvature) to red (positive curvature).

Let $B_\epsilon(M)$ denote the closed ball with radius ϵ around M with respect to this metric. Geometrically speaking, N is in the set $B_\epsilon(M)$ if each vertex n_i of N lies in the ball of radius ϵ around the corresponding vertex m_i of M.

Now, we can state the optimization problem.

Problem 4.1 (constrained fairing) *Given a polyhedral surface M and a positive ϵ, find a polyhedral surface N that minimizes the discrete Willmore energy over all candidates $\widetilde{N} \in B_\epsilon(M)$.*

4.3 Minimization procedure

The constraints define a feasible region in $\mathbb{R}^3$ for every vertex. The shape of the region depends on which norm on $\mathbb{R}^3$ we use. In the case of the standard Euclidean norm, it is a sphere of radius ϵ. For the maximum norm, it is an axis aligned cube with side length 2ϵ. For our experiments, we use the maximum norm because the resulting constraints are box (or bound) constraints and there are many specialized optimization strategies for box constraints. *Active set Newton solvers* with gradient projection are among the most effective solvers for large-scale box constrained non-linear optimization problems. For a general introduction to active set and gradient projection methods we refer to [87]. For an analysis and discussion of solvers of this type for large-scale problems, see [75, 70] and references therein. First, we briefly describe the general scheme. Then, in Section 4.3.1, we discuss how to approximate the required second-order information in an efficient and robust way.

By listing the coordinates of all the vertices, we identify a polyhedral surface with a point in $\mathbb{R}^n$ where n equals three times the number of vertices. Let

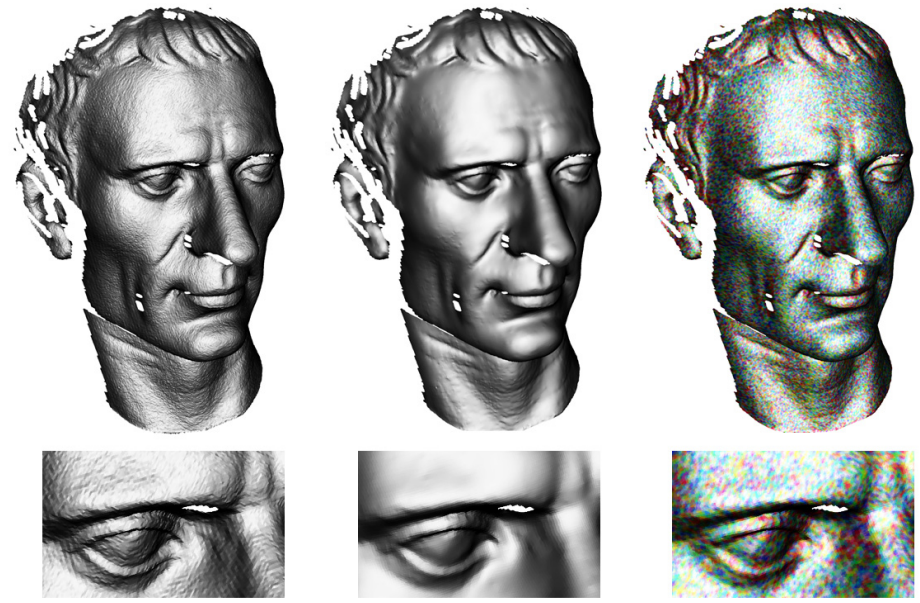

FIGURE 4.2. Noise removal from a range image. The maximum tolerance is 0.1 mm and the height of the object is 30 cm. The right image shows the smoothed surface colored by the distance between the initial (noisy) to the smoothed surface.

$x^0 \in \mathbb{R}^n$ be the point representing the initial surface. Then the feasible set $\Omega_{x^0,\epsilon}$ is the n-dimensional cube with edge length ϵ and midpoint x^0. The projection P of a point x in $\mathbb{R}^n$ onto $\Omega_{x^0,\epsilon}$ can be computed by projecting each coordinate x_i of x onto the interval $[x_i^0 - \epsilon, x_i^0 + \epsilon]$, where x_i^0 is the i^{th} coordinate of x^0. In the minimization process, we use so-called *projected rays*, which are rays that are *bent* whenever they hit the boundary such that they stay within the feasible set. The projected ray starting at a point x with initial direction v is obtained by projecting the ray $x + t\,v$ onto the feasible set, *i.e.*, it is given by

$$r(t) = P(x + t\,v).$$

This describes a piecewise linear path that, after first hitting a face of the feasible set, travels along the boundary.

The *set of active constraints* for a point $x \in \Omega_{x^0,\epsilon}$ is defined as

$$A(x) = \{i \in \{1, 2, ..., n\} \mid \left|x_i - x_i^0\right| = \epsilon\}.$$

For a point away from the boundary, the active set is empty, and for a vertex of the cube $\Omega_{x^0,\epsilon}$, all constraints are active. Let $E : \Omega_{x^0,\epsilon} \to \mathbb{R}$ be our energy, and let $H(x)$ denote the Hessian and $g(x)$ the gradient. The Newton direction $v(x)$ at a point $x \in \Omega_{x^0,\epsilon}$ is

$$v(x) = -(H(x))^{-1} g(x).$$

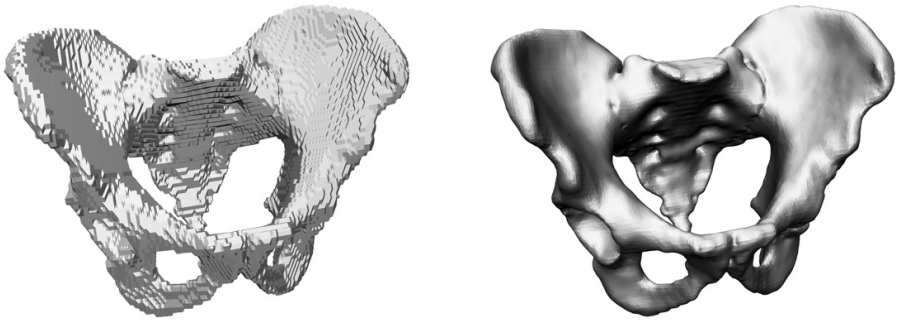

FIGURE 4.3. Removing marching cubes artifacts from a human pelvis (~ 28 cm width) model extracted from computed tomography data. The maximum deviation of the smoothed mesh (right) from the initial surface is 1 mm.

The active set method iterates the following two steps until a local minimum is reached. Let x^k be the current point after the k^{th} iteration.

1. Cauchy step. Compute the gradient direction $g(x^k)$. Find a point y^k along the projected path $P(x^k + t\ g(x^k))$ that produces a sufficient reduction of energy, *i.e.*, a point y^k such that

$$E(y^k) < E(x^k) - \lambda \left\langle g(x^k), y^k - x^k \right\rangle, \tag{4.3}$$

where $\lambda < 1$ is a constant. In our experiments, we set $\lambda = 0.01$. A point satisfying (4.3) is called a Cauchy point.

2. Subspace minimization step. The point y^k lies in some face of the feasible cube $\Omega_{x^0,\epsilon}$ (which may be the cube itself). In this step, we perform a minimization step constrained to this face. More specifically: determine the active set $A(y^k)$ of y^k and compute the reduced Hessian H_r and the reduced gradient g_r with respect to the free variables. Here, reduced means: for all $i \in A(y^k)$ remove the i^{th} column and row from H and the i^{th} entry from g. Then compute the reduced Newton direction $v_r^k = H_r^{-1} g_r$ and lift the vector v_r^k to $\mathbb{R}^n$ by adding zeros for the removed entries. The next iterate x^{k+1} is a point on the projected path $P(y^k + t\ v_r^k)$ that is itself a Cauchy point, *i.e.*, satisfies (4.3), and has less energy than the Cauchy point computed in step 1.

In steps 1 and 2, we search along a projected ray $r(t)$ for a point that satisfies a descent condition. Since we can efficiently evaluate $r(t)$ for any t, any line search algorithm can be applied for this. We use an iterative procedure that starting from an initial guess $t = \tilde{t}$, either monotonically increases or monotonically decreases the value of t. It is increasing if the guessed point $r(\tilde{t})$ satisfies the descent condition and is otherwise decreasing. In each iteration, the value of t is multiplied by a factor of 2 (increasing case) or 0.5 (decreasing case). The iteration terminates if the descent condition is no longer fulfilled (increasing

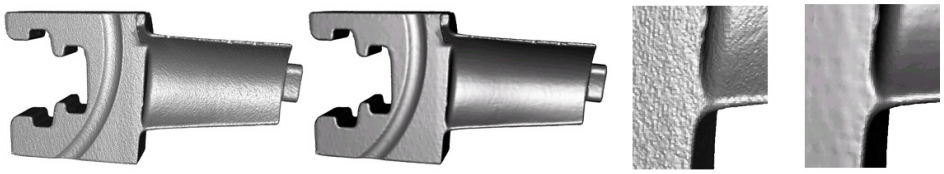

FIGURE 4.4. Noise removal from the scanned blade model with 390 k triangles. Details are shown on the right.

case) or if they are fulfilled (decreasing case). If the sequence is increasing, the last value satisfying the descent condition is used. In each Cauchy and subspace minimization step, we use the result of the previous iteration as an initial guess for t.

4.3.1 Approximation of the Hessian

Since the Hessian of the discrete Willmore energy is not necessarily positive definite, there is no guaranty that the Newton direction is indeed a descent direction. One way to deal with this issue is to replace the Hessian by a positive definite approximation. This technique is used by inexact Newton methods.

To approximate the Hessian of the Willmore energy, we use the Hessian of the thin plate energy with the initial surface as the parameter domain. This matrix has the form $S\,M^{-1}\,S$, where S is the usual cotan matrix, see Section 3.3, and M contains the masses, *e.g.*, M is a diagonal matrix containing the Voronoi areas. Since the matrix S has a kernel consisting of the constant functions, we add the constant value 0.1 to all diagonal entries of S. The resulting approximation of the Hessian is positive definite, can be written as the square of a matrix, and decouples the x, y, and z coordinates. Therefore the linear systems that need to be solved are better conditioned (the condition number is only the square root of the original), have higher sparsity and are of lower dimension. As a result, the method can be be applied to larger models. This is demonstrated on the Chinese lion model with $1.3\,m$ triangles in Figure 4.1.

A related approximation of the Hessian of the Willmore energy has been proposed and used to accelerate the integration of Willmore flow in [107]. One difference between this method and ours is that the approximate Hessian we use is a product of square matrices whereas their approximation is a product of non-square matrices.

Efficiently solving the linear system. To compute the descent direction, we need to solve the linear system

$$(S\,M^{-1}\,S)_r\,v_r = g_r, \tag{4.4}$$

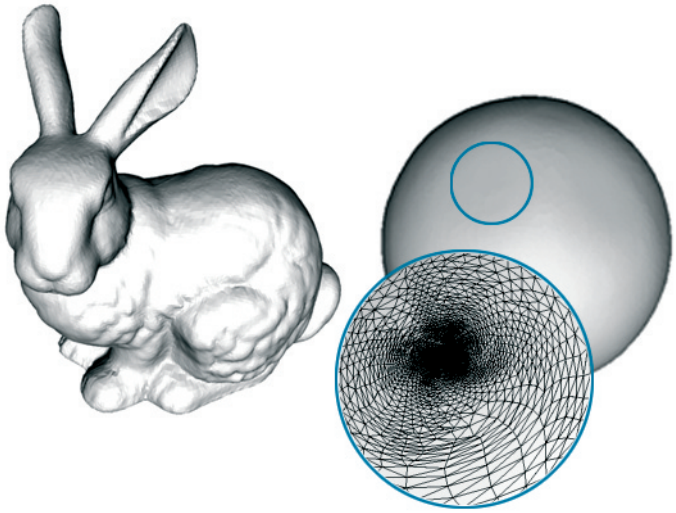

FIGURE 4.5. The bunny model (70k triangles) is shown on the left and after the unconstrained minimization of its discrete Willmore energy on the right. We zoom in to show the difference in size of the triangles corresponding to the region around an ear. This demonstrates the robustness of the discrete energy.

where g is the gradient of the discrete Willmore energy (4.1). Note that we solve only the reduced system. We do not completely solve the system, but compute an approximate solution by performing only a few iterations of preconditioned conjugate gradients. Such a strategy is commonly used for large-scale problems. It proved to be more efficient to spend less effort for each iteration at the cost of having to perform more steps. This type of method is called a Newton–CG method. The performance of the CG solver essentially depends on the choice of a preconditioner. We compute a sparse Cholesky factorization of S only once as a preprocessing step and use the factorization in each iteration to build a *constraint preconditioner* [87] for solving the reduced system (4.4).

4.4 Experiments

We have tested our method on laser-scanned real-world models, with the exception of the pelvis model shown in Figure 4.3 that has been extracted from computed tomography data. No artificial noise has been added to the models; we tested the method with the noise inherent to the scanned data. The only exceptions are Figures 4.7 and 4.8, where artificial noise has been added to the models in order to have a *ground truth* for the comparison of methods.

Noise removal from range images is shown in Figures 4.2 and 4.6. These models have a regular quad connectivity which we triangulated in order to

FIGURE 4.6. Noise removal from a range image of a part of a Neptune statue (height $\sim$10 cm) with a maximum deviation tolerance of 0.04 mm.

get planar faces. The two range images differ in size and resolution: the image of the Caesar model has 190 k triangles with a height of 30 cm and the Neptune model has 270 k triangles with a height of 10 cm. Accordingly, we specified a smaller value for the maximum deviation tolerance for Neptune than for Caesar: 0.04 mm for Neptune and 0.1 mm for Caesar. These values are much smaller than the size of features like the eyelids or wrinkles, which are preserved. The third image of Figure 4.2 shows the smoothed Caesar colored by the distance of the initial (noisy) to the smoothed surface. The colors seem to be randomly distributed, which indicates that mainly noise has been removed and that few structured deviations, like shrinkage of features, have taken place. The Figures 4.1 and 4.4 show models with clean connectivity and filled holes. The Chinese lion model has 1.3 m triangles with a height of 10 cm and the blade has 390 k triangles and measures about one meter in height. We used a 0.1 mm maximum deviation tolerance for the Chinese lion and a 1 mm maximum for the blade.

The pelvis model (Figure 4.3) suffers from aliasing and terracing artifacts caused by a rudimentary volume-extraction method. The ϵ maximum deviation for this model is 1 mm which suffices to produce a smooth model.

We compare our method to the feature-preserving anisotropic diffusion as described in [59] on the armadillo model in Figure 4.8. Despite the larger amount of noise used in this example, our method produces a result that comes close to the original surface. The anisotropic diffusion focuses on preserving the features and even enhances them, *e.g.*, the teeth are sharper than in the original model. On the other hand the noise is also preserved for a longer time.

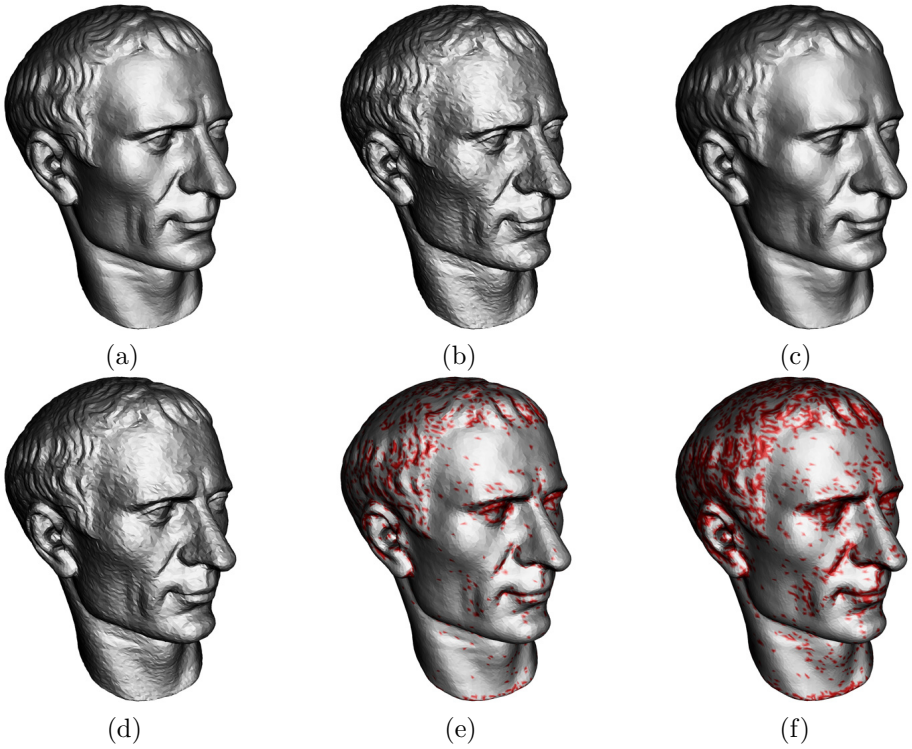

FIGURE 4.7. Comparison of the constrained optimization and the unconstrained gradient flow of the Willmore energy on the Caesar model (a). The model has been artificially corrupted by random noise with 0.2 mm maximum deviation (b), where the height of the object is 30 cm. The constrained optimization (c) keeps all vertices within 0.2 mm distance. The bottom row shows the gradient flow at different times. Vertices that leave the 0.2 mm distance are colored red. The first vertices leave the 0.2 mm distance (d). When the same Willmore energy is reached (e), the maximum distance is 2 mm and shrinkage effects appear, for example, at the eyelids. Further time steps (f) induce more shrinkage.

At the instant when the noise is removed, the non-feature regions are already oversmoothed. For the goal of reproducing the original shape, our method produces visually better results.

We compare our method to the unconstrained gradient flow of the Willmore energy on the Caesar model in Figure 4.7. The model has been corrupted by random noise with a maximal deviation of 0.2 mm, where the height of the object is 30 cm. The constrained optimization (top row right) keeps all vertices within 0.2 mm distance to the noisy surface. The bottom row shows snapshots of the unconstrained evolution. Vertices that leave the 0.2 mm distance are colored red. The first image shows the moment when the first vertices leave the 0.2 mm distance. The model is still very noisy. When the fairness energy equals the fairness energy of the surface produced by the constrained optimization, the

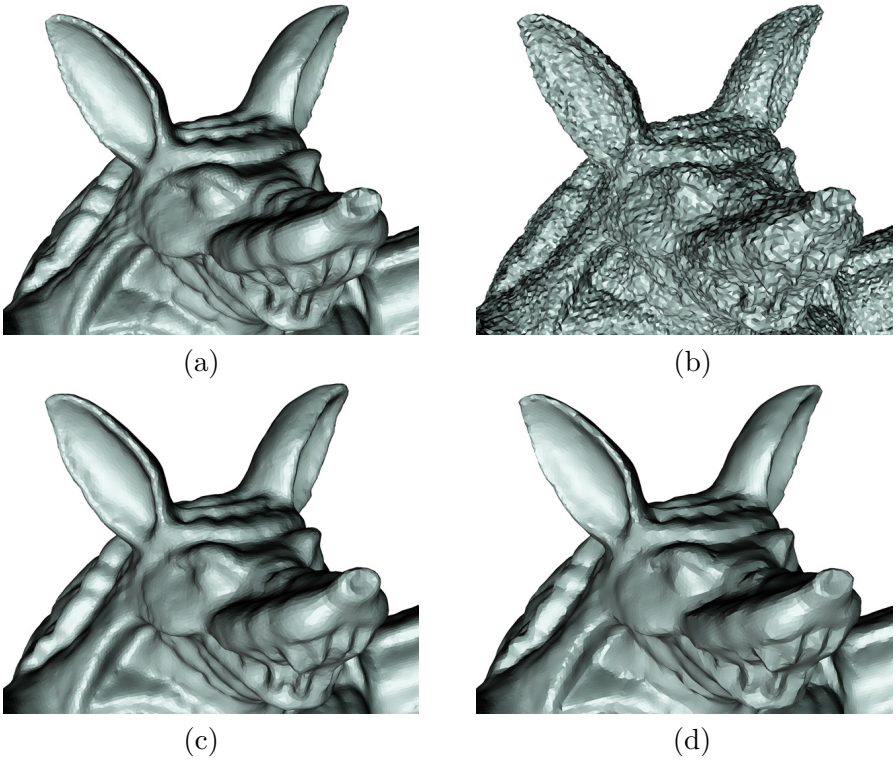

FIGURE 4.8. On the armadillo model (a) that has been artificially corrupted with random noise (b), we compare our method (c) with feature preserving anisotropic diffusion (d). The anisotropic flow sharpens features, but regarding the reproduction of the original model, our method produces better results.

maximum distance is already 2 mm and shrinkage effects appear in regions with high curvature, *e.g.*, at the eyelids. Further time steps induce more shrinkage.

Optimization procedure. The active set Newton scheme produces a rapid decrease of energy. All presented examples, including the 1.3 m-triangle Chinese lion model, were stopped after 10-25 iterations. The most time consuming operation in each iteration is the computation of the Newton direction, which requires solving a linear system. Compared to this, the procedure that finds the new position along a projected ray $r(t)$ is fast.

An alternative optimization procedure to the proposed Newton scheme would be an explicit projected gradient descent, *i.e.*, to skip the subspace minimization step. A benefit of this is that one does not need to compute the Newton direction, which simplifies the implementation and decreases the computational cost of an iteration. On the other hand, it is well known that for this type of problem, an explicit gradient descent usually requires a large number of steps. The comparison shown in Table 4.1 demonstrates that the explicit gradient descent is only efficient if the surface has nicely shaped triangles and the devi-

Model	#T	Max. Tol. in mm	Newton		Exp. Gradient	
			#iter	cost (s)	#iter	cost (s)
Caesar	190 k	0.1	20	103	95	172
Caesar	190 k	0.3	20	101	> 500	> 850
Blade	390 k	1	15	216	90	364
Blade	390 k	3	15	209	> 500	> 2000
Blade*	100 k	1	15	48	250	278

TABLE 4.1. A comparison of running times of the proposed Newton scheme and an explicit gradient descent is shown. Different values of the maximum deviation tolerance were tested on the Caesar and the blade model. The procedures were stopped at equal values of the energy. The last row shows running times of the methods on an irregular mesh generated by simplifying the blade model.

ation tolerance is very small whereas the Newton scheme performs well on all the examples. An implicit gradient descent can handle irregular meshes and larger steps, but the computation of an implicit step itself requires solving a nonlinear equation, cp. [107]. Even if the equation is linearized (semi-implicit scheme), the cost of computing the gradient direction is comparable to the cost of computing the Newton direction.

Bibliography

[1] R. A. Adams. *Sobolev Spaces*. Academic Press, 1975.

[2] M. Alexa. Wiener filtering of meshes. In *Proceedings of Shape Modeling International*, pages 51–57. IEEE Computer Society, 2002.

[3] M. Alexa and M. Wardetzky. Discrete Laplacians on general polygonal meshes. *ACM Trans. Graph.*, 30(4):102:1–102:10, 2011.

[4] N. Amenta, S. Choi, T. Dey, and N. Leekha. A simple algorithm for homeomorphic surface reconstruction. *Proceedings of the ACM Symposium on Computational Geometry*, pages 213–222, 2000.

[5] D. N. Arnold, R. S. Falk, and R. Winther. Finite element exterior calculus, homological techniques, and applications. *Acta Numerica*, 15:1–155, 2006.

[6] C. Bajaj and G. Xu. Anisotropic diffusion on surfaces and functions on surfaces. *ACM Transactions on Graphics 22*, pages 4–32, 2003.

[7] T. Banchoff. Critical points and curvature for embedded polyhedra. *J. Differential Geometry*, 1:257–268, 1967.

[8] T. Banchoff. Critical points and curvature for embedded polyhedral surfaces. *Amer. Math. Monthly*, 77:475–485, 1970.

[9] J. W. Barrett, H. Garcke, and R. Nürnberg. Parametric approximation of Willmore flow and related geometric evolution equations. *SIAM J. Sci. Comput.*, 31(1):225–253, 2008.

[10] U. Bauer, K. Polthier, and M. Wardetzky. Uniform convergence of discrete curvatures from nets of curvature lines. *Discrete Comput. Geom.*, 43(4):798–823, 2010.

[11] M. Belkin and P. Niyogi. Laplacian eigenmaps for dimensionality reduction and data representation. *Neural Comput.*, 15(6):1373–1396, 2003.

[12] M. Belkin and P. Niyogi. Towards a theoretical foundation for Laplacian-based manifold methods. *J. Comput. Syst. Sci.*, 74:1289–1308, 2008.

[13] M. Belkin, J. Sun, and Y. Wang. Discrete Laplace operator for meshed surfaces. In *Proceedings of the ACM Symposium on Computational Geometry*, pages 278–287, 2008.

[14] M. Belkin, J. Sun, and Y. Wang. Constructing Laplace operator from point clouds in $\mathbb{R}^d$. In *Proceedings of the ACM-SIAM Symposium on Discrete Algorithms*, pages 1031–1040, 2009.

[15] M. Berger. *A Panoramic View of Riemannian Geometry*. Springer Verlag, 2003.

[16] Z. Bian and R. Tong. Feature-preserving mesh denoising based on vertices classification. *Computer Aided Geometric Design*, 28:50–64, January 2011.

[17] W. Blaschke. *Vorlesungen ber Differentialgeometrie, III: Differentialgeometrie der Kreise und Kugeln*, volume 29 of *Grundlehren der Mathematischen Wissenschaften*. Springer, 1929.

[18] A. Bobenko, H. Pottmann, and J. Wallner. A curvature theory for discrete surfaces based on mesh parallelity. *Mathematische Annalen*, 348:1–24, 2010.

[19] A. I. Bobenko. A conformal energy for simplicial surfaces. *Combinatorial and Computational Geometry*, 52:133–143, 2005.

[20] A. I. Bobenko, T. Hoffmann, and B. Springborn. Minimal surfaces from circle patterns: Geometry from combinatorics. *Ann. of Math.*, 164:231–264, 2006.

[21] A. I. Bobenko and U. Pinkall. Discrete isothermic surfaces. *J. Reine Angew. Math.*, 475:187–208, 1996.

[22] A. I. Bobenko and P. Schröder. Discrete Willmore flow. In *Proceedings of the ACM SIGGRAPH/Eurographics Symposium on Geometry Processing*, pages 101–110, 2005.

[23] A. I. Bobenko, P. Schröder, J. M.Sullivan, and G. M. Ziegler. *Discrete Differential Geometry*, volume 38 of *Oberwolfach Seminars*. Birkhäuser, 2008.

[24] A. I. Bobenko and B. A. Springborn. A discrete Laplace–Beltrami operator for simplicial surfaces. *Discrete Comput. Geom.*, 38(4):740–756, 2007.

[25] A. Bonito, R. H. Nochetto, and M. Sebastian Pauletti. Parametric FEM for geometric biomembranes. *J. Comput. Phys.*, 229:3171–3188, 2010.

[26] M. Botsch, L. Kobbelt, M. Pauly, P. Alliez, and B. Levy. *Polygon Mesh Processing*. AK Peters, 2010.

[27] K. Brakke. The surface evolver. *Experimental Mathematics*, 1(2):141–165, 1992.

[28] D. Burago, Y. Burago, and S. Ivanov. *A Course in Metric Geometry*, volume 33 of *Graduate Studies in Mathematics*. American Mathematical Society, 2001.

[29] F. Cazals and M. Pouget. Estimating differential quantities using polynomial fitting of osculating jets. *Computer Aided Geometric Design*, 22:121–146, 2005.

[30] U. Clarenz, U. Diewald, G. Dziuk, M. Rumpf, and R. Rusu. A finite element method for surface restoration with smooth boundary conditions. *Comput. Aided Geom. Des.*, 21:427–445, 2004.

[31] U. Clarenz, U. Diewald, and M. Rumpf. Anisotropic geometric diffusion in surface processing. *Proceedings of IEEE Visualization*, pages 397–405, 2000.

[32] D. Cohen-Steiner and J.-M. Morvan. Restricted Delaunay triangulations and normal cycles. *ACM Symposium on Computational Geometry*, pages 237–246, 2003.

[33] D. Cohen-Steiner and J.-M. Morvan. Second fundamental measure of geometric sets and local approximation of curvatures. *J. Differential Geom.*, 73(3):363–394, 2006.

[34] K. Deckelnick and G. Dziuk. Error analysis for the Willmore flow of graphs. *Interfaces Free Boundaries*, 8:21–46, 2006.

[35] H. Delingette. On smoothness measures of active contours and surfaces. In *Proceedings of the IEEE Workshop on Variational and Level Set Methods*, Washington, DC, USA, 2001. IEEE Computer Society.

[36] A. Demlow. Higher-order finite element methods and pointwise error estimates for elliptic problems on surfaces. *SIAM J. Numer. Anal.*, 47(2):805–827, 2009.

[37] M. Desbrun, E. Grinspun, P. Schröder, and M. Wardetzky. Discrete Differential Geometry: An applied introduction. In *ACM SIGGRAPH ASIA Courses*, 2008.

[38] M. Desbrun, A. Hirani, M. Leok, and J. Marsden. Discrete exterior calculus. preprint, arXiv:math.DG/0508341, 2005.

[39] M. Desbrun, M. Meyer, P. Schröder, and A. H. Barr. Implicit fairing of irregular meshes using diffusion and curvature flow. *Proceedings of ACM SIGGRAPH*, pages 317–324, 1999.

[40] T. K. Dey, P. Ranjan, and Y. Wang. Convergence, stability, and discrete approximation of Laplace spectra. In *Proceedings of the ACM-SIAM Symposium on Discrete Algorithms*, pages 650–663. SIAM, 2010.

[41] M. Droske and M. Rumpf. A level set formulation for Willmore flow. *Interfaces and Free Boundaries*, 6(3):361–378, 2004.

[42] R. J. Duffin. Distributed and lumped networks. *Journal of Mathematics and Mechanics*, 8:793–826, 1959.

[43] R. J. Duffin. Potential theory on a rhombic lattice. *Journal of Combinatorial Theory*, 5(3):258–272, 1968.

[44] G. Dziuk. Finite elements for the Beltrami operator on arbitrary surfaces. In S. Hildebrandt and R. Leis, editors, *Partial Differential Equations and Calculus of Variations*, Lecture Notes in Mathematics 1357. Springer Verlag, 1988.

[45] G. Dziuk. Computational parametric Willmore flow. *Numerische Mathematik*, 111(1):55–80, 2008.

[46] K. Ecker. *Regularity theory for mean curvature flow.* Birkhäuser, 2004.

[47] H. Federer. Curvature measures. *Trans. Am. Math. Soc.*, 93:418–491, 1959.

[48] H. Federer. *Geometric measure theory.* Springer Verlag, 1969.

[49] S. Fleishman, I. Drori, and D. Cohen-Or. Bilateral mesh denoising. *Proceedings of ACM SIGGRAPH*, pages 950–953, 2003.

[50] R. L. Foote. Regularity of the distance function. *Proceedings of the American Mathematical Society*, 92(1):153–155, 1984.

[51] J. Fu. Curvature measures and generalized morse theory. *J. Diff. Geom.*, 30:619–642, 1989.

[52] S. F. F. Gibson. Constrained elastic surface nets: Generating smooth surfaces from binary segmented data. In *Medical Image Computing and Computer-Assisted Intervention - MICCAI*, pages 888–898. Springer, 1998.

[53] J. Goldfeather and V. Interrante. A novel cubic-order algorithm for approximating principal direction vectors. *ACM Transactions on Graphics*, 23:45–63, 2004.

[54] M. Gromov. *Metric Structures for Riemannian and Non-Riemannian Spaces*, volume 152 of *Progress in Mathematics*. Birkhäuser, 1999.

[55] M. Gross and M. Pauly. Spectral processing of point-sampled geometry. *Proceedings of ACM SIGGRAPH*, pages 379–386, 2001.

[56] L. P. Hari, D. Givoli, and J. Rubinstein. Computation of open Willmore-type surfaces. *Applied Numerical Mathematics*, 37:257–269, 2001.

[57] M. Hein, J.-Y. Audibert, and U. von Luxburg. From graphs to manifolds - weak and strong pointwise consistency of graph Laplacians. In *Proceedings of the 18th Conference on Learning Theory*, pages 470–485. Springer, 2005.

[58] C.-J. Heine. Isoparametric finite element approximation of curvature on hypersurfaces. Preprint, Universität Freiburg, 2004.

[59] K. Hildebrandt and K. Polthier. Anisotropic filtering of non-linear surface features. *Computer Graphics Forum*, 23(3):391–400, 2004.

[60] K. Hildebrandt and K. Polthier. Constraint-based fairing of surface meshes. In *ACM Siggraph/Eurographics Sympos. Geom. Processing*, pages 203–212, 2007.

[61] K. Hildebrandt and K. Polthier. Generalized shape operators on polyhedral surfaces. *Computer Aided Geometric Design*, 28(5):321–343, 2011.

[62] K. Hildebrandt and K. Polthier. On approximation of the Laplace–Beltrami operator and the Willmore energy of surfaces. *Computer Graphics Forum*, 30(5):1513–1520, 2011.

[63] K. Hildebrandt and K. Polthier. Consistent discretizations of the Laplace–Beltrami operator and the Willmore energy of surfaces. Oberwolfach Reports No. 34, 2012.

[64] K. Hildebrandt, K. Polthier, and M. Wardetzky. On the convergence of metric and geometric properties of polyhedral surfaces. *Geometricae Dedicata*, 123:89–112, 2006.

[65] T. Hoffmann. Discrete rotational cmc surfaces and the elliptic billiard. In H.-C. Hege and K. Polthier, editors, *Mathematical Visualization*, pages 117–124. Springer-Verlag, 1998.

[66] M. Holst and A. Stern. Geometric variational crimes: Hilbert complexes, finite element exterior calculus, and problems on hypersurfaces. *Found. Comput. Math.*, 12(3):263–293, 2012.

[67] L. Hsu, R. Kusner, and J. Sullivan. Minimizing the squared mean curvature integral for surfaces in space forms. *Experimental Mathematics*, 1(3):191–207, 1992.

[68] H. Huang and U. Ascher. Surface mesh smoothing, regularization, and feature detection. *SIAM J. Sci. Comput.*, 31(1):74–93, Oct. 2008.

[69] T. R. Jones, F. Durand, and M. Desbrun. Non-iterative, feature-preserving mesh smoothing. *Proceedings of ACM SIGGRAPH*, 2003.

[70] C. Kanzow. An active set-type newton method for constrained nonlinear systems. In M. Ferris, O. Mangasarian, and J.-S. Pang, editors, *Complementarity: Applications, Algorithms and Extensions*, pages 179–200. Kluwer Academic Publishers, 2001.

[71] H. Karcher and K. Polthier. Construction of triply periodic minimal surfaces. *Phil.Trans. Royal Soc. Lond.*, 354:2077–2104, 1996.

[72] W. Kühnel. *Differential Geometry: Curves - Surfaces - Manifolds*, volume 16 of *Student Mathematical Library*. AMS, second edition, 2005.

[73] M. Levoy, K. Pulli, B. Curless, S. Rusinkiewicz, D. Koller, L. Pereira, M. Ginzton, S. Anderson, J. Davis, J. Ginsberg, J. Shade, and D. Fulk. The digital michelangelo project: 3D scanning of large statues. In *Proceedings of ACM SiGGRAPH*, pages 131–144, 2000.

[74] B. Lévy and H. Zhang. Spectral mesh processing. In *ACM SIGGRAPH ASIA Courses*, pages 1–47, 2009.

[75] C.-J. Lin and J. J. Moré. Newton's method for large bound-constrained optimization problems. *SIAM Journal on Optimization*, 9(4):1100–1127, 1999.

[76] R. MacNeal. *The solution of partial differential equations by means of electrical networks*. PhD thesis, California Institute of Technology, 1949.

[77] D. S. Meek and D. J. Walton. On surface normal and Gaussian curvature approximations given data sampled from a smooth surface. *Computer Aided Geometric Design*, 17(6):521–543, 2000.

[78] C. Mercat. Discrete Riemann surfaces and the Ising model. *Comm. Math. Phys.*, 218(1):177–216, 2001.

[79] H. P. Moreton and C. H. Séquin. Functional optimization for fair surface design. In *Proceedings of ACM SIGGRAPH*, pages 167–176, 1992.

[80] J.-M. Morvan. *Generalized Curvatures*. Springer Verlag, 2008.

[81] J.-M. Morvan and B. Thibert. Approximation of the normal vector field and the area of a smooth surface. *Discrete and Computational Geometry*, 32(3):383–400, 2004.

[82] J. R. Munkres. *Some Applications Of Triangulation Theorems*. PhD thesis, University Of Michigan, 1955.

[83] J. R. Munkres. Obstructions to the smoothing of piecewise-differentiable homeomorphisms. *Annals of Mathematics*, 72(3):521–554, 1960.

[84] A. Nealen, T. Igarashi, O. Sorkine, and M. Alexa. Laplacian mesh optimization. In *Proceedings of ACM GRAPHITE*, pages 381–389, 2006.

[85] J. C. Nédélec. Curved finite element methods for the solution of singular integral equations on surfaces in $\mathbb{R}^3$. *Computer Methods in Applied Mechanics and Engineering*, 8(1):61–80, 1976.

[86] G. M. Nielson, G. Graf, R. Holmes, A. Huang, and M. Phielipp. Shrouds: Optimal separating surfaces for enumerated volumes. In *Symposium on Visualization*. Eurographics Association, 2003.

[87] J. Nocedal and S. J. Wright. *Numerical Optimization (2nd edition)*. Springer Series in Operations Research. Springer-Verlag, New York, NY, 2006.

[88] N. Olischläger and M. Rumpf. Two step time discretization of Willmore flow. In *Proceedings of the IMA International Conference on Mathematics of Surfaces*, pages 278–292. Springer-Verlag, 2009.

[89] J. Peng, V. Strela, and D. Zorin. A simple algorithm for surface denoising. *Proceedings of IEEE Visualization*, 2001.

[90] P. Perona and J. Malik. Scale space and edge detection using anisotropic diffusion. *IEEE Computer Society Workshop on Computer Vision*, 1987.

[91] U. Pinkall and K. Polthier. Computing discrete minimal surfaces and their conjugates. *Experim. Math.*, 2:15–36, 1993.

[92] K. Polthier. Polyhedral surfaces of constant mean curvature. Habilitationsschrift, Technische Universität Berlin, 2002.

[93] K. Polthier. Unstable periodic discrete minimal surfaces. In S. Hildebrandt and H. Karcher, editors, *Geometric Analysis and Nonlinear Partial Differential Equations*, pages 127–143. Springer Verlag, 2002.

[94] K. Polthier and E. Preuss. Identifying vector field singularities using a discrete Hodge decomposition. In H.-C. Hege and K. Polthier, editors, *Visualization and Mathematics III*. Springer Verlag, 2003.

[95] K. Polthier and W. Rossmann. Counterexample to the maximum principle for discrete minimal surfaces. Electronic Geometry Model No. 2000.11.040, 2001. `www.eg-models.de/2000.11.040`.

[96] K. Polthier and M. Schmies. Straightest geodesics on polyhedral surfaces. In H.-C. Hege and K. Polthier, editors, *Mathematical Visualization*, pages 135–150. Springer-Verlag, 1998.

[97] M. Reuter, S. Biasotti, D. Giorgi, G. Patanè, and M. Spagnuolo. Discrete Laplace–Beltrami operators for shape analysis and segmentation. *Computers & Graphics*, 33(3):381–390, 2009.

[98] O. Sorkine and D. Cohen-Or. Least-squares meshes. In *Proceedings of Shape Modeling International*, pages 191–199. IEEE Computer Society Press, 2004.

[99] H. Sprekeler. On the relation of slow feature analysis and Laplacian eigenmaps. *Neural Comput.*, 23(12):3287–3302, 2011.

[100] T. Tasdizen, R. Whitaker, P. Burchard, and S. Osher. Geometric surface smoothing via anisotropic diffusion of normals. *Preceedings of IEEE Visualization*, pages 125–132, 2002.

[101] G. Taubin. A signal processing approach to fair surface design. *Proceedings of ACM SIGGRAPH*, 1995.

[102] C. Tomasi and R. Manduchi. Bilateral filtering for gray and color images. In *Proceedings of the Sixth International Conference on Computer Vision*, pages 839–846, 1998.

[103] M. Troyanov. Les surfaces euclidiennes à singularités coniques. *Enseign. Math.*, 32(2):79–94, 1986.

[104] L. Váša and J. Rus. Dihedral angle mesh error: a fast perception correlated distortion measure for fixed connectivity triangle meshes. *Computer Graphics Forum*, 31(5):1715–1724, 2012.

[105] T. Volodine, D. Vanderstraeten, and D. Roose. Smoothing of meshes and point clouds using weighted geometry-aware bases. In *Proceedings of Geometric Modeling and Processing*, pages 687–693, 2006.

[106] M. Wardetzky. *Discrete Differential Operators on Polyhedral Surfaces - Convergence and Approximation*. PhD thesis, Freie Universität Berlin, 2006.

[107] M. Wardetzky, M. Bergou, D. Harmon, D. Zorin, and E. Grinspun. Discrete Quadratic Curvature Energies. *Computer Aided Geometric Design*, 24:499–518, 2007.

[108] M. Wardetzky, S. Mathur, F. Kälberer, and E. Grinspun. Discrete Laplace operators: No free lunch. In *ACM Siggraph/Eurographics Sympos. Geom. Processing*, pages 33–37, 2007.

[109] P. Wintgen. Normal cycle and integral curvature for polyhedra in Riemannian manifolds. In G. Soós and J. Szenthe, editors, *Differential Geometry*, volume 31 of *Colloq. Math. Soc. János Bolyai*, pages 805–816. North-Holland, Amsterdam, 1982.

[110] G. Xu. Convergence of discrete Laplace–Beltrami operators over surfaces. *Comput. Math. Appl.*, 48:347–360, 2004.

[111] Z. Xu, G. Xu, and J.-G. Sun. Convergence analysis of discrete differential geometry operators over surfaces. In *Mathematics of Surfaces XI.*, volume 3604 of *LNCS*, pages 448–457. Springer Verlag, 2005.

[112] S. Yoshizawa, A. Belyaev, and H.-P. Seidel. Smoothing by example: Mesh denoising by averaging with similarity-based weights. In *Proceedings of the IEEE International Conference on Shape Modeling and Applications*. IEEE, 2006.

[113] S. Yoshizawa and A. G. Belyaev. Fair triangle mesh generation with discrete elastica. In *Proceedings of Geometric Modeling and Processing*, pages 119–123. IEEE Computer Society, 2002.

[114] M. Zähle. Integral and current representations of Federer's curvature measures. *Arch. Math.*, 46:557–567, 1986.

Zusammenfassung

Die diskrete Differentialgeometrie ist ein mathematisches Gebiet, in dem diskrete Entsprechungen zu Begriffen und Konzepten der klassischen und modernen Differentialgeometrie glatter Mannigfaltigkeiten konstruiert und analysiert werden. Die Entwicklung in diesem Gebiet wird katalysiert durch die Anwendbarkeit der Resultate in der Computergraphik, der Geometrieverarbeitung, der numerischen Physik und der Architekturgeometrie.

In dieser Arbeit befassen wir uns mit polyedrischen Flächen im $\mathbb{R}^3$. Im ersten Kapitel fassen wir Resultate zusammen, die die Grundlage dieser Arbeit bilden. Insbesondere betrachten wir die Approximation des metrischen Tensors einer glatten Fläche und die Definition von Funktionenräumen auf polyedrischen Flächen.

Im zweiten Kapitel beschäftigt uns die Frage, wie sich Krümmungen polyedrischer Flächen beschreiben lassen. In der klassischen Differentialgeometrie glatter Flächen wird dafür die Weingartenabbildung verwendet. Da polyedrische Flächen im $\mathbb{R}^3$ nur Lipschitz–Untermannigfaltigkeiten sind, lässt sich die klassische Definition der Krümmungen nicht anwenden. Wir führen daher eine verallgemeinerte Weingartenabbildung ein, die ein vektorwertiges Funktional auf einem Sobolevraum schwach differenzierbarer Vektorfelder ist und sich rigoros auf polyedrischen Flächen definieren lässt. Zur Rechtfertigung des Konzepts zeigen wir, wie die verallgemeinerte Weingartenabbildung einer polyedrischen Fläche benutzt werden kann, um die klassische Weingartenabbildung einer glatten Fläche zu approximieren.

Im dritten Kapitel beschäftigen wir uns mit diskreten Laplace–Beltrami–Operatoren polyedrischer Flächen. Wir zeigen, wie die starke (oder klassische)

Form des Laplace–Beltrami–Operators konsistent diskretisiert werden kann. Darüber hinaus betrachten wir die Willmore–Energie, ein wichtiges geometrisches Funktional, und führen eine konsistente Diskretisierung der Willmore–Energie auf polyedrischen Flächen ein.

Im vierten Kapitel entwickeln wir ein Verfahren zur Glättung verrauschter Flächen. Die Besonderheit dieses Verfahrens ist, dass die maximale Abweichung jedes Punktes von seiner gemessenen Position beschränkt werden kann.